Energy Storage and Conversion

ACADEMIC
ACADEMIC PUBLISHING PTE LTD

2023 VOLUME 1 ISSUE 1
ISSN: 3029-2778 (Online)

http://ojs.acad-pub.com/index.php/ESC

1

Editorial Board

Editor-in-Chief

Associate Editor

Editorial Board Members

Volume 1 Issue 1 • 2023

Energy Storage and Conversion

Editor-in-Chief

Prof. Jinlian Hu

City University of Hong Kong, Hong Kong

ACADEMIC
ACADEMIC PUBLISHING PTE LTD

2023 | Volume 1 | Issue 1

Energy Storage and Conversion

https://ojs.acad-pub.com/index.php/ESC/index

Contents

Original Research Articles

Review Articles

Energy Storage and Conversion 2023; 1(1): 138.
Original Research Article

Compozit structures $Ba_{0.5}Sr_{0.5}Co_{1-x}Fe_xO_{3-z}$, synthesized on the big solar furnace

M. S. Payzullakhanov*, F. Ernazarov, O. Rajamatov, N. Karshieva, A. Holmatov

Institute of Materials Science of the Academy of Sciences of the Republic of Uzbekistan, Tashkent 100084, Uzbekistan

*** Corresponding author:** M. S. Payzullakhanov, fayz@bk.ru

ARTICLE INFO

Received: 20 July 2023
Accepted: 16 August 2023
Available online: 8 October 2023

doi: 10.59400/esc.v1i1.138

ABSTRACT: Anion-deficient structures based on the composition $Sr_{0.5}Ba_{0.5}Co_{1-x}Fe_xO_{3-z}$ synthesized from a melt in a solar furnace in a stream of concentrated solar radiation with a density of 100–200 W/cm^2 have been studied. Briquettes of the form of tablets based on a stoichiometric mixture of carbonates and oxides of the corresponding metals ($SrCO_3$ + $BaCO_3$ + Co_1O_3 + Fe_2O_3) were melted on the focal spot of the big solar furnace. Drops of the melt flowed into the water, cooling at a rate of 10^3 deg/s. Drops of the melt flowed into the water, cooling at a rate of 10^3 deg/s. The castings were crushed to a fineness of 63 μm, dried at 400 °C, molded into tablets (samples) (20 mm in diameter and 10 mm high). Samples of the material were sintered in the temperature range of 1050 °C–1250 °C. The structure, water absorption, and degradation in a carbon dioxide medium were studied in the samples. The crystal lattice of the material had a perovskite structure with a unit cell parameter a = 4.04 Å. The material samples showed increasing water absorption with increasing sintering temperatures. There is also a dependence on the resistance of the material structure to the effects of carbon dioxide and water vapor on the sintering temperature. The observed values of structural parameters indicate that the material based on the perovskite $Sr_{0.5}Ba_{0.5}Co_{1-x}Fe_xO_{3-z}$ structures can be used as a catalyst in the production of hydrogen and synthesis gas by reforming and methane oxidation. Preliminary experiments on obtaining synthesis gas showed that the perovskite structures of the composition are not inferior to phosphogypsum in terms of efficiency. However, the implementation of such approaches requires the development and creation of special equipment that makes it possible to control the flows of gases and water into the reaction chamber irradiated by a concentrated flux of high-density solar radiation.

KEYWORDS: synthesis from a melt; concentrated flow; hydrogen production; synthesis gas; perovskite catalytic structures

1. Introduction

In the fundamental triad “composition-structure-properties”, one can trace the manifestation of unique properties (high-temperature superconductivity, magnetoresistance, ferroelectricity, catalytic activity) of materials with the ABO_3 perovskite structure[1–6]. Because of this, such materials are widely used in various promising areas[7–9]. For example, in obtaining synthesis gas[10,11].

Anion-deficient $ABO_{3-\delta}$ structures with transition metals in B positions (Mn, Fe, Co, Ni, and Cu) can be distinguished from the class of perovskites. A feature of such structures, for example, $SrBaCo_{1-x}Fe_xO_{3-z}$, is mixed oxygen-electronic conductivity, which makes it possible to use them as oxygen-reversible ($ABO_{3-\delta} + 1/2\delta O_2 \leftrightarrow ABO_3$) electrode materials, replacing expensive platinum in solid oxide fuel cells (SOFC). Oxygen-permeable membranes, reducing the cost of producing synthesis gas and sorbents with 100% oxygen selectivity[12–16]. Interest in materials of this class is especially growing under the conditions of rapidly developing hydrogen energy[17,18]. However, this material interacts well with carbon dioxide and decomposes into carbonates and oxides, which limits its applicability[19]. Perovskites are used in solid-oxide fuel cells to convert chemical energy into electricity. At the same time, such devices have high efficiency (more than 80%) and very low emissions of harmful gases. with high efficiency, low emissions, and fuel flexibility. In addition, perovskites are successfully used in membrane reactors based on oxygen-conducting membranes (OTMs). Such devices combine separation and chemical reactions in one unit[20].

It was shown in the study of Pan et al.[21] that oxygen-conducting materials based on phosphogypsum significantly increase the efficiency of producing hydrogen-enriched synthesis gas (72.51% was established) at a reaction temperature of about 1023 K.

In this work, the material of the perovskite structure of the composition $Ba_{0.5}Sr_{0.5}Co_{1-x}Fe_xO_{3-z}$, was studied. The purpose of the work was to show the possibility of synthesizing perovskite structures in a solar furnace.

2. Methodology of experiments

A concentrated flux of solar radiation through mirror concentrating systems is widely used for heating, processing, and melting a wide range of materials. For example, a large solar furnace (BSP) with a thermal power of 1 MW was recently used to extract metals from industrial waste[22], hydrogen from water[23]. The technological capabilities of BSP were also used to synthesize high-temperature materials[24].

From mixtures of iron and cobalt oxides with barium and strontium carbonates ($BaCO_3 + SrCO_3 + Fe_2O_3 + Co_2O_3$) in a stoichiometric ratio after grinding (63 μm) and molding by semi-dry pressing (100 MPa), samples were made in the form of a cylinder Æ 20 mm, which were installed on a water-cooled melting unit located on the focal plane of the solar furnace. A concentrated flux of solar radiation with a density of the order of Q = 150 W/cm^2 was directed to the sample. This value of the flux density is according to Stefan Boltzmann's law.

$$T = \sqrt[4]{\frac{Q}{\varepsilon\sigma}}$$

where Q is the flux density of the concentrated flux of solar radiation, 250 W/cm^2, ε is the emissivity, and σ = 5.67 × 10^{-8} W/m^{2}K is the Stefan Boltzmann constant, corresponds to the temperature of the heated body of 2200 K. At this temperature, the sample melts, and melt drops fall into the water and are cooled at a rate of 10^3 deg/s. Such cooling conditions made it possible to fix the high-temperature structural states of the material.

Drops of the melt, loaded into the water, cracked into small glass-like particles of arbitrary shape. The melt quenched into water was crushed to a fineness of 60 μm and molded into cylinders 8 mm in diameter and 2 mm high. Cylindrical samples were sintered at different temperatures.

X-ray phase analysis of samples of the obtained materials was performed on a Panalytical Empyrean diffractometer with software in the Bragg-Brentano reflection geometry with CuKα radiation (λ = 1.5418 Å). Data was taken between 10° and 64° in 0.5° increments.

Studies of the morphology and microstructural features of the material samples were done by scanning electron microscopy (SEM).

Thermogravimetric (TG) curves were obtained on a TG50 instrument either running in air at a heating rate of 10 ″C/min using about 50 mg of sample.

The temperature coefficient of thermal expansion was measured on a cathetometer in the temperature range of 300–1250 K. The electrical resistance was measured by the four-contact method in the temperature range of 300–1300 K.

The relative density of the samples was determined as the ratio of the density of the material sample to 4.87 g/cm^3.

3. Results and discussion

We have studied perovskite structures $Ba_{0.5}Sr_{0.5}Co_{0.8}Fe_{0.2}O_{3-\delta}$ synthesized from a melt in a solar furnace.

Figure 1 shows a Panalytical Empyrean X-ray diffractometer with CuKα radiation of a sintered sample at 1100 °C.

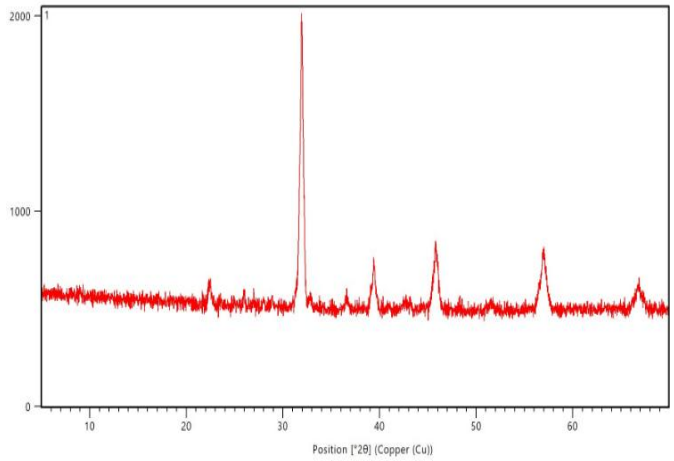

Figure 1. X-ray pattern of a material sample obtained by synthesis from a melt in a solar furnace of composition $Sr_{0.5}Ba_{0.5}Co_{0.8}Fe_{0.2}O_{2.78}$.

An analysis of the X-ray diffraction patterns showed that the obtained oxides have a cubic perovskite-like structure with a lattice parameter a = 4.04 Å of the Pm3m space group. It was also found that such structures are characterized by significant nonstoichiometry in oxygen. The estimated region of homogeneity of the resulting complex compositions of $Sr_{0.5}Ba_{0.5}Fe_{1-x}Co_xO_{3-\delta}$ lies in the range from x = 0.0 to x = 0.7.

Figure 2 shows the dependence of shrinkage on the sintering temperature, and **Figure 3** shows the dependence of density on the sintering temperature.

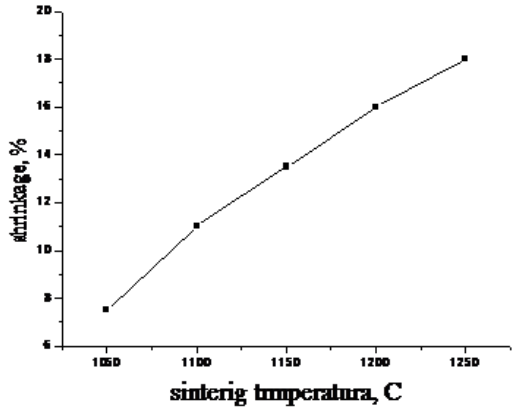

Figure 2. Dependence of shrinkage on sintering temperature.

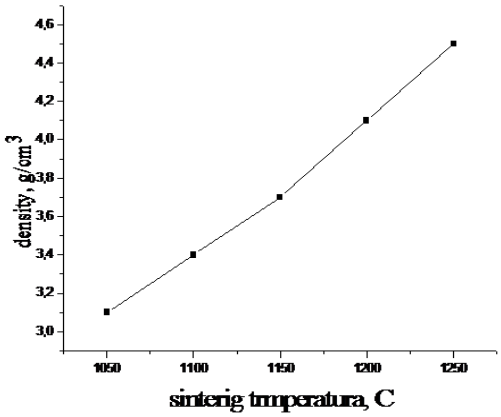

Figure 3. Dependence of density on sintering temperature.

As can be seen from **Figures 2** and **3**, with an increase in the sintering temperature of ceramics, an increase in shrinkage and density is observed. At the same time, a decrease in the porosity of the material is observed.

Figure 4 shows the dependence of electrical resistance on the sintering temperature of material samples. As can be seen in **Figure 4**, with increasing temperature, an increase in electrical resistance is observed, i.e., samples of the material show a metallic character of conductivity.

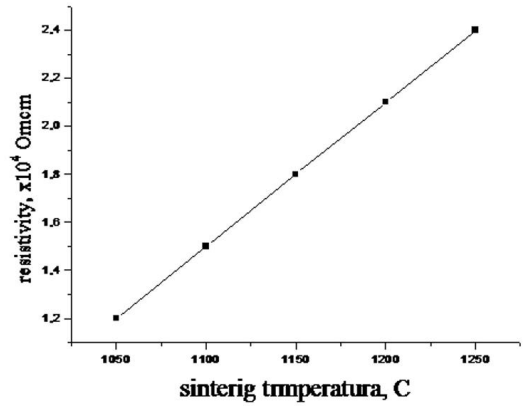

Figure 4. Dependence of electrical resistance on sintering temperature.

Figure 5 shows the dependence of the water absorption of the material sample on the sintering temperature. As can be seen from **Figure 5**, an increase in the ceramic sintering temperature to 1200 °C

causes a decrease in water absorption. Thus, by the method of synthesis from a melt in a solar furnace, it is possible to obtain a material resistant to carbon dioxide and water vapor with low water absorption.

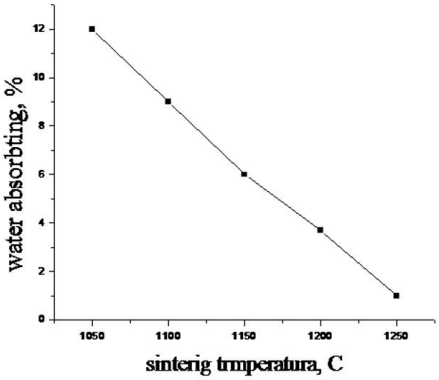

Figure 5. Dependence of water absorption on sintering temperature.

From the above, we can conclude that the material based on $Sr_{0.5}Ba_{0.5}Co_{0.8}Fe_{0.2}O_{2.78}$ perovskite structures can be used as a catalyst in the production of hydrogen and synthesis gas by reforming and oxidizing methane:

$$H_2O + CH_4 \rightarrow CO + 3H_2$$

$$CO_2 + CH_4 \rightarrow 2CO + 2H_2$$

$$CH_4 + (1/2)O_2 \rightarrow CO + 2H_2$$

$$CH_4 + 2O_2 \rightarrow CO_2 + 2H_2O$$

Preliminary experiments on obtaining synthesis gas showed that the perovskite structures of the composition are not inferior to phosphogypsum in terms of efficiency.

However, the implementation of such approaches requires the development and creation of special equipment that makes it possible to control the flows of gases and water into the reaction chamber irradiated by a concentrated flux of high-density solar radiation.

4. Conclusion

Perovskite structures $Sr_{0.5}Ba_{0.5}Co_{1-x}Fe_xO_{3-z}$ were synthesized from a melt in a solar furnace in a stream of concentrated solar radiation with a density of 100–200 W/cm^2.

The material had a cubic structure with a unit cell parameter a = 4.04 Å and showed resistance to carbon dioxide and water vapor and low water absorption.

The material can be used as a catalyst in the production of hydrogen and synthesis gas by reforming and oxidizing methane.

Author contributions

Conceptualization, MSP; methodology MSP; software, FE and OR; validation, FE, OR, NK and AH; supervision, MSP; project administration, MSP. All authors have read and agreed to the published version of the manuscript.

Funding

The work was carried out within the framework of international projects AL-4821023123 “Technology of hydrogen storage in an absorbed form in porous materials” and IL-4821091562

"Peculiarities of phase transitions in ceramics synthesized using a solar furnace of the Institute of Materials Science of the Academy of Sciences of the Republic of Uzbekistan".

Conflict of interest

The authors declare no conflict of interest.

References

1. Galasso FS. Structure, Properties and Preparation of Perovskite-Type Compounds. Pergamon Press; 1968.
2. Goodenough JB. Electronic and ionic transport properties and other physical aspects of perovskites. Reports on Progress in Physics. 2004, 67(11): 1915-1993. doi: 10.1088/0034-4885/67/11/R01
3. Peña MA, Fierro JLG. Chemical structures and performances of perovskite oxides. Chemical Reviews. 2001, 7(101): 1981-2017. doi: 10.1021/cr980129f
4. Yang JB, Kim J, Woo YS, et al. Magnetoresistance in double perovskites $Ba_{2-x}La_xFeMoO_6$. Journal of Magnetism and Magnetic Materials. 2007, 310(2): e664-e665. doi: 10.1016/j.jmmm.2006.10.916
5. Burns G, Dacol FH. Glassy polarization behavior in ferroelectric compounds $Pb(Mg_{\{1\}/\{3\}}Nb_{\{2\}/\{3\}})O_3$ and $Pb(Zn_{\{1\}/\{3\}}Nb_{\{2\}/\{3\}})O_3$.Solid State Communications. 1983, 48(10): 853-856. doi: 10.1016/0038-1098(83)90132-1
6. Kharton VV, Patrakeev MV, Waerenborgh JC, et al. Methane oxidation over perovskite-related ferrites: Effects of oxygen nonstoichiometry. Solid State Sciences. 2005, 7(11): 1344-1352. doi: 10.1016/j.solidstatesciences.2005.08.004
7. Sharma S, Tomar M, Kumar A, et al. Photovoltaic effect in $BiFeO_3/BaTiO_3$ multilayer structure fabricated by chemical solution deposition technique. Journal of Physics and Chemistry. 2016, 93: 63-67. doi: 10.1016/j.jpcs.2016.02.010
8. Zhang J, Gao X, Deng Y, et al. Comparison of life cycle environmental impacts of different perovskite solar cell systems. Solar Energy Materials and Solar Cells. 2017, 166: 9-17. doi: 10.1016/j.solmat.2017.03.008
9. Vassilakopoulou A, Papadatos D, Koutselas I. Light emitting diodes based on blends of quasi-2D lead halide perovskites stabilized within mesoporous silica matrix. Microporous and Mesoporous Materials. 2017, 249: 165-175. doi: 10.1016/j.micromeso.2017.05.001
10. Arutyunov VS. Oxidative Conversion of Natural Gas (Turkish). Krasand; 2011.
11. da Rosa AV, Ordóñez JC. Fundamentals of Renewable Energy Processes, 4th ed. Elsevier; 2022. pp. 419-470.
12. Bouwmeester HJM, Burggraf AJ. Dence ceramic membranes for oxygen separation. In: Gellings PJ, Bouwmeester HJM (editors). Handbook of Solid State Electrochemistry, 1st ed. CRC Press; 1997. pp. 481-553.
13. Tang M, Xu L, Fan M. Progress in oxygen carrier development of methane-based chemical-looping reforming: A review. Applied Energy. 2015, 151: 143-156. doi: 10.1016/j.apenergy.2015.04.017
14. Teraoka Y, Zhang H, Furukawa S, Yamazoe N. Oxygen permeation through perovskite-type oxides. Chemistry Letters. 1985, 14(11): 1743-1746. doi: 10.1246/cl.1985.1743
15. Shao Z, Yang W, Cong Y, et al. Investigation of the permeation behavior and stability of a $Ba_{0.5}Sr_{0.5}Co_{0.8}Fe_{0.2}O_{3-\delta}$ oxygen membrane. Journal of Membrane Science. 2000, 172(1-2): 177-188. doi: 10.1016/S0376-7388(00)00337-9
16. Chang X, Zhang C, He Y, et al. A comparative study of the performance of symmetric and asymmetric mixed-conducting membranes. Chinese Journal of Chemical Engineering. 2009, 17(4): 562-570. doi: 10.1016/S1004-9541(08)60245-1
17. Payzullakhanov MS, Parpiev OR, Avezova NR, Shermatov Z. Hydrogen storage in porous ceramic materials of aluminosilicate composition. Applied Solar Energy. 2022, 58(5): 722-724. doi: 10.3103/S0003701X22601338
18. Allaev KR, Avezova NR. Hydrogen—The future of power engineering for the world and Uzbekistan. Applied Solar Energy. 2021, 57: 575-583. doi: 10.3103/S0003701X21060025
19. Zeng Q, Zuo Y, Fan C, Chen C. CO_2-tolerant oxygen separation membranes targeting CO_2 capture application. Journal of Membrane Science. 2009, 335(1-2): 140-144. doi: 10.1016/j.memsci.2009.03.012
20. Sunarso J, Hashim SS, Zhu N, Zhou W. Perovskite oxides applications in high temperature oxygen separation, solid oxide fuel cell and membrane reactor: A review. Progress in Energy and Combustion Science. 2017, 61: 57-77. doi: 10.1016/j.pecs.2017.03.003

21. Pan Q, Ma L, Du W, et al. Hydrogen-enriched syngas production by lignite chemical looping gasification with composite oxygen carriers of phosphogypsum and steel slag. Energy. 2022, 241: 122927. doi: 10.1016/j.energy.2021.122927
22. Paizullakhanov MS, Parpiev OR, Yu RY, Suvanova SL. Features of the extraction of metals from waste in a solar furnace. Applied Solar Energy. 2022, 58(3): 433-437. doi: 10.3103/S0003701X2203015X
23. Akhatova JS, Ahmadova KS. Extraction of hydrogen from water using CeO_2 in a solar reactor using a concentrated flux of solar radiation. Applied Solar Energy. 2022, 58(6): 889-894. doi: 10.3103/S0003701X22060032
24. Paizullakhanov MS, Shermatov ZZ, Nodirmatov EZ, et al. Synthesis of materials by concentrated solar radiation. High Temperature Material Processes. 2021, 25(2): 17-29. doi: 10.1615/HighTempMatProc.2021038543

Energy Storage and Conversion 2023; 1(1): 215.
Original Research Article

Prefeasibility analysis of the Pumped Hydro Storage (PHS) system in Türkiye: A case study on a hybrid system

Muhammed Fatih Saltuk

Development and Investment Bank of Türkiye, Istanbul 34000, Turkey; fatih.saltuk@kalkinma.com.tr

ARTICLE INFO

Received: 30 August 2023
Accepted: 5 October 2023
Available online: 17 October 2023

doi: 10.59400/esc.v1i1.215

ABSTRACT: Pumped Hydro Storage (PHS) power plants aim to exploit the price difference between storing and generating electricity. These power plants operate by pumping water from the lower reservoir to the upper reservoir, consuming energy, and generating electricity by transferring water from the upper reservoir to the lower reservoir. There is no pumped storage power plant in Turkey yet, and it is in the planning stage. This study aims to provide a preliminary feasibility analysis of this investment from an economic and technical point of view and to contribute to this issue through the recently announced feed-in tariff for PHS. The planned PHS at Gökçekaya Dam was considered a proposal in this study and was carried out using a developed algorithm. The algorithm determines the optimal installed capacity of hybrid energy. This feasibility analysis is based on two scenarios. The difference between the first and second scenarios is due to the investment cost of the PHS system. Additionally, the second scenario considers an integrated hybrid Solar Hydroelectric (SHE) system. Each scenario is evaluated in terms of base price, average price, maximum feed-in price, and market peak price. The result of the study is that only the market price represents a remarkable payback period for pumped storage power plants. As a result of the study, it was found that it's possible to support the pumped storage power plant with a hybrid solar power system and market price if only the storage volume is increased. The feed-in tariff should be set to cover the demand. In the first scenario, only the PHS was evaluated, and after completing the economic analysis, the investment has a payback period of 28.39 years for the market peak price. If the PHS facility is supported by a hybrid solar energy system for internal energy needs, the payback periods can be reduced. In the first scenario, the investment has a payback period of 18.05 years, supported by integrated hybrid solar energy. In the second scenario, the PHS investment has a payback period of 9.63 years for the highest price on the market. The investment has a payback period of 8.66 years, which is supported by the integrated hybrid solar energy. Due to the high self-consumption of energy, integrated hybrid solar energy is suitable for the PHS projects.

KEYWORDS: Pumped Hydro Storage (PHS); energy management; solar energy; Solar-Hydroelectric (SHE)

1. Introduction

Pumped Hydro Storage power plants are hydroelectric power plants aimed at generating additional electricity. The concept of such plants is to pump the reservoir from a lower level to a higher level and then, when needed, release that volume of water back into the lower reservoir. The water is pumped into the upper reservoir during off-peak hours when electricity prices are low and released into the lower reservoir during peak hours when electricity prices are high, resulting in an economic gain. A typical Pumped Hydro Storage (PHS) plant is shown in **Figure 1**.

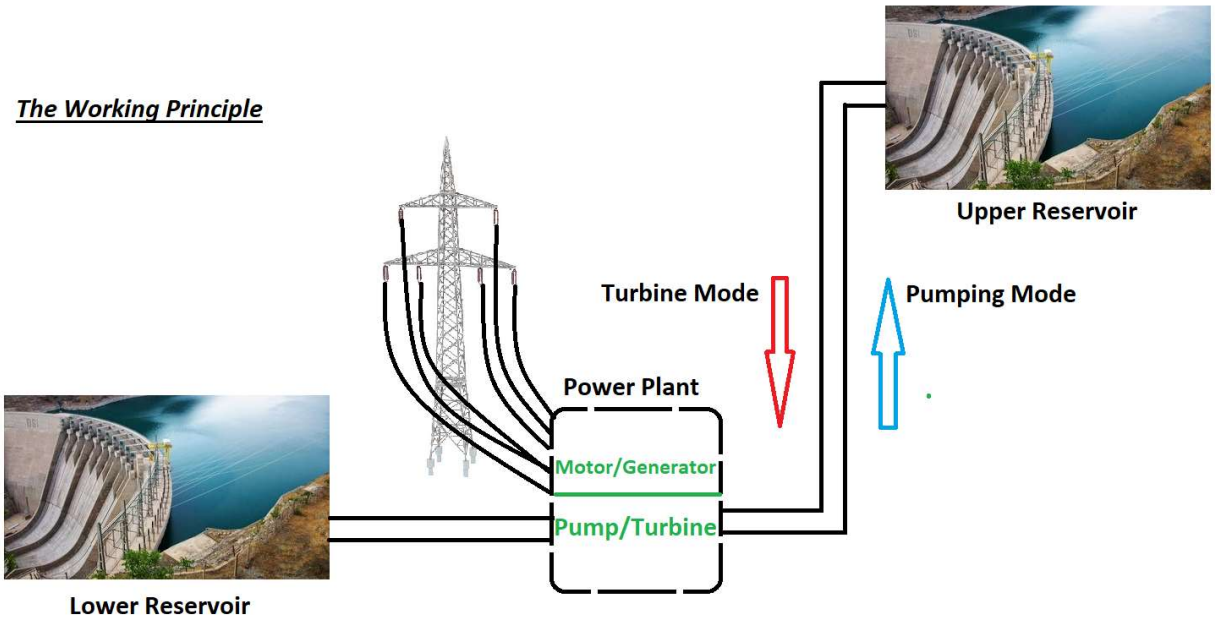

Figure 1. An illustration of Pumped Hydro Storage (PHS) system[1].

The largest share among renewable energy sources is accounted for by hydropower plants. The dams, or storage facilities, are used not only for electricity generation but also for irrigation and flood control. Recently, hydropower plants with pumped storage have been on the agenda in all countries. These plants are considered in the context of physical storage. The aim is to increase the volume of conventional water storage or to make profits by exploiting the price differential between pumping and power generation. Hydroelectric Power Plant (HEPP) systems with pumped storage are used as an alternative to other storage systems. Since battery technology is more expensive to implement and the annual operating cost/renewal cost/battery life isn't what is expected, pumped storage has been chosen, which can be a physical storage method. The table below provides a cost comparison between other storage and pumped storage HEPP facilities. This table is prepared with 2021 indicators by Pumped Hydro Storage International Forum (PHSIF). According to the Pumped Hydro Storage capabilities and costs study of this forum, storage costs are still much higher. Information on storage types and unit costs is provided in **Table 1** below[2].

Table 1. Comparison of energy storage technologies[2].

Costs 2020	PHS	LFP	LAB	Vanad. RF	CAES	Hydrogen
Average power CAPEX (USD/kW)	2,202	3,565	3,558	3,994	1,089	3,117
Average energy CAPEX(USD/kWh)	220	356	356	399	109	312
Average fixed O&M (USD/kWh/yr)	30	8.82	12.04	11.3	8.74	28.5
Effective CAPEX (USD/kW)*	2,910	10,570	11,720	16,170	3,110	8,890

*80 years economic life time, 6% discount rate.

Here PHS stands for pumped storage power plants, LFP for lithium-ion battery storage, LAB for lead-acid batteries, Vanad. RF for vanadium battery storage RF, CAES for compressed air storage, and Hydrogen for hydrogen combined with fuel cells. All the technologies mentioned in the table are methods of energy storage. Pumped Hydro Storage plants are one type of mechanical energy storage, other general methods are electrochemical, thermal, electrical, and hydrogen storage. Each of these types of storage has its own characteristics. When we compare these energy models with each other, we find that they differ in terms of charging/discharging times and size specifications. Thanks to these features, they can be used in different areas. Basically, we can divide the common usage areas into three sections that clarify reserve and response services, transmission and distribution support grids, and bulk power management. Pumped Hydro Storage is the energy storage method that requires the highest charge-discharge time and maximum installed capacity. In **Figure 2** below, all energy storage methods used in detail, and their comparisons between themselves and Pumped Hydro Storage are given[3].

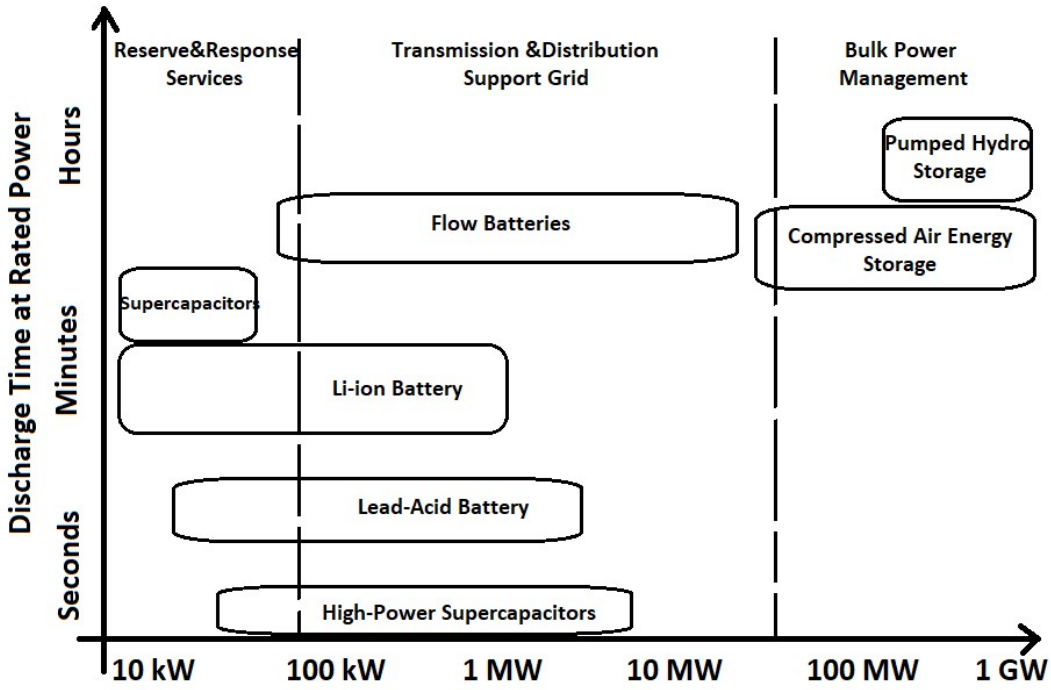

Figure 2. Comparison of the energy storage systems in terms of storage capacity and discharge time[3].

According to the IHA 2022 Status Report, there are pumped storage power plants worldwide with an installed capacity of about 162 GW. The five countries with the highest installed capacity are listed in **Table 2** below[4].

Table 2. Leadership countries for PHS[4].

Countries with Pumped Hydro Storage	Installed Capacity (GW)
China	36.0
Japan	27.5
United States of America	22.0
Italy	7.6
Germany	6.2

Most countries prepare feasibility studies and analyze studies to determine the above pumped storage power plant. In Turkey, feasibility studies for the development of pumped storage power plants have been carried out for a long time, and there is no plant in operation yet. Under the legislation published in the Official Gazette on 12 February 2020, the first step was taken for HEPP with pumped storage. The Gökçekaya PHS, to be completed between 2020 and 2032, will have a total installed capacity of 1.400 MW and is to be completed in Turkish-Japanese cooperation with a value of TL 6.3 billion, according to the legislation that came into force. Türkiye Elektrik İletişim A.Ş. under the coordination of the abolished Electricity Works Survey Administration. (TEİAŞ) and Japan International Cooperation Agency (JICA) under the "Optimal Power Generation Project for Meeting the Peak Demand in Türkiye", which started on 2 February 2010 and was completed in February 2011. HEPP projects were also developed by Tokyo Power Company (TEPCO) experts[5].

Although pumped storage plants are a new challenge for the world, the plants need to be developed in a short time, especially in terms of the supply of energy and water resources, and many studies have been conducted on this mechanism. Rehman et al. evaluated pumped storage technology, the suitability of hybrids, and studies on the islanding of Pumped Hydro Storage systems[6]. Blakers et al. emphasized that pumped hydro energy offers a longer storage time than other battery storage methods[7]. Steffen investigated the application areas of Pumped Hydro Storage for Germany[8]. Ma et al. analyzed the use of pumped storage power plants and battery storage for islands that meet their energy needs from renewable sources[9]. This study is a kind of research article that consists of energy storage technologies, like electrochemical (battery) and mechanical (Pumped Hydro Storage-(PHS)) facilities, for the system in Hong Kong. A case study is performed to clarify the relationship between energy storage systems and the grid. Within the scope of this study, the authors aim to reveal the potential of energy storage systems and lead project sponsors. A comparison of energy storage systems is examined by the levelized cost of energy (LCOE), life-cycle costs (LCC), and LCC ratio methodologies. At the end of this comparison, Pumped Hydro Storage is defined as the optimal solution for the system, with the lowest LCC ratios. Additionally, due to the charge/discharge period of the Pumped Hydro Storage facilities, the system, which is connected to the grid with PHS, is more feasible than the battery option. Yang and Jackson conducted a SWOT analysis of pumped storage power plant use in the United States[10]. Hunt et al. evaluated existing and proposed pumped storage power plants[11]. They emphasized that integrated hybrid energy is a trend, combined with renewable sources like wind and solar energy. The main problem with this synergy is defined as the instability of renewable energy. So, they examined energy storage options in their study. They exhibited the positive and negative sides of the Pumped Hydro Storage facilities. They examined the cost of water storage. Sivakumar et al. studied and projected the long-term use of pumped storage power plants in India[12]. Foley et al. evaluated Pumped Hydro Storage (PHS) that can be operated in the long term with respect to wind energy[13]. They stated that Pumped Hydro Storage facilities are so important for the grid connection. The most compelling part of this investment is the financial structure. So, economic analysis is the vital evaluation of this project. In general, economic indicators like the payback period are taken into account by project sponsors or decision-makers. In this study, they offer to combine Pumped Hydro Storage with wind energy. Pumped Hydro Storage can be used as mechanical energy storage in this mix generation facility. Additionally, a better economic analysis can be obtained from this combined energy system. Javed et al. studied the interoperability of renewable energy sources such as wind, solar, and pumped storage power plants in a hybrid structure[14]. They emphasized that energy storage is the future of energy. They attracted attention to renewable energy penetration. The most optimal solution is offered as solar-wind-Pumped Hydro Storage in their study. This combined energy facility structure is considered preferential basis in terms of economic, environmental, and technical aspects. Within the scope of this penetration, they offered an optimization. Renewable hybrid storage facilities can lead to ongoing alternatives to subsidize the flabbiness

of each other and will be up-and-coming areas for the next generation of investigation. Ma et al. studied the feasibility of a hybrid renewable energy structure for an island in a city, including a pumped storage power plant park order[15]. Kusakana studied the optimization of distributed energy systems using pumped storage power[16]. He stated that the electrification system in rural areas is still a challenge. Renewable energy sources are the most promising technologies. However, the flexile generation profile of solar and wind resources, as well as the flexile electricity consumption, restrain these energy systems from being trustworthy without applicable energy storage systems. In general, solar and wind energy are good candidates for the grid structure of a country; however, energy storage systems are not taken into account in this penetration. In this study, a combined structure is designed with wind energy, solar energy, Pumped Hydro Storage, and diesel generators to satisfy the electricity demand. This study aims to reduce the operational expenditure of the system. The demonstration of this structure has been conducted using the MATLAB software program. The proposed simulation model provides a balanced energy structure for the rural area. Barbour et al. studied the international energy value of pumped storage power plants[17]. Lin et al. have worked on a small system of photovoltaic and residential pumped storage[18]. Ding et al. have studied the energy management of a system of wind and pumped storage power[19]. They designed an energy structure combined with wind energy and a pumped hydro structure for reliable prediction of wind energy. In the first step, the mixed integer programming (MIP) formula is used to determine the limitations of the unit total on and off frequencies, as well as the unit among pumping and generating. The designed simulation offers more reliable energy management for wind energy. Javed et al. analyzed a hybrid structure consisting of a battery and pumped storage[20]. Kocaman and Modi conducted a performance analysis for pumped-storage hydro in a hybrid system[21]. Kim et al. studied the operation of air and pumped storage in a hybrid structure[22]. Kapsali et al. focused on an economic analysis of a pumped storage power plant using solar energy[23]. Stocks et al. studied closed-loop systems that provide no outflow, one of the types of pumped storage power plants[24]. Fan et al. prepared a pre-feasibility study for the use of pumped storage power plants at a currently abandoned mine site[25]. Bredeson and Cicilio, reviewed the Pumped Hydro Storage for Alaska region[26]. Baniya et al. stated that the Himalaya is so suitable for pumped storage facilities because of its geographical advantages[27]. Soucek et al. analyzed computational fluid dynamics by using numerical modelling, standards, and scientific literature for Pumped Hydro Storage plant[28]. Hu et al. performed a quantitative study of the liquid behaviour of the manifold in a seawater-pumped storage facility[29]. Wang et al. organized the energy management of a hydropower plant as Pumped Hydro Storage by using other renewable sources[30]. Ghanjati and Tnani analyzed the optimum installed capacity of a hybrid energy facility, including the photovoltaic (PV)/battery/pumped Hydro Storage structure by using artificial intelligence methodology[31]. Lei et al. focused on the operating conditions of Pumped Hydro Storage[32]. They analyzed the adaptability of the vane under the complicated conjuncture of the Pumped Hydro Storage. Lan et al. stated that Pumped Hydro Storage is so important for renewable energy integration. They focused on the transient process of the facility and performed a case study in China[33]. Huang et al. reviewed the selected project site of the Pumped Hydro Storage such as an abandoned mine site. They tried to reveal the heavy metal impact on water and environment[34]. Liu et al. optimized a strategy for the operation conjuncture of Pumped Hydro Storage[35]. Yi et al. indicated that supercapacitors/batteries can be used in biomedical equipment, aerospace, electric vehicles, military industry, transportation industry, and portable electronic equipments[36]. This energy storage systems are used in quick-response technologies. The charge and discharge times of these systems are so short. These technologies can be defined as electronic equipment. Pumped Hydro Storage has so many different project characteristics. Pumped Hydro Storage can be larger than these technologies for mechanical energy storage. Liu et al. clarified the recent development of lithium-ion batteries[37]. This technology is a kind of electrochemical energy storage system. In recent years, lithium-ion battery technology has become the most popular technology in energy storage systems. It can be used as a

supportive vehicle for the Pumped Hydro Storage facilities. Ma et al. reviewed the economic life of the supercapacitors under various conditions[38]. These technologies are used in quick-response electronic devices. They have a short charge and discharge period. The cycle of this tool is shorter than that of other energy storage systems. These tools are used in high-tech applications. Previous studies have focused primarily on battery technologies, which are electrochemical energy storage methods, and pumped storage has generally been considered an example of mechanical energy storage. In previous case studies, it was assumed that these mechanical energy storage systems would contribute to the environment and the economy if they were built. In contrast to previous studies, this study evaluated the investment period for pumped storage power plants and examined the conditions required for the construction of this structure. This study demonstrated the conditions under which such a structure can be economically evaluated. In contrast to previous studies, the feasibility of a pumped storage power plant was demonstrated, taking into account the contribution of the integrated hybrid Solar Hydroelectric (SHE) system.

In this study, PHS and the suitability of the solar system for pumped storage power utilization were analyzed. The designed algorithm was used in determining the appropriate size of the solar power plant. The algorithm works with the support of a benefit-cost methodology. The algorithm uses the Matlab database as a data center. The yield resulting from the amount of energy generated in each cycle step is compared to the cost of the system. The purpose with the best proportional result gives the main applicable installed energy amount. It was found that the obtained result of solar hydropower is a support for the proposed pumped storage power plant. There are many methods of energy storage that can be used, given current technologies. Pumped storage power is one of them, as is mechanical energy storage. Although the charging and discharging times of mechanical energy storage systems are much longer than those of other energy storage systems, these systems have advantages in terms of the size of their installed capacity, durability, number of cycles, and maintenance and repair requirements. In this study, it is shown that the planned pumped storage power plant will be more successful if it is supported by integrated hybrid renewable energy. The economic analysis was carried out in assumed scenarios, both alone and with integrated hybrid SHE systems. The main objective of this study is to provide an economic analysis of the conditions under which meaningful pumped storage power can be established. The second objective is to demonstrate the effect of integrated hybrid Solar-Hydroelectric (SHE) systems on energy management and process optimization.

2. Materials and methods

An algorithm is designed for hybrid power optimization. Definitions of algorithm are given in below.

$$Ghyd = \ actual\ electricity\ generation\ of\ the\ PHS \tag{1}$$

$$Gsol = calculated\ electricity\ generation\ of\ solar\ energy \tag{2}$$

$$G\ (x) = \ Ghyd + Gsol\ (x) \tag{3}$$

$$Chyd = \ actual\ cost\ of\ the\ PSH\ energy \tag{4}$$

$$Csol = calculated\ cost\ of\ solar\ energy \tag{5}$$

$$C(x) = Chyd + Csol\ (x) \tag{6}$$

$$P = feed - in - tariff \tag{7}$$

$$B(x) = G(x) \times P \tag{8}$$

$$\mathrm{Loop(x)} = \frac{\mathrm{B}(x)}{C(x)} \tag{9}$$

$$foptimum(x) = \max\ (\mathrm{Loop(x)}) \tag{10}$$

where $Ghyd$ is the realized generation of hydro energy, $Gsol$ is the predicted generation of solar energy, G is the total generation of hybrid facility, x is the repetitive step number, $Chyd$ is the realized cost of hydropower, $Csol$ is the estimated investment cost of solar energy, C is the total cost, P is the feed-in-tariff, B is the benefit value of hybrid system, Loop is the ratio of benefit/cost, $foptimum$ is the optimum point of algorithm function. The optimum point determines the optimal installed capacity of hybrid Solar Power Plant (SPP) part. Designed algorithm is given in **Figure 3** below. This algorithm is not an embedded program, designed by the author for the optimization of the solar energy installed capacity.

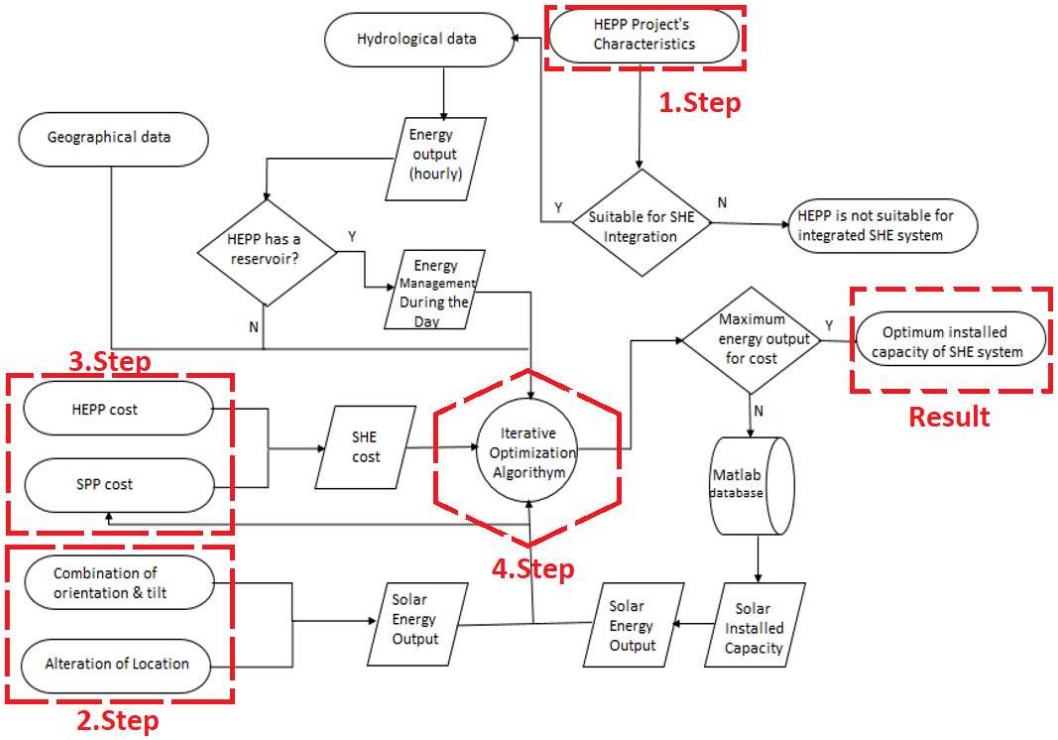

Figure 3. The SHE optimization algorithm.

The algorithm can be clarified as four parts;

- Hydro part of the system (1. Step)
- Solar part of the system (2. Step)
- Cost of the system (3. Step)
- Benefit/Cost cycle of the system-Iteration (4. Step)

The developed algorithm is evaluated based on the benefit-cost methodology. Currently, energy generated by hydropower is supplemented by solar energy, taking into account grid-connected transformer capacity. The algorithm evaluates the solar energy that can be generated without idle capacity, bringing the value to a more reasonable level. The goal of the algorithm is to maximize the benefit achieved per unit. The optimal installed capacity is determined by applying this algorithm to existing hydropower/PHS facilities. PHS consumes power to pump volume from a lower to an upper reservoir. The installed power of the pump that provides the specified amount of consumption is calculated using the following equation.

$$P = \frac{Q \times H \times \rho}{367 \times \eta h} \times ef \tag{11}$$

where P, is the transferred power of pump (kW), Q, is the flow (m^3/h), H, is the height (m), ρ, is the density (kg/m^3), 367 is the conversion coefficient, ηh, is the hydraulic efficiency (%), ef, is the security factor. In general, ηh, is a value between 40-80 % proportions. Security factors can be change according to required power.

3. Results and discussion

A case study examines the economic analysis of pumped storage power plants. The existing Gökçekaya Dam and HEPP plant were used for the case study. Although storage has gained importance in recent years, physical storage is still the most commonly used form of energy storage. Two scenarios are discussed as part of the case study. The results are compared when pumped storage is supplemented with stand-alone and hybrid solar hydropower. When evaluating hydropower with pumped storage alone, the energy needed for the pump is purchased from the grid at lower unit prices. When the same structure is supported by a solar plant, the energy needed for pumping is obtained from the SHE plant. The optimal size of the SHE plant was found considering the prevailing HEPP. The capability that is the subject of the case study can be seen in **Figure 4** below.

Figure 4. The existing hydro power plant demonstration[39]

Project characteristics is given in the **Table 3** below.

Table 3. The hydropower plant project's characteristics.

Projects Characteristics	
Installed Capacity	278,400 kW
Height	115 m
Electricity Generation (2021)	215,000,000 kWh
Capacity Utilization Rate (2021)	8.82 %

Using the data from the Gökçekaya reservoir, the designed algorithm is executed. In the study, the actual power generation for the year 2021 is obtained from the transparency platform of the Istanbul Energy Exchange (EXIST). The algorithm is used to determine the optimal hybrid system, SPP, as a hybrid structure. In addition, two scenarios are carried out for this study. The scenarios are the pumped storage power plant and the pumped storage power plant supported by the hybrid structure. The designed algorithm was applied to the selected Gökçekaya HEPP plant. The assumptions made for the evaluation are listed below:

- The power generation amount of Gökçekaya Dam in 2021 was taken from the transparency platform EXIST. This website is a platform on which the amount of electricity generated is tracked and disclosed to the public by the government[40].
- The grid connection is limited to 278.4 MW for energy generation (278.4 MW is the installed capacity of Gökçekaya Dam and HEPP). This is the legal grid restriction for the facility. Energy generation above this limit value cannot be supplied to the grid. The excess generated energy is interrupted by facility control management before being given to the grid.
- The economic life of the SPP plant is assumed to be 25 years. The stated economic lifetime is the period specified in the datasheets for the First Solar brand PV panels used in the study. The electromechanical equipment of turbines and generators in hydropower plants has a similar economic lifetime. The economic lifetime is a factor that affects the levelized cost of energy (LCOE). The longer this period is, the lower the LCOE[41].
- The installed capacity of the PHS is accepted as 1,400 MW. This installed capacity was officially announced by the government[42].
- The unit cost is assumed to be 857 USD/kW for the SPP facility. The cost of SPP affects LCOE and payback period (PP) calculations. The higher the cost is, the higher the LCOE[43].
- Within the scope of the study, a performance comparison was carried out by analyzing two scenarios.
- In the first scenario, a feed-in tariff is used for the revenue calculation of the PHS.
- In the second scenario, the energy consumption of the PHS is met by a hybrid SPP facility, and this scenario considers an integrated hybrid SHE facility.
- The cost of installed PHS capacity is from the 2021 Pumped Hydro Storage Forum report (2,202 USD/kW) (PHSIF 2021). Under the legislation published in the Official Gazette on February 12, 2020, the Gökçekaya PHS, to be completed between 2020 and 2032, will have a total installed capacity of 1,400 MW and is to be completed in Turkish-Japanese cooperation with a value of TL 6.3 billion. So, 1,046,250,000 USD (equivalent to TL 6.3 billion according to the February 12, 2020 Central Bank forex buying value) is used as an alternative PHS's construction cost. The cost of facilities affects LCOE and payback period (PP) calculations. The higher the cost is, the higher the LCOE and PP[44].
- The amount of power generation from combined hybrid energy is determined by the algorithm. This electricity generation by facilities affects LCOE and payback period (PP) calculations. The higher generation is, the lower the LCOE and PP.
- The payback period calculations assume that the investment is completed in one year and can be commissioned within the next year, according to the assumptions. The longer this period is, the higher the PP.
- The calculation of the payback period was made very roughly; aspects such as Value Added Tax (VAT), taxes, maintenance investments, and depreciation weren't taken into account in the calculation. The additional cost of this expenditure has an adverse impact on LCOE and PP.
- Only revenue and expense differences are considered in the payback period calculation. In this study, the nominal payback period is taken into account. The discount rate has an adverse impact on PP.
- A feed-in tariff is used as the price of electricity generation. This tariff was announced on 1 May 2023 by the government. If the feed-in tariff is low, this situation will affect LCOE and PP calculations adversely[45].

- Electricity sales prices are supported by night, day, and peak unit prices valid for 3 months as of 1.4.2023 announced by Energy Market Regulatory Authority (EMRA). Related prices are given in the table below[46].
- 1 USD equivalent is accepted as 19.7607 TL (18.05.2023 Central Bank Forex Buying). Possible changes in the exchange rate affect, in particular, the prices per unit of goods/price in Turkish lira[47].
- The investment cost of SPP is predicated on the 2021 IRENA renewable energy costs report[42].
- The designed algorithm was run with 45,000 cycles; each step size was taken as 25 kW.
- The 2019 IRENA renewable energy costs report relies on the expense assumptions of renewable energy sources. Within the IRENA renewable energy costs report, it's stated that the annual disbursement for solar energy plants varies between 9.5 and 18.3 USD/kW. For the solar energy plant, 14 USD/kW is accepted because of the unit disbursement. It's stated in the report that the fixed disbursement for hydroelectric power plants is 0.06% of the whole investment cost, and therefore the variable disbursal is 0.003 USD/kWh. In PHS, the identical figures, excluding electricity consumption expenses, are accepted as operating expenses[43]. The higher cost of this operational expenditure has an adverse impact on LCOE and PP. The announced feed-in tariff is given in **Table 4.** The announced energy consumption unit price is given in **Table 5** below.

Table 4. Feed-in tariff.

	Average Price	**Price Cap**	**Base Price**
Energy Price for PHS (USDcent/kWh)	10.50	11.55	9.45
Energy Price for Solar Energy (USDcent/kWh)	5.50	6.05	4.95

Table 5. Energy consumption unit price.

	Medium (7 am–6 pm)	**Peak (6 pm–11 pm)**	**Low (11 pm–7 am)**
Energy Price (kr/kWh)	281.2067	425.3925	166.4840
Energy Price (USDcent/kWh)	14.2306	21.5272	8.4250

In the second step of the algorithm, the program contains a section on the generation of solar energy. The amount of solar energy used for the internal hybrid energy is determined. The solar radiation and the meteorological data provided by NASA for any point on the Earth. A sample year of original solar radiation data obtained from the official website of NASA is given in **Figure 5** below[48].

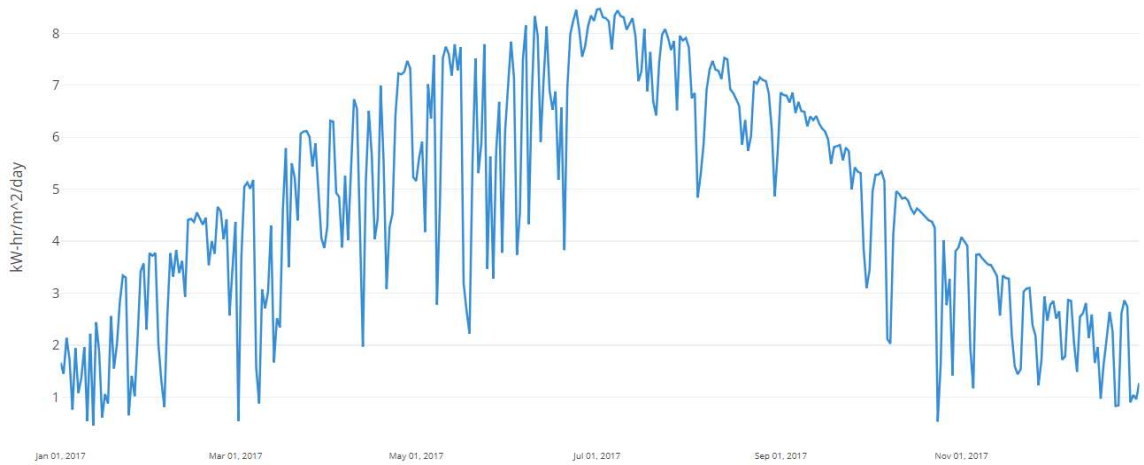

Figure 5. The daily solar radiation obtained from the NASA website (365 days)[48].

The NASA database provides data daily, and solar radiation must be determined on an hourly basis to ensure energy management and optimization of installed power. The two models used when obtaining solar radiation amounts on an hourly basis are the econometric model and the empirical model. While conducting the study, it was decided to use an empirical model for the reasons stated below.

- Ability to convert daily data
- Availability and usage of public data
- The high correlation coefficient
- Prediction of the long-term data

The study, which includes an empirical model, was used to obtain the amount of solar radiation on an hourly basis using MATLAB. In **Figure 6** below, the results obtained for sample days and the amount of solar radiation obtained for the whole year are given. While obtaining the amount of solar energy, the amount of solar radiation on an hourly basis and the current-voltage response of the PV panel to temperature and radiation were used.

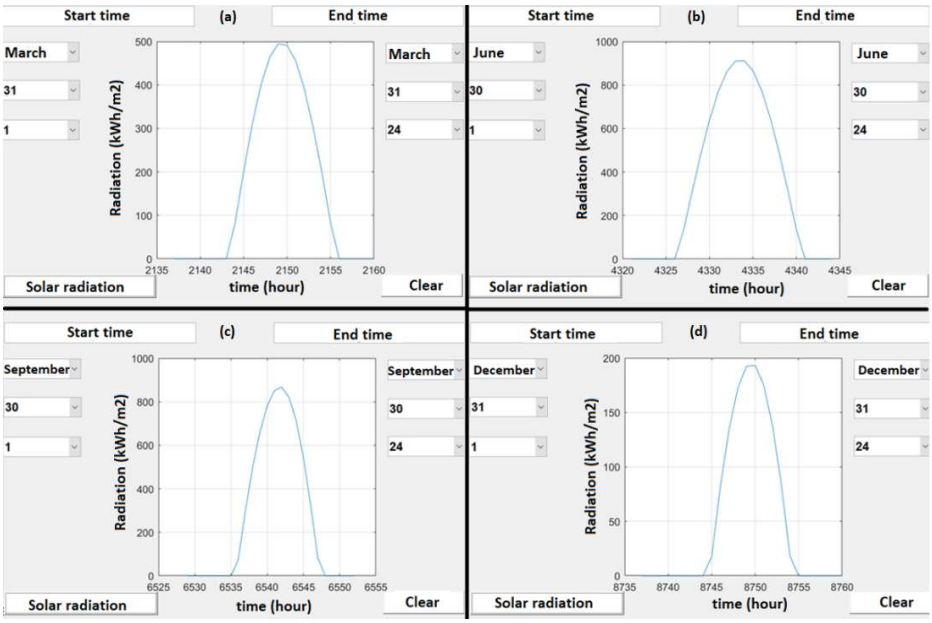

Figure 6. Estimation of the hourly based solar radiation by using the empirical model in Matlab GUI **(a)** 31st March, **(b)** 30th June, **(c)** 30th September and **(d)** 31st December.

The daily radiation amounts were taken from the NASA website for the solar energy plant located within the Gökçekaya HEPP. This original hourly based dataset is given within the **Figure 7** below.

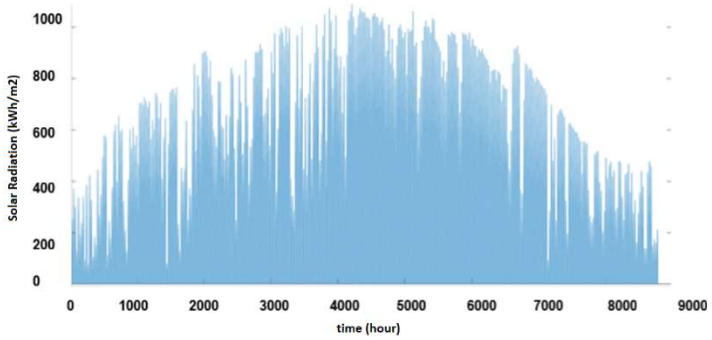

Figure 7. The hourly based solar irradiance obtained from the daily solar irradiance dataset (8760 hours = 24 hours/day × 365 day).

After determining the hourly solar radiation in the selected region, the amount of solar energy is calculated using the designed algorithm. When calculating the solar energy generation, information obtained from the PV data sheet is used. PV data sheet information includes current-voltage information and variations that can be obtained under nominal conditions (1000 W/m^2, AM 1.5, 25 ℃) and radiation. The fluctuations are mainly due to temperature fluctuations. The first Solar brand PV panels, model FS-6450, with an installed capacity of 450 watts, were selected for the case study. **Table 6** below contains PV specifications taken from First Solar's official website[41].

Table 6. Nominal values of PV panel.

Model types and ratings at standard test conditions (1,000 W/m², AM 1.5, 25 °C)								
Nominal values		FS-6430	FS-6435	FS-6440	FS-6445	FS-6450	FS-6455	FS-6460
Nominal power	Pmax (W)	430	435	440	445	450	455	460
Efficiency	%	17.4	17.6	17.8	18.0	18.2	18.4	18.6
Voltage at pmax	Vmax (V)	182.6	183.6	184.7	185.7	186.8	187.8	188.8
Current at pmax	Imax (A)	2.36	2.37	2.38	2.40	2.41	2.42	2.44
Open circuit voltage	Voc (V)	219.2	219.6	220	220.4	221.1	222	222.9
Short circuit current	Isc (A)	2.54	2.55	2.55	2.56	2.57	2.58	2.59
Maximum system voltage	Vsys (V)	1,500[5]						
Limiting reverse current	Ir (A)	5						
Maximum series fuse	Icf (A)	5						

Once all the steps specified in the algorithm had been completed, the installed output of the SHE system, which can be implemented as an integrated hybrid system, was determined. Once the contribution of solar energy had been determined, the economic analysis studies began. Taking into account the conditions previously discussed in the "Acceptance" section, the LCOE and payback period were determined as the key indicators. The revenues and costs were calculated according to the specified scenarios. Results are given in **Table 7** below.

Table 7. Evaluation results.

	1st Scenario		**2nd Scenario**	
Evaluation	**PHS**	**PHS+SHE**	**SHE**	**PHS+SHE**
Gökçekaya HEPP installed capacity (MW)	278.4	278.4	278.4	278.4
PHS installed capacity (MW)	1,400	1,400	1,400	1,400
Energy requirement of pumping (MWh)	1,397,500	1,397,500	1,397,500	1,397,500
PHS energy generation (MWh)	1,075,000	1,075,000	1,075,000	1,075,000
PHS investment cost (million USD)	3,082,800	3,082,800	1,046,250	1,046,250
SPP installed capacity (kW)	-	904,500	-	548,775
Total hybrid installed capacity (MW)	1,400	2,304.5	1,400	1,948.775
SPP energy generation (MWh)	-	1,450,369	-	879,962
Net hybrid generation—Consumption (MWh)	−322,500	1,127,869	−322,500	557,462
Hybrid SPP investment cost (million USD)	-	775.16	-	470.30
Annual revenue (million USD)-Feed-in Tariff-Base	101,588	104,205	101,588	101,588
Annual revenue (million USD)-Feed-in Tariff-Average	112,875	115,783	112,875	112,875
Annual revenue (million USD)-Feed-in Tariff-Cap	124,163	127,362	124,163	124,163
Annual revenue (million USD)-Market Peak Price	231,417	231,417	231,417	231,417
Energy cost of pumping (million USD)	117,739	-	117,739	43,603
Annual PHS operational expenditure (m USD)	5.075	5.075	5.075	5.075
Annual SPP operational expenditure (m USD)	-	12.663	-	7.683
Annual hybrid operational expenditure (m USD)	5.075	17.738	5.075	12.758

Table 7. (*Continued*).

	1st Scenario		2nd Scenario	
Evaluation	**PHS**	**PHS+SHE**	**SHE**	**PHS+SHE**
Annual gross cash surplus (million USD)-Feed-in tariff-base	−21.226	86.467	−21.226	45.407
Annual gross cash surplus (million USD)- Feed-in tariff-base	−9.939	98.045	−9.939	56.514
Annual gross cash surplus (million USD)- Feed-in tariff-base	1.349	109.624	1.349	67.802
Annual gross cash surplus (million USD)- Market peak price	108.603	213.679	108.603	175.056
Payback period (year-nominal)- Feed-in tariff-base	-	44.61	-	33.40
Payback period (year-nominal)- Feed-in tariff-average	-	39.35	-	26.83
Payback period (year-nominal)- Feed-in tariff-cap	-	35.19	-	22.37
Payback period (year-nominal)- Market peak price	28.39	18.05	9.63	8.66
Levelized cost of energy-LCOE (USD/kWh)	5.724	3.996	3.829	1.496

$$\mathrm{LCOE(x)} = \frac{\mathrm{INVCost}(x) + (ELxOPEX(x)}{ELxGEN(x)} \tag{11}$$

$$\mathrm{PP(x)} = \frac{\mathrm{INVCost}(x)}{Revenue(x) - OPEX(x)} \tag{12}$$

where $LCOE$, is the levelized cost of energy (USD/kWh), PP, is the nominal payback period of the facility (year). $INVCost$, is the investment cost (USD), EL, is the economic life of the facility (years), $OPEX$, is the annual operational expenditure (USD/y), GEN is the electricity generation of the facility (kWh/y), $Revenue$, is the revenue of the facility (USD/y).

The energy generation from Gökçekaya Dam will be about 215 million kWh in 2021. During the construction of the pumped storage power plant, it was planned to pump the discharge from the lower basin to the upper basin. The pumped storage power plant will be built in the future. Since the pumped storage power plant has the same water flow as the existing Gökçekaya power plant, it can produce 1075 million kWh with an analogous generation profile. It was calculated that a pump with an installed capacity of 1400 MW. In the 2021 calculations, it was determined that the Gökçekaya HEPP would require an energy consumption of approximately 1397 million kWh to pump this reservoir from the lower level to the upper level. In the economic evaluation, it was assumed that the required energy consumption would be covered by relatively low prices for the unit of demand (at night) and that it would be sold during the peak period, which implies a high price for the unit of measurement when selling energy. In addition to this evaluation, feed-in tariff base/average/cap situations are taken into account. In the first scenario, only the PHS was evaluated, and after completing the economic analysis, the investment has a payback period of 28.39 years for the market peak price. Other feed-in tariff options cause meaningless results or long-term payback periods. If the PHS facility is supported by a hybrid solar energy system for internal energy requirements, payback periods can be shortened. In the first scenario, the investment has a payback period of 18.05 years, which is supported by integrated hybrid solar energy. In the second scenario, the PHS investment has a payback period of 9.63 years for the market peak price. The investment has a payback period of 8.66 years, which is supported by integrated hybrid solar energy. The difference in the first and second scenarios is due to the investment cost of the PHS facility. In the first scenario, the size of the plant SPP, which can be installed as a hybrid plant within the existing Gökçekaya dam and the HEPP plant, is optimized using the developed algorithm in addition to the HEPP pumped storage plant. It is shown that a plant SPP with an installed capacity of 904.5 MW (36,180th stage × 25 kW) can be constructed. In the second scenario, it is shown that a plant SPP with an installed capacity of 548.775 MW (21,951th stage × 25 kW) can be constructed. The cost-benefit analysis is shown in **Figure 8** below.

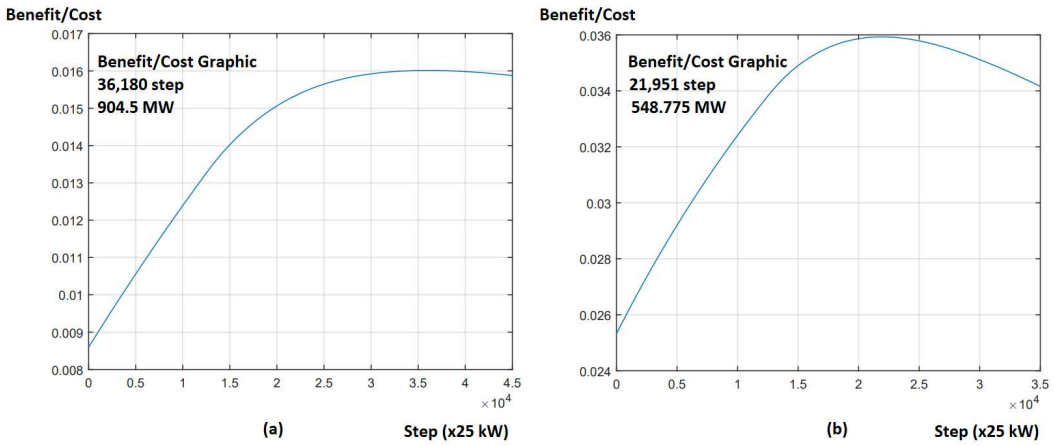

Figure 8. Benefit/Cost graphic of hybrid SHE system **(a)** 1st scenario **(b)** 2nd scenario.

When an evaluation is created to incorporate the pumped-storage HEPP with the contribution of the hybrid SPP structure, it's observed that the second scenario pays back the investment in 8.66 years. During this study, it's assumed that the amount of energy required by the pumped-storage HEPP facility is met by the SPP facility, while the increased energy production is sold during market demand. The daytime demand unit prices supported by sales are the unit prices announced by EMRA and valid for three months as of 01.04.2023. The increases in energy costs experienced in recent months are reflected in unit prices. The best benefit/cost optimization point, SHE system energy amount, and current HEPP/SHE system comparison are given within the graphics in **Figure 9** below.

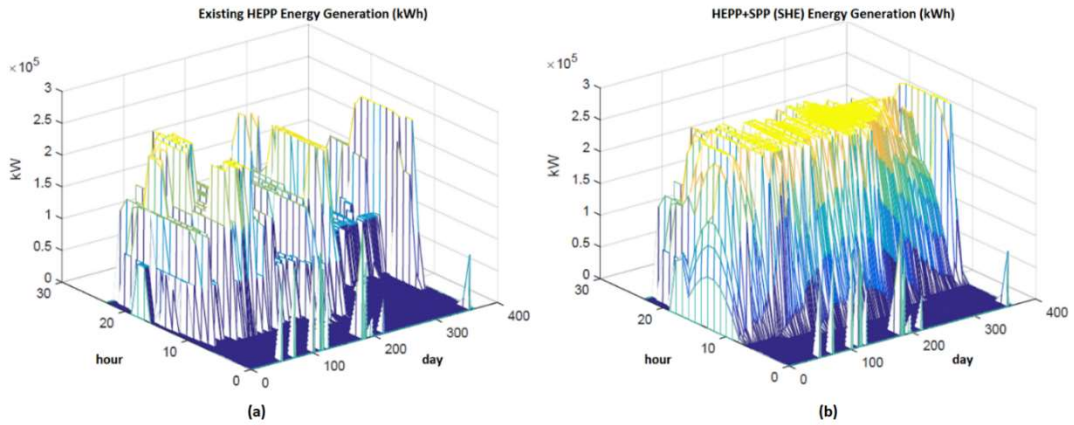

Figure 9. Energy generation comparison of existing HEPP **(a)** and Hybrid SHE **(b)** facilities.

As can be seen in **Figure 9**, the energy generation of the existing HEPP plant is sensitive to climatic and meteorological changes. So, energy management is quite difficult. It also goes without saying that the existing HEPP plant has a low capacity utilization rate for the energy of the facility shown in the graph. A low utilization rate is an indicator of inefficient operation of the plant. In the other graphic, the integrated hybrid structure, it is observed that solar and hydro energy complement each other in terms of energy generation. The generation of the HEPP facility is high in the spring months when the amount of solar energy is relatively low, and the generation of the SPP facility is high during the period when rainfall is low, and these two energy sources complement each other perfectly. This situation leads to more efficient operation of the facility and higher capacity utilization rates. Additionally, the energy efficiency of the transformer is ensured.

4. Conclusion

Pumped storage power plants can provide additional water volume and profits by taking advantage of the energy sales differential between pumping and power generation. Solar hydropower (SHE) is a hybrid structure of solar and hydropower that uses the same electrical infrastructure. In this study, a PHS system with the new feed-in tariff is investigated. In addition, an integrated hybrid solar power system uses an algorithm to achieve optimal installed power. Solar energy is an option for hybrid energy because of its applicability. Two scenarios were discussed in the case study. The difference between the first and second scenarios is due to the investment cost of the PHS facility. Each scenario is evaluated in terms of the base, average, and maximum feed-in price, as well as the market peak price. In the first scenario, only the PHS is examined, and after completing the economic analysis, the investment has a payback period of 28.39 years at a market peak price. In the first scenario, the investment has a payback period of 18.05 years, supported by integrated hybrid solar energy. The economic analysis performed in this assessment assumes that the electricity used for pumping is consumed at low unit prices and that the electricity generated is offered in the market at high prices. The algorithm developed is based on the benefit-cost method. The solar generation profile, compatible with and complementary to the installed profile of the existing hydropower plant when it's low, was determined using the Matlab database. The optimal installed capacity was determined by comparing it with the amount of electricity generated by the sun and the associated investment costs. In the second scenario, it's envisioned that the electricity requirement for pumping will be generated from hybrid solar energy. The electricity consumption required by the pump was covered by solar energy, and the increased solar energy was also fed into the grid at average unit prices (07:00–18:00). Other feed-in tariff options cause meaningless results or long-term payback periods. If the PHS facility is supported by a hybrid solar energy system for internal energy requirements, payback periods can be shortened. In the first scenario, the investment has a payback period of 18.05 years, which is supported by integrated hybrid solar energy. In the second scenario, the PHS investment has a payback period of 9.63 years for the market peak price. The investment has a payback period of 8.66 years, which is supported by integrated hybrid solar energy.

The COVID-19 pandemic and, consequently, the recent and ongoing tensions between Russia and Ukraine have led to an increase in commodity, goods, oil, and energy prices. Accordingly, with a with a feed-in tariff that consists only of pumped hydroelectric storage or is supported by an integrated hybrid solar energy system, no economically viable result can be achieved. The only market price that can be applicable for this investment. If the PHS facility is supported by integrated hybrid solar energy for its internal energy consumption, the results will be more effective. As a result, storage remains a more expensive technology today. It's expected that investment and operating costs per unit will decrease with technological development. However, physical storage is expected to be more sustainable to meet current large-capacity needs. In addition, pumped storage is believed to be a response to warming and the water scarcity expected in the future. As a result of the study, it was found that it's possible to support the pumped storage power plant with a hybrid solar system and market prices if only the storage volume is increased. In addition to this, the feed-in tariff should be determined as a price sufficient to meet the requirement.

Conflict of interest

The author declares no conflict of interest.

References

1. Andritz. Pumped storage. Available online: https://www.andritz.com/products-en/hydro/products/pumped-storage (accessed on 1 July 2023).
2. Capabilities, Costs & Innovation Working Group. Pumped Storage Hydropower capabilities and costs. Available online: https://assets-global.website-files.com/5f749e4b9399c80b5e421384/61432796645661f940f277a8_IFPSH%20-%20PSH%20Capabilities%20and%20Costs_15%20Sept.pdf (accessed on 1 July 2023).
3. Møller KT, Jensen TR, Akiba E, et al. Hydrogen - A sustainable energy carrier. Progress in Natural Science: Materials International. 2017, 27(1): 34-40. doi: 10.1016/j.pnsc.2016.12.014
4. International Hydropower Association. 2021 Hydropower Status Report: Sector Trends and Insights. International Hydropower Association; 2022.
5. Çiçek Ö, Özdemir M. Örnek Bir Hidroelektrik Santrali İçin Pompaj Depolamalı Hidroelektrik Santrali Tasarımı. Gazi Journal of Engineering Sciences. 2021, 7(1): 26-35. doi: 10.30855/gmbd.2021.01.04
6. Rehman S, Al-Hadhrami LM, Alam MdM. Pumped hydro energy storage system: A technological review. Renewable and Sustainable Energy Reviews. 2015, 44: 586-598. doi: 10.1016/j.rser.2014.12.040
7. Blakers A, Stocks M, Lu B, et al. A review of pumped hydro energy storage. Progress in Energy. 2021, 3(2): 022003. doi: 10.1088/2516-1083/abeb5b
8. Steffen B. Prospects for pumped-hydro storage in Germany. Energy Policy. 2012, 45: 420-429. doi: 10.1016/j.enpol.2012.02.052
9. Ma T, Yang H, Lu L. Feasibility study and economic analysis of Pumped Hydro Storage and battery storage for a renewable energy powered island. Energy Conversion and Management. 2014, 79: 387-397. doi: 10.1016/j.enconman.2013.12.047
10. Yang CJ, Jackson RB. Opportunities and barriers to pumped-hydro energy storage in the United States. Renewable and Sustainable Energy Reviews. 2011, 15(1): 839-844. doi: 10.1016/j.rser.2010.09.020
11. Hunt JD, Zakeri B, Lopes R, et al. Existing and new arrangements of pumped-hydro storage plants. Renewable and Sustainable Energy Reviews. 2020, 129: 109914. doi: 10.1016/j.rser.2020.109914
12. Sivakumar N, Das D, Padhy NP, et al. Status of pumped hydro-storage schemes and its future in India. Renewable and Sustainable Energy Reviews. 2013, 19: 208-213. doi: 10.1016/j.rser.2012.11.001
13. Foley AM, Leahy PG, Li K, et al. A long-term analysis of Pumped Hydro Storage to firm wind power. Applied Energy. 2015, 137: 638-648. doi: 10.1016/j.apenergy.2014.07.020
14. Javed MS, Ma T, Jurasz J, et al. Solar and wind power generation systems with Pumped Hydro Storage: Review and future perspectives. Renewable Energy. 2020, 148: 176-192. doi: 10.1016/j.renene.2019.11.157
15. Ma T, Yang H, Lu L, et al. Technical feasibility study on a standalone hybrid solar-wind system with Pumped Hydro Storage for a remote island in Hong Kong. Renewable Energy. 2014, 69: 7-15. doi: 10.1016/j.renene.2014.03.028
16. Kusakana K. Optimal scheduling for distributed hybrid system with Pumped Hydro Storage. Energy Conversion and Management. 2016, 111: 253-260. doi: 10.1016/j.enconman.2015.12.081
17. Barbour E, Wilson IAG, Radcliffe J, et al. A review of pumped hydro energy storage development in significant international electricity markets. Renewable and Sustainable Energy Reviews. 2016, 61: 421-432. doi: 10.1016/j.rser.2016.04.019
18. Lin S, Ma T, Shahzad Javed M. Prefeasibility study of a distributed photovoltaic system with Pumped Hydro Storage for residential buildings. Energy Conversion and Management. 2020, 222: 113199. doi: 10.1016/j.enconman.2020.113199
19. Ding H, Hu Z, Song Y. Stochastic optimization of the daily operation of wind farm and pumped-hydro-storage plant. Renewable Energy. 2012, 48: 571-578. doi: 10.1016/j.renene.2012.06.008
20. Javed MS, Zhong D, Ma T, et al. Hybrid pumped hydro and battery storage for renewable energy based power supply system. Applied Energy. 2020, 257: 114026. doi: 10.1016/j.apenergy.2019.114026
21. Kocaman AS, Modi V. Value of Pumped Hydro Storage in a hybrid energy generation and allocation system. Applied Energy. 2017, 205: 1202-1215. doi: 10.1016/j.apenergy.2017.08.129
22. Kim YM, Shin DG, Favrat D. Operating characteristics of constant-pressure compressed air energy storage (CAES) system combined with Pumped Hydro Storage based on energy and exergy analysis. Energy. 2011, 36(10): 6220-6233. doi: 10.1016/j.energy.2011.07.040
23. Kapsali M, Anagnostopoulos JS, Kaldellis JK. Wind powered pumped-hydro storage systems for remote islands: A complete sensitivity analysis based on economic perspectives. Applied Energy. 2012, 99: 430-444. doi: 10.1016/j.apenergy.2012.05.054
24. Stocks M, Stocks R, Lu B, et al. Global Atlas of Closed-Loop Pumped Hydro Energy Storage. Joule. 2021, 5(1): 270-284. doi: 10.1016/j.joule.2020.11.015

25. Fan J, Xie H, Chen J, et al. Preliminary feasibility analysis of a hybrid pumped-hydro energy storage system using abandoned coal mine goafs. Applied Energy. 2020, 258: 114007. doi: 10.1016/j.apenergy.2019.114007
26. Bredeson L, Cicilio P. Hydropower and Pumped Storage Hydropower Resource Review and Assessment for Alaska's Railbelt Transmission System. Energies. 2023, 16(14): 5494. doi: 10.3390/en16145494
27. Baniya R, Talchabhadel R, Panthi J, et al. Nepal Himalaya offers considerable potential for pumped storage hydropower. Sustainable Energy Technologies and Assessments. 2023, 60: 103423. doi: 10.1016/j.seta.2023.103423
28. Souček J, Nowak P, Kantor M, et al. CFD as a Decision Tool for Pumped Storage Hydropower Plant Flow Measurement Method. Water. 2023, 15(4): 779. doi: 10.3390/w15040779
29. Hu J, Wang Q, Meng Z, et al. Numerical Study of the Internal Fluid Dynamics of Draft Tube in Seawater Pumped Storage Hydropower Plant. Sustainability. 2023, 15(10): 8327. doi: 10.3390/su15108327
30. Wang Z, Fang G, Wen X, et al. Coordinated operation of conventional hydropower plants as hybrid pumped storage hydropower with wind and photovoltaic plants. Energy Conversion and Management. 2023, 277: 116654. doi: 10.1016/j.enconman.2022.116654
31. Ghanjati C, Tnani S. Optimal sizing and energy management of a stand-alone photovoltaic/pumped storage hydropower/battery hybrid system using Genetic Algorithm for reducing cost and increasing reliability. Energy & Environment. 2022, 34(6): 2186-2203. doi: 10.1177/0958305x221110529
32. Lei L, Chen D, Ma C, et al. Optimization and decision making of guide vane closing law for pumped storage hydropower system to improve adaptability under complex conditions. Journal of Energy Storage. 2023, 73: 109038. doi: 10.1016/j.est.2023.109038
33. Lan X, Gu N, Egusquiza M, et al. Parameter optimization decision framework for transient process of a pumped storage hydropower system. Energy Conversion and Management. 2023, 286: 117064. doi: 10.1016/j.enconman.2023.117064
34. Huang G, Rao X, Shao X, et al. Distribution of heavy metals influenced by pumped storage hydropower in abandoned mines: Leaching test and modelling simulation. Journal of Environmental Management. 2023, 326: 116836. doi: 10.1016/j.jenvman.2022.116836
35. Liu B, Zhou J, Guo W, et al. A many-objective optimization strategy for unified optimal operation of pumped storage hydropower station under multiple load rejection conditions. Energy for Sustainable Development. 2023, 74: 34-49. doi: 10.1016/j.esd.2023.03.011
36. Yi Z, Chen Z, Yin K, et al. Sensing as the key to the safety and sustainability of new energy storage devices. Protection and Control of Modern Power Systems. 2023, 8(1). doi: 10.1186/s41601-023-00300-2
37. Liu Y, Wang L, Li D, et al. State-of-health estimation of lithium-ion batteries based on electrochemical impedance spectroscopy: a review. Protection and Control of Modern Power Systems. 2023, 8(1). doi: 10.1186/s41601-023-00314-w
38. Ma N, Yin H, Wang K. Prediction of the Remaining Useful Life of Supercapacitors at Different Temperatures Based on Improved Long Short-Term Memory. Energies. 2023, 16(14): 5240. doi: 10.3390/en16145240
39. Available online: https://www.dsi.gov.tr/ (accessed on 1 July 2023.)
40. Available online: https://www.epias.com.tr/en/ (accessed on 1 July 2023).
41. Available online: https://www.firstsolar.com/-/media/First-Solar/Technical-Documents/Series-6-Datasheets/ (accessed on 1 July 2023).
42. Available online: https://openjicareport.jica.go.jp/pdf/12019790.pdf (accessed on 1 July 2023).
43. International Renewable Energy Agency. Renewable Power Generation Costs in 2021. International Renewable Energy Agency; 2022.
44. International Renewable Energy Agency. Renewable Power Generation Costs in 2019. International Renewable Energy Agency; 2020.
45. Available online: https://www.resmigazete.gov.tr/fihrist?tarih=2023-05-01 (accessed on 1 July 2023).
46. Available online: https://www.epdk.gov.tr/Home/En (accessed on 1 July 2023).
47. Available online: https://www.tcmb.gov.tr/kurlar/kurlar_tr.html (accessed on 18 May 2023).
48. Available online: https://www.earthdata.nasa.gov/topics/atmosphere/atmospheric-radiation/solar-irradiance (accessed on 1 July 2023).

Energy Storage and Conversion 2023; 1(1): 351.
Original Research Article

Integrating self-powered disaster recovery networks with environmental monitoring for enhanced disaster preparedness and response

Qutaiba I. Ali[1,*], Nawar A. Ibrahim[2,*]

[1] *Computer Engineering Department, University of Mosul, Mosul 00964, Iraq*

[2] *Computer Techniques Engineering Department, Northern Technical University, Mosul 00964, Iraq*

*** Corresponding author:** Qutaiba I. Ali, Qut1974@gmail.com; Nawar A. Ibrahim, nawar.ali@ntu.edu.iq

ARTICLE INFO

Received: 20 November 2023
Accepted: 18 December 2023
Available online: 23 December 2023

doi: 10.59400/esc.v1i1.351

ABSTRACT: This paper investigates a comprehensive approach to enhancing environmental monitoring services within a self-powered Disaster Recovery Network (DRN) infrastructure. The study introduces a variety of solutions aimed at overcoming logistical challenges associated with establishing an environmentally conscious DRN infrastructure. Moreover, the research explores the intrinsic factors governing the system's behavior, defines essential evaluation metrics, and delineates performance measurements. The Wireless Solar Router (WSR) is specifically introduced using the Ubicom IP 2022 platform to realize the Ad hoc wirelessly networked nodes of the DRN infrastructure. To advance the field further, the paper proposes an experimental platform for comprehensive evaluation, assessing network performance, practicality, power efficiency, and resilience to various scenarios. A comprehensive design process is illustrated, and the required values of the system elements, i.e., the number of solar cell panels, the capacity of the battery cells, etc., are adjusted to fulfill the design purposes. In order to reduce the power utilization of the recommended WSR and to lengthen the duration of their batteries, a new distributed power management scheme called Duty Cycle Estimation-Event Driven Duty Cycling (DCE-EDDC) was suggested and installed locally in the WSRs in order to decrease their power consumption and extend the lifetime of their batteries. The suggested method is compared with other duty cycling methods, and the proposed DRN system is also compared with other real-world implementations to show its usefulness in building a green DRN infrastructure.

KEYWORDS: environmental monitoring services; DRN infrastructure; network reliability; wireless solar router; solar energy harvesting; power management; fault tolerance techniques

1. Introduction

Natural disasters, encompassing phenomena like earthquakes, hurricanes, and floods, frequently afflict regions across the globe, resulting in substantial destruction to both lives and properties[1–3]. In the face of these catastrophic events, numerous stakeholders must swiftly make critical decisions related to rescue operations. However, the disruption of terrestrial communication infrastructures and other interconnections, such as power facilities, poses a formidable challenge in facilitating communication

between the disaster-affected areas and the outside world[4–6]. In such scenarios, the restoration of the communication system becomes of paramount importance to enable the timely exchange of vital information pertaining to location, events, and the severity of the situation, serving both victims and rescue teams.

Several research articles explore various issues related to emergency communication networks. These articles delve into:

- Content and space analysis of existing networks and big data: Investigating how existing emergency communication networks handle information and its geographical spread[2–4].
- Wireless emergency response systems: Analyzing the specific details and functionalities of wireless systems for emergency response[5–7].
- Emerging communication technologies for disasters: Exploring the potential of technologies like IoT, D2D communication, vehicle networks, cloud and fog computing, UAVs, and WSNs in disaster scenarios[8–10].
- Disaster emergency management networks: Systematically summarizing the overall framework and components of disaster management networks[11–13].
- Advancements in emergency communication technology: Highlighting the latest developments and existing technologies in the field[13–15].
- Communication strategies for mobile Ad hoc networks in emergencies: Classifying different communication approaches within mobile Ad hoc networks for disaster situations[16–18].

Comprehensive environmental monitoring encompasses a spectrum of advanced sensors, from temperature and humidity to pressure, rainfall, wind speed and direction, solar radiation, air quality, and UV radiation. These sensors are strategically deployed to provide real-time, high-resolution data on various environmental quantities. This paper introduces a new paradigm for disaster resilience that centers on the seamless integration of comprehensive environmental monitoring, which includes advanced weather monitoring, with sustainable communication infrastructure, creating a unified system that empowers more effective disaster preparedness and response. The system is self-contained and not reliant on previous models or research, offering a fresh perspective on disaster resilience.

Nonetheless, significant research opportunities remain within this field. This paper aims to address key questions regarding the implementation of a self-powered DRN infrastructure, which is particularly vital in catastrophic scenarios with high probabilities of electrical power source unavailability. These questions encompass:

1) What logistical prerequisites are essential for constructing a self-powered DRN infrastructure?
2) What factors influence system behavior, and how can they be evaluated and measured for performance assessment?
3) How can different environmental monitoring services be effectively integrated with a solar energy-powered system?
4) What criteria should be applied when assessing the entire system in terms of network performance, practicality, and power consumption?

In our work, the distinctive features related to energy conversion and storage in the context of Disaster Recovery Network (DRN) infrastructure set it apart from other works. Here are the key differences:

1) New power management approach: Our work introduces a novel approach to power management by proposing the use of Wireless Solar Routers (WSRs) within the DRN infrastructure. These routers

are designed to harness and store energy from the surrounding environment, with a specific emphasis on solar energy. This innovative approach stands out from conventional methods of power supply and contributes to the eco-friendliness of the DRN.

2) Ad hoc networking for efficiency: Our work emphasizes the use of Ad hoc networking technology within the DRN infrastructure to enhance reliability. Unlike some conventional wireless and wired methods, Ad hoc networks establish connections among nodes without relying on centralized infrastructure or administrative oversight. This results in reduced ownership, installation, and maintenance costs, providing a more efficient and cost-effective solution.
3) Integration of weather monitoring services: Another distinguishing aspect of our work is the integration of a portable self-powered weather station within the DRN infrastructure. This versatile node plays a crucial role in delivering essential DRN and weather monitoring services to various clients. This integrated approach adds a layer of functionality that may not be present in other works focused solely on communication aspects.
4) Extended coverage area through environmental energy harvesting: Our work addresses the limitation of coverage area associated with traditional localized placement of WSRs near wired electricity sources. By proposing energy harvesting from the environment, particularly through solar energy, we overcome this constraint and significantly extend the coverage area of the DRN infrastructure. This approach enhances the adaptability and resilience of the network in diverse geographical locations.

In summary, our work distinguishes itself through an innovative energy conversion and storage strategy, incorporating self-powered WSRs, environmental energy harvesting, and the integration of weather monitoring services. These elements collectively contribute to a more sustainable, resilient, and mobile Disaster Recovery Network infrastructure compared to other works in the field.

2. Disaster recovery network infrastructure

In this section, we explore the requirements and logistics involved in building a robust and eco-friendly Disaster Recovery Network (DRN) infrastructure. We delve into the challenges of self-sufficiency, power management, and connectivity that such a network must overcome. Moreover, we introduce the concept of a green DRN infrastructure.

In this paper, we propose an approach to enhance the reliability of Disaster Recovery Network (DRN) communication systems by leveraging wireless Ad hoc network technology. Our strategy involves the deployment of a wireless network that becomes active when traditional network services fail or when responding to a disaster event. The envisioned DRN infrastructure comprises a variety of wireless nodes, both fixed and mobile, each tailored to fulfill specific tasks dictated by the requirements of different applications.

A key component of this network is the integration between a Wireless Solar Router (WSR) and a portable self-powered weather station, a versatile node responsible for delivering a range of essential DRN and weather monitoring services to various clients within a designated network area. These services encompass transmitting data and weather sensor signals between critical and industrial facilities, facilitating text messaging, and even supporting multimedia services. WSRs, as integral elements of the DRN infrastructure, receive data packets from diverse sources and subsequently relay them to a local server situated within a Mobile Rescue Office (MRO). These WSRs collaborate to create an Ad hoc network, enabling them to collectively transport data packets to their intended destinations.

Consequently, an efficient Ad hoc routing protocol is required to manage this intricate network, as depicted in **Figure 1(a)**.

Furthermore, within the Ad hoc network, each WSR functions as a router, enabling the forwarding of traffic originating from other WSRs towards their respective destinations. The adoption of Ad hoc networking to enhance the reliability of DRN systems offers substantial advantages over conventional wireless and wired methods. Ad hoc networks establish connections among nodes without relying on centralized infrastructure or administrative oversight, resulting in significantly reduced ownership, installation, and maintenance costs in comparison to other networking approaches.

To meet power supply requirements, WSRs are typically situated in proximity to wired electricity sources. However, this localized placement limits the coverage area of the proposed DRN infrastructure and, consequently, the reach of its services. To overcome this constraint, we suggest the implementation of self-powered WSRs. In this context, we propose that WSRs harness and store the energy they require from the surrounding environment, with a particular emphasis on solar energy, as illustrated in **Figure 1(b)**. This innovative approach enables the deployment of WSRs in virtually any location, independent of power supply availability, thereby extending the coverage area of the DRN infrastructure to a considerable extent.

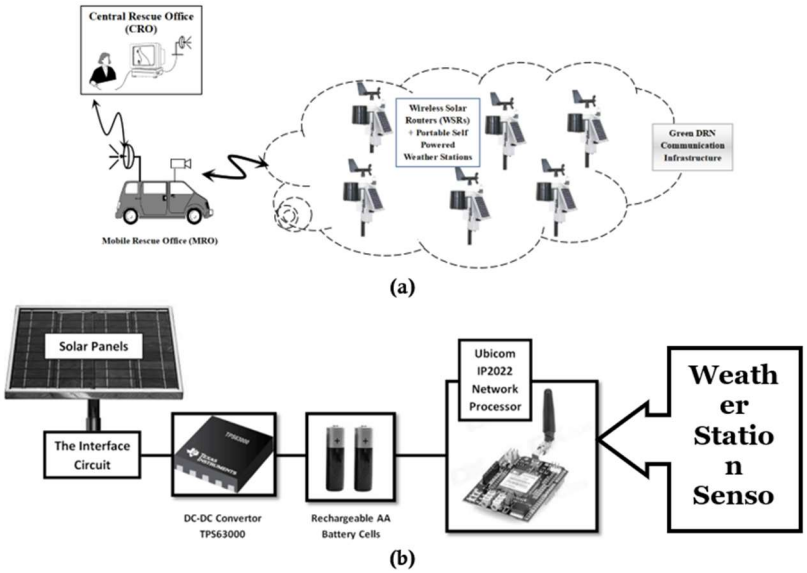

Figure 1. Self-powered DRN infrastructure. **(a)** DRN topology. **(b)** WSR architecture.

Traditional environmental monitoring systems often rely on centralized infrastructure and wired connections, making them vulnerable to disruption during disasters. This can lead to blind spots in data collection and hinder timely responses to environmental threats.

Self-powered DRNs, on the other hand, offer several advantages in disaster scenarios:

- Resilience: DRNs are designed to operate independently of the power grid and traditional communication infrastructure. They use solar panels, wind turbines, or other renewable energy sources to power themselves and communicate wirelessly. This makes them highly resilient to power outages and disruptions caused by natural disasters.
- Real-time data collection: DRNs can be equipped with a variety of sensors to monitor air quality, water quality, radiation levels, and other environmental parameters. These sensors can collect data in real-time, even in remote areas affected by disasters.

- Early warning and rapid response: By providing real-time data on environmental threats, DRNs can enable authorities to issue early warnings and take rapid response measures to protect people and property. For example, if a DRN detects a sudden spike in air pollution levels caused by a chemical spill, authorities can evacuate nearby residents and deploy emergency response teams.
- Improved disaster preparedness: DRNs can be used to collect data on environmental conditions before, during, and after disasters. This data can be used to improve disaster preparedness planning and response efforts. For example, data on floodplains and landslide zones can be used to identify areas at risk and develop evacuation plans.

Here are some specific examples of how self-powered DRNs can be used in disaster scenarios:

- Monitoring air quality after a wildfire: DRNs can be deployed in areas affected by wildfires to monitor air quality levels and provide real-time data to firefighters and residents. This data can be used to determine when it is safe for people to return home and to track the spread of smoke and other pollutants.
- Monitoring water quality after a flood: DRNs can be used to monitor water quality in rivers and streams after a flood to ensure that the water is safe to drink. This data can help prevent the spread of waterborne diseases.
- Monitoring radiation levels after a nuclear accident: DRNs can be used to monitor radiation levels in areas affected by a nuclear accident. This data can help protect people from exposure to radiation.

Overall, integrating self-powered DRNs with environmental monitoring can significantly improve the ability to respond to environmental threats in disaster scenarios. This can lead to a safer and more resilient system.

3. Sustainable power management

Our paper introduces a cutting-edge power management system, the "Duty Cycle Estimation (DCE)—Event Driven Duty Cycling (EDDC)" technique, to efficiently harness solar energy and sustain network operations. This section provides a comprehensive explanation of this technique, emphasizing its role in green communication infrastructure.

In this study, we have opted for the versatile UBICOM IP2022 platform[16] to realize our envisioned Wireless Solar Router (WSR) due to its multifunctional capabilities. As integral members of the Disaster Recovery Network (DRN) infrastructure, WSRs encounter varying network traffic conditions, significantly affecting their power consumption and operational lifespan. Our primary objective in this research is to provide an alternative power source for WSRs and implement an energy management strategy that optimally governs the utilization of energy stored in the WSRs' battery cells.

To fulfill the first goal, we introduce a solar energy harvesting module, as illustrated in **Figure 1(b)**. At the core of this module lies the harvesting circuit, responsible for harvesting energy from the solar panels, managing energy storage, and directing power to the intended system. In our setup, we employ a DC-DC converter, specifically the Texas Instruments TPS63000 low-power boost-buck DC-DC converter[16], to ensure a consistent supply voltage to the embedded system.

Concurrently, we introduce a novel duty cycling methodology aimed at efficiently controlling power consumption within the WSR circuitry. Duty cycling involves the periodic transition of embedded nodes between energy-intensive states (active) and low-energy states (sleep) with the intention of conserving energy[17]. During active states, nodes can perform their regular functions, whereas in low-energy states, nodes limit their operations to specific tasks to save energy[17]. We refer to this methodology as "Duty

Cycle Estimation (DCE)—Event Driven Duty Cycling (EDDC)," which consists of two key components: dynamic duty cycle estimation and the management of WSR behavior during active periods.

Duty Cycle Estimation (DCE) Algorithm: Within the scope of this paper, we propose that WSRs should adjust their operations based on the available energy, specifically linking the service rate of the WSR to its power budget. In this algorithm, sleep periods are dynamically determined each day, taking various factors into account, including WSR power consumption, weather conditions, and the amount of stored energy. To achieve this, we establish a relationship among Duty Cycling periods, Average Service Rate (ASR), and Available Energy (AE). The key terms in this context include:

- Average Service Rate (ASR): This represents the average of the total traffic (in bps) transmitted and received by the WSR.
- Duty cycling periods: Time is divided into time slots, making Duty Cycle the ratio of sleep periods to the total slot time.
- Available energy (AE): This encompasses the sum of residual energy in the batteries from the previous day plus the anticipated energy for the next day.

Our approach follows the steps illustrated in **Figure 2(a)**. Each time slot is divided into active and sleep periods, with a WSR initially entering the sleep period for a predetermined duration calculated in accordance with AE. When the active period commences, the WSR awakens and processes the stored packets in the WLAN NIC, as depicted in **Figure 2(a)**. At the commencement of each working day, the nodes compute the pre-specified Accumulated Energy (AE). It is imperative to underscore that, throughout the entire workday, the nodes must continuously gauge the current flowing to and from the batteries to facilitate the computation of the Remaining Energy (RE). The measurement procedure involves capturing samples every second, with subsequent computation of average current values on an hourly basis. To enhance forecasting precision, we advocate for the CRO to disseminate weather forecasts and the effective charging period for the region, providing critical inputs for determining the Expected Energy (EE). This forecast encompasses anticipated weather conditions (sunny, cloudy, or rainy) and the approximate charging hours available. Leveraging historically recorded current values under analogous weather conditions, the nodes predict the expected current value. Consequently, the Energy Efficiency (EE) is derived, with nodes storing the average current values for each day categorized by climate conditions (sunny, cloudy, or rainy) in a local database file. Subsequently, the Average Energy (AE) for each weather condition is computed. The subsequent step involves calculating the State of Readiness (SR) of each node based on the determined AE value. The correlation between SR and AE is established by evaluating the power consumed during node activities. Mapping the SR value to varied rates of the applied load constitutes the subsequent stage, necessitating adaptability to fluctuations in the network load. This mapping stage is crucial for accommodating changes in the Service Rate (SR) for medium-load conditions. Anticipating future load based on past behavior is integral to this stage, ensuring responsiveness to variations in network load. The final stage entails determining the Sleep Period (SP) allocated to each time slot. Employing the same mapping process previously discussed, the nodes calculate varying SP values in tandem with fluctuations in the applied network load. This comprehensive process aligns the nodes' energy management with dynamic forecasting, load mapping, and responsiveness to real-world conditions, fostering an efficient and adaptive energy utilization system.

Event Driven Duty Cycling (EDDC): Within our paper, we propose that WSR behavior during active periods is governed by two factors: scheduled tasks and responses to packet reception events targeting specific WSRs. The suggested Event Driven Duty Cycling (EDDC) technique leverages a critical feature known as "Clock Stop Mode". In this mode, the system clock may be disabled,

deactivating the CPU core clock and, consequently, the WSR's motherboard. While the system clock is disabled, the interrupt logic continues to function, and a sleep timer remains active. Transitioning from the clock stop mode (sleep mode) to normal execution is feasible through sleep timer interrupts or in response to an external interrupt from the WLAN NIC. Importantly, this method doesn't reset the chip, allowing program execution to resume from where it was paused. This mode shifts only the WSR motherboard to a power-saving mode, turning off its circuitry (except the external interrupt circuits, sleep timer, and program memory). Whenever an interrupt is triggered, such as packet reception by the WLAN NIC or the expiration of the sleep timer, the board promptly awakens within a few clock cycles to execute the necessary actions, as depicted in **Figure 2(b)**.

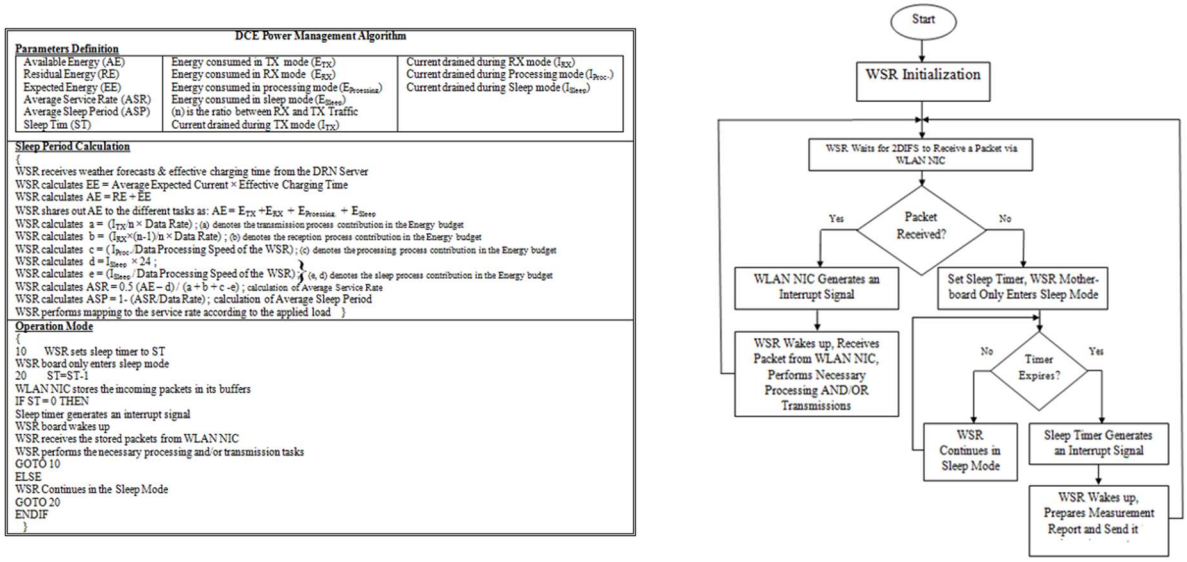

(a) **(b)**

Figure 2. DCE-EDDC algorithm. **(a)** DCE algorithm. **(b)** Flowchart of EDDC algorithm.

4. Evaluation and experimentation

To validate the proposed infrastructure, we suggest an experimental platform for thorough evaluation. This section outlines the metrics used to assess network performance, practicality, power consumption, and its resilience in the face of various failure events.

To fulfill the networking and energy-saving prerequisites of the proposed DRN, it is viable to deploy the suggested power management and other algorithms on platforms equipped with specific features[19,20]. These features include: 1) fast wake-up time from sleep to active mode (less than 10 clock cycles); 2) clock stop mode; 3) data saving during the clock stop mode; 4) low power consumption (below 15 mA during sleep mode); 5) sufficient networking and processing capabilities (exceeding 18 Mbps) to meet DRN application demands[19]; 6) support for a wide range of applications and networking protocols in the TCP/IP stack; 7) open-source development and programming environment; 8) reasonable cost. Based on these criteria, the recommended Ubicom IP2022 platforms for the integrated "weather station-WSR".

To assess the power consumption of the proposed Ubicom Wireless Solar Router (WSR) under real-world Disaster Recovery Network (DRN) traffic scenarios, we propose an experimental framework, as illustrated in **Figure 3**. This framework entails the generation of diverse DRN traffic profiles, which are then input into a simulation model. This model serves as a representative depiction of a DRN infrastructure and aids in creating the necessary network traffic. Subsequently, a traffic generator PC utilizes this network traffic to simulate the behavior of the DRN in interaction with a WSR.

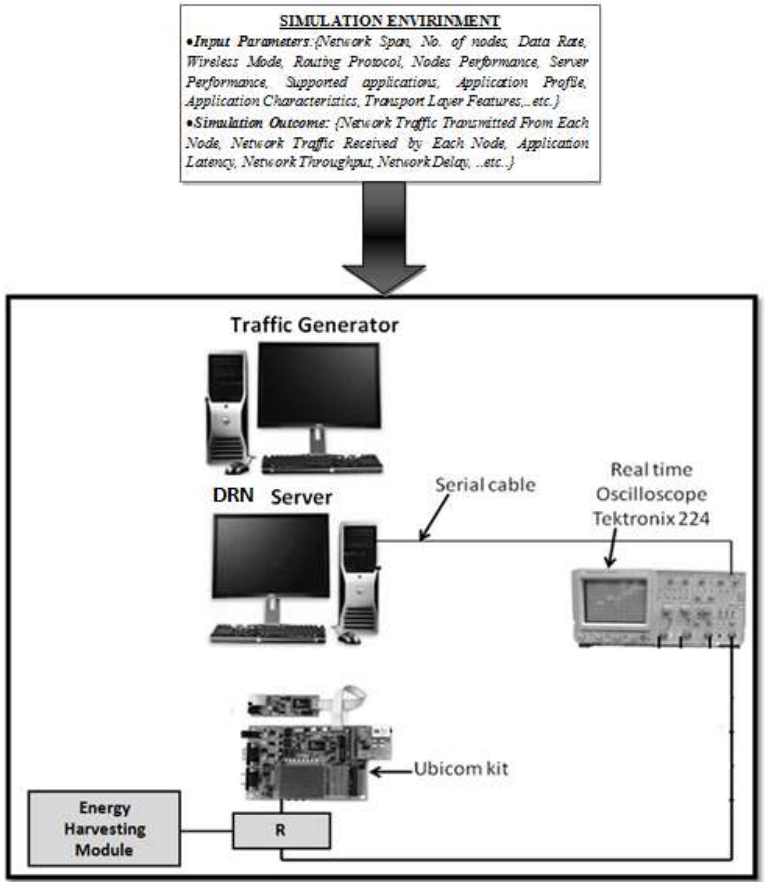

Figure 3. The experimental framework.

The initial step involves the selection of a real-world map for the installation of Wireless Solar Routers (WSRs). This map serves as a representation of a Disaster Recovery Network (DRN) infrastructure, covering an area of 5 × 5 square km and accommodating 40 WSRs[16]. Based on a prior analysis[16], it was determined that Optimized Link State Routing (OLSR) outperforms other Ad hoc routing protocols in a dynamic Ad hoc topology, making it the protocol of choice for our simulation model. The OLSR protocol's functionalities are governed by a predefined set of parameters specified in OLSR RFC 3626[16], which we incorporated into our simulation model, as outlined in **Table 1**. To evaluate the performance of our simulated network, various environmental monitoring services were introduced[2], as detailed in **Table 1**.

Table 1. Simulation model parameters.

Simulation time (min)	60
No. of WSR nodes	40
Network span area (km^2)	25
WSR modeling parameters	Packets processing rate (packet/s) = 2000 Memory = 2 M byte
WLAN settings	Data rate (Mbps): 18 for IEEE802.11a
OLSR settings	Hello interval (s) = 2 TC interval (s) = 5 Neighbor hold time (s) = 6 Topology hold time (s) = 15 Duplicate message hold time (s) = 30

Table 1. (*Continued*).

Weather station applications	**Weather sensors**	3 sensors/station Sensors to WSR packet length = (128–512) bit Sensors to WSR packets rate = (20–1000) packet/s
	Text messaging	Message inter-arrival time = 10 s Message size = (200 – 1000) byte [uniformly distributed]
	Environmental file transfer	1024 × 768 pixels (JPEG compression) File size = (0.5–1) M byte Inter-request interval = 180 s [poisson distribution]
	Multimedia streaming	352 × 288 @ 15 fps 197–421 Kb/s H.264/AVC

In our forthcoming experiments, we intend to measure two key parameters:

- Current consumption in normal mode: In this mode, the Ubicom board, along with its associated accessories, operates without any power management strategies in place.
- Current consumption in sleep mode: In this mode, the power consumption of the Ubicom board and its accessories adheres to the DCE-EDDC power management scheme.

To demonstrate the advantages of implementing the suggested duty cycling methods, we plan to conduct a series of tests utilizing the proposed experimental test bed, as depicted in **Figure 3**.

We will assess the impact of the DCE algorithm in various scenarios, with initial settings detailed in **Table 2**. These experiments aim to evaluate the DCE algorithm's adaptability under diverse operational conditions, considering variations in Available Energy (AE) levels. **Table 3** lists the corresponding values of Average Service Rate (ASR) and Average Sleep Period (ASP) from these scenarios, with Residual Energy (RE) representing battery charging levels and (N) indicating the number of paralleled solar panels. Notably, the proposed DCE algorithm exhibits the ability to dynamically adjust duty cycling based on available energy levels, ensuring that the WSR continues to operate in a pre-planned and managed manner.

Table 2. Initial settings of DCE experiments.

Data rate	18 Mbps (IEEE802.11a)
Traffic characteristics	n = $(\frac{RX\ Traffic}{TX\ Traffic})$= 4
Data processing speed of the WSR	24 Mbps
I_{TX}	150 mA
I_{RX}	120 mA
$I_{Proc.}$	150 mA
I_{Sleep}	1 mA
Battery characteristics	3 v, 2800 mAh
Solar panel	SP1
Average current produced in a sunny day, effective charging time	34 mA 15 h
Average current produced on a cloudy day, effective charging time	20.5 mA 13 h
Average current produced in a rainy day, effective charging time	14.4 mA 11 h

Table 3. ASR and ASP values under different conditions.

RE (% of battery capacity)	N	Weather condition	AE (mAh)	ASR (Mbps)	ASP (s)
100%	1	Sunny	4960	7.75	0.57
100%	1	Cloudy	3801	5.94	0.67
100%	1	Rainy	3482	5.44	0.70
75%	1	Sunny	4260	6.66	0.63
75%	1	Cloudy	3101	4.85	0.73
75%	1	Rainy	2782	4.35	0.76
50%	1	Sunny	3560	5.56	0.69
50%	1	Cloudy	2401	3.75	0.79
50%	1	Rainy	2082	3.25	0.82
25%	1	Sunny	2860	4.47	0.75
25%	1	Cloudy	1701	2.66	0.85
25%	1	Rainy	1382	2.16	0.88
100%	2	Sunny	7120	11.13	0.38
100%	2	Cloudy	4802	7.50	0.58
100%	2	Rainy	4164	6.51	0.64
75%	2	Sunny	6420	10.03	0.44
75%	2	Cloudy	4102	6.41	0.64
75%	2	Rainy	3464	5.41	0.70
50%	2	Sunny	5720	8.94	0.50
50%	2	Cloudy	3402	5.32	0.70
50%	2	Rainy	2764	4.32	0.76
25%	2	Sunny	5020	7.84	0.56
25%	2	Cloudy	2702	4.22	0.77
25%	2	Rainy	2064	3.23	0.82

Furthermore, we aim to assess the efficacy of the suggested DCE-EDDC power management method in defending against unmanaged network traffic conditions, such as those stemming from an Energy Exhaustive Denial of Service (DoS) Attack[15]. Various network traffic rates will be directed at the WSR, both with and without the implementation of the proposed power management method. **Figure 4** will provide insights into how well the properly managed WSR sustains its battery life, irrespective of fluctuations in incoming traffic rates. In contrast, the unmanaged power consumption resulting from varying traffic rates significantly diminishes the battery life of the WSR.

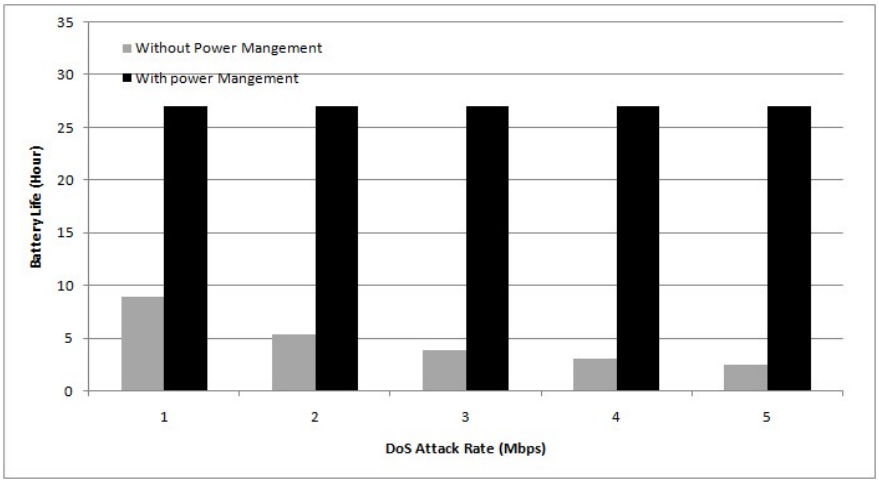

Figure 4. WSR battery life according to different DoS attack rates.

To complete our design process, it is crucial to estimate the requisite number of solar panels arranged in parallel, determine the quantity of parallel AA battery pairs, and ascertain their capacities to fulfill the power requirements of the WSR. Our analysis begins by adopting a realistic approach to assessing power needs under demanding conditions:

This study concentrates on three panels of monocrystalline solar cells sharing the same technology but differing in dimensions, resulting in varying values of voltage, current, power, and, consequently, distinct power-generating capabilities (refer to **Table 4**). **Table 5** provides details on various tests conducted at different times of the year in Mosul city/Iraq[13]. Key observations from these experiments reveal that the electrical current generated by the solar cell panels primarily depends on the characteristics of the solar cells, prevailing weather conditions, and the daytime period (effective charging time). The Maximum Operation Period (MOP) without charging battery cells extends to 14 h per day, representing the longest night period. In contrast, the least average charging current is obtained during rainy days, with a minimum day period of 10 h. These findings form the basis of our planning procedure.

Table 4. Solar panels characteristics.

Solar panel class	Dimensions, (height (cm) × width (cm))	Mean voltage (v)	Mean current (mA)	Rated power (w)
Solar panel 1 (SP1)	17 × 10	4	100	0.4
Solar panel 2 (SP2)	23 × 15	4	220	1
Solar panel 3 (SP3)	36 × 29	4	360	1.5

Table 5. Solar panel testing.

Daily average current produced by solar panel 1 (SP1) in Mosul City/Iraq			Daily average current produced by solar panel 2 (SP2) in Mosul City/Iraq			Daily average current produced by solar panel 3 (SP3) in Mosul City/Iraq		
Sunny (summer)	**Cloudy (winter)**	**Rainy (winter)**	**Sunny (summer)**	**Cloudy (winter)**	**Rainy (winter)**	**Sunny (summer)**	**Cloudy (winter)**	**Rainy (winter)**
34 mA	20.5 mA	14.4 mA	70 mA	40 mA	30 mA	144 mA	77 mA	62 mA

To calculate the battery capacity, we employ the following relationship:

$$BC = I_{WSR}. MOP \quad (1)$$

here, BC represents the battery capacity (in mAh), I_{WSR} is the current drained by an WSR, and MOP is the Maximum Operation Period of an WSR.

To determine the required number of paralleled solar panels, we need to establish their duties in generating the necessary current to supply the WSR for the shortest day period while simultaneously charging the batteries. This is calculated using the Equation (2) below:

$$\text{No. of Parallel Solar Panels} = SP_{WSR} + SP_{BC} \quad (2)$$

where SP_{WSR} is the number of solar panels required to power the WSR, expressed as:

$$SPWSR = \left(\frac{\text{Current Drained by the WSR}}{\text{Current Produced by a Single Solar Panel}}\right) \quad (3)$$

On the other hand, SP_{BC} is the number of solar panels needed to energize the battery cells, expressed as:

$$SPBC = \left(\frac{\text{Battery Capacity}}{\text{Minimum Day Period} \,.\, \text{Current Produced by a Single Solar Panel}}\right) \quad (4)$$

Table 6 highlights that the WSR, when operating in sleep mode, demands a significantly lower number of paralleled solar panels and a reduced battery capacity to support multiple weather station applications. These findings underscore the effectiveness of the proposed power management scheme in extending the lifespan of solar energy-harvested battery-based roadside units, enhancing their reliability and availability, which positively impacts the construction of a dependable DRN infrastructure.

Table 6. Solar panels and battery cells required for various conditions.

Average (daily) network load %	Normal mode					Sleep mode				
	No. of parallel solar cells			Battery capacity (mAh)		No. of parallel solar cells			Battery capacity(mAh)	
	SP1	SP2	SP3	Calculated	Standard	SP1	SP2	SP3	Calculated	Standard
25%	18	9	4	1540	1600	2	1	1	182	200
50%	19	9	5	1624	1800	3	2	1	252	300
75%	21	10	5	1792	1800	5	2	1	371	400
100%	24	12	6	2058	2300	8	4	2	677	750

Next, we will assess the performance of the proposed power management technique in comparison to traditional duty cycling methods, namely Fixed Duty Cycling (FDC)[18] and Artificial Neural Network-based Adaptive Duty Cycling (ANN-ADC)[17]. The evaluation of these methods is based on the following metrics:

- Missed events percentage (ME%): This metric quantifies the percentage of received data lost due to improper sleeping states.
- False wakeup percentage (FW%): Defined as the percentage of slot time spent in the wakeup state without performing any action, indicating unnecessary energy consumption.

The performance of the three duty cycling methods was assessed using the previously mentioned evaluation metrics, as presented in **Table 7**. It is evident that the suggested method exhibits superior performance in terms of data loss and extra power consumption. This enhanced performance is attributed, firstly, to the precise selection of sleep periods based on the timing requirements of scheduled tasks and, secondly, to the fast wakeup mechanism triggered by an external WLAN NIC interrupt, ensuring the reception of all incoming packets without loss. Conversely, the FDC method demonstrates suboptimal performance, with higher energy consumption (indicated by the highest FW% values) and a tendency to lose a higher percentage of received data (indicated by the highest ME% values). The ANN-ADC method displays acceptable performance, which could be further improved through an extensive training procedure. However, it's worth noting that the ANN training is computationally and power-demanding, placing an additional load on platforms with limited resources.

Table 7. Performance of different duty cycling methods.

%AME	%FW	%AME	%FW	%AME	%FW
43%	255%	0%	2.9%	0%	0%

A comparison of the main features between the current work and other DRN solutions is presented in **Table 8**. The suggested system offers a broader array of solutions, encompassing all necessary elements for constructing a dependable and secure DRN infrastructure.

Table 8. Comparison with other DRN solutions.

	Current work	OEMAN[14]	TeamPhone[2]
Network type	Wireless mesh network (WMN)	Multihop access networks	Cellular networks, Ad hoc networks and opportunistic networks
DRN node	Wireless solar router (WSR)	Smart phone, laptop PCs	Smart phone
Power source	Solar energy, battery cells	Battery cells	Battery cells
Routing protocol	OLSR	Simple routing in tree-based topology	AODV, DTN2
Power management	DCE-EDDC	None	Wake-up scheduling
Research methodology	Simulation, experimental work	Experimental work	Experimental work
Supported applications	Text messaging, field measurements, file transfer, multimedia streaming	Internet access	Text messaging

Finally, **Table 9** compiles the statistical findings derived from a range of experiments, taking into consideration the influence of the proposed power management techniques and the DRN clustering algorithm. The data presented in **Table 7** underscores the substantial reduction in the number of paralleled solar panels and the decreased battery capacity required for WSRs when operating in sleep mode to support multiple environmental monitoring applications. These results underscore the remarkable effectiveness of the suggested power management scheme in extending the lifespan of solar energy-harvested battery-based WSRs and enhancing their reliability, ultimately contributing positively to the establishment of a dependable and available Disaster Recovery Network (DRN) infrastructure. Additionally, the network's performance, installation time, and cost have all met the stipulated requirements within the acceptable range for DRN operations[10–12].

Table 9. Evaluation metrics of green environmental monitoring DRN infrastructure.

Network type		**Wireless mesh network (WMN)**
Ad hoc routing protocol		Optimized link state routing (OLSR)
WSR node		Ubicom IP2022 network processor platform, 120 MHZ CPU, 2 Mbyte memory
Wi Fi standard		IEEE802.11a, 18 MHZ
WSR transmit power (W)		25 dBm
Antenna type		Omni antenna 2.4 GHz/5 GHz dual band Gain: 1.5 dBi (2.4 GHZ)/4.5 dBi (5 GHZ)
WSR radial transmit range (m)		300
Average installation time/WSR		30 min
Estimated Cost/WSR		$150
Quality of service (QoS) support		Yes
Remote WSR management		Yes, via simple network management protocol (SNMP)
Network performance	Average network access delay (s)	0.00169
	Average file transfer latency (s)	6
	Average video streaming latency (s)	0.5
Requirements of solar system	Solar panel dimensions (height (cm)×width (cm))	36 × 29
	Mean voltage (v)	4
	Mean current (mA)	360
Requirements of solar system	Rated power (w)	1.5
	No. of paralleled solar panels required [normal mode]	6
	No. of paralleled solar panels required [sleep mode]	2
	Battery capacity (mAh) [normal mode]	2300
	Battery capacity (mAh) [sleep mode]	750
Power consumption analysis	Average drained current (mA) [normal mode]	150
	Average drained current (mA) [sleep mode]	70
	Battery life (h)/normal mode [2800 mAh battery cells]	15
	Battery life (h)/sleep mode [2800 mAh battery cells]	29

5. Conclusion

This paper introduces an effective approach to deploying a self-powered and dependable Disaster Recovery Network (DRN) infrastructure designed to support various environmental monitoring applications. Our work distinguishes itself through an innovative energy conversion and storage strategy, incorporating self-powered WSRs, environmental energy harvesting, and the integration of weather monitoring services. These elements collectively contribute to a more sustainable, resilient, and mobile Disaster Recovery Network infrastructure compared to other works in the field. The paper explores a range of methodologies and algorithms to facilitate the realization of such an infrastructure. Several valuable insights can be gleaned from this study. Foremost, the pivotal determinant for the successful execution of an "energy harvesting-battery-based" embedded system is the intelligent power management algorithm's capacity to adapt to diverse DRN operational scenarios. The adoption of the suggested "Duty Cycle Estimation (DCE)—Event-Driven Duty Cycling (EDDC)" method offers numerous advantages, including simplified implementation, optimized utilization of energy resources, and heightened network performance. Notably, this approach also bears substantial economic benefits, requiring fewer solar panels and a suitable battery capacity. Furthermore, it's imperative for management strategies to strike a balance between a highly reliable and a well-performing system, considering the embedded nature of a Wireless Solar Router (WSR). Additionally, the network's performance, installation time, and cost have all met the stipulated requirements within the acceptable range for DRN operations. To the best of our knowledge, the integration of these disaster recovery algorithms and techniques with a solar energy-powered system represents a novel and unexplored frontier in prior research endeavors. This innovative combination holds the promise of advancing the fields of disaster recovery and environmental monitoring, offering enhanced reliability and performance while also addressing sustainability and economic considerations.

Author contributions

Conceptualization, QIA and NAI; methodology, QIA; software, QIA; validation, QIA and NAI; formal analysis, QIA; investigation, QIA; resources, QIA; data curation, QIA and NAI; writing—original draft preparation, QIA and NAI; writing—review and editing, QIA; visualization, QIA; supervision, QIA; project administration, QIA; All authors have read and agreed to the published version of the manuscript.

Conflict of interest

The authors declare no conflict of interest.

References

1. Qian G, Wei F. Summary of global earthquake disasters in 2020. Earthquake Research Advances. 2021, 51: 289-296.
2. Zeng Y, Zhang R, Lim TJ. Throughput Maximization for UAV-Enabled Mobile Relaying Systems. IEEE Transactions on Communications. 2016, 64(12): 4983-4996. doi: 10.1109/tcomm.2016.2611512
3. Heleno S, Fernandes CA, Felício JM, et al. Development of TETRA Radio Backhaul Network Redundancy Plan for Disaster Recovery in Mission Critical Communications. In: Proceedings of the 2023 17th European Conference on Antennas and Propagation (EuCAP); 26-31 March 2023; Firenze, Italy. doi: 10.23919/eucap57121.2023.10133791
4. Macrì D, Gentile AF. Avoiding Information Disorder in Disaster Recovery Through Internet of Things. In: Proceedings of the 2023 IEEE International Conference on Web Intelligence and Intelligent Agent Technology (WI-IAT). 26-29 October 2023; Venice, Italy. doi: 10.1109/wi-iat59888.2023.00077
5. Wu Q, Zeng Y, Zhang R. Joint Trajectory and Communication Design for Multi-UAV Enabled Wireless Networks. IEEE Transactions on Wireless Communications. 2018, 17(3): 2109-2121. doi:

10.1109/twc.2017.2789293
6. Yang D, Wu Q, Zeng Y, et al. Energy Tradeoff in Ground-to-UAV Communication via Trajectory Design. IEEE Transactions on Vehicular Technology. 2018, 67(7): 6721-6726. doi: 10.1109/tvt.2018.2816244
7. Chakraborty S, Park J, Saraswat G, et al. Emergency Power Supply System for Critical Infrastructures: Design and Large Scale Hardware Demonstration. IEEE Access. 2023, 11: 114509-114526. doi: 10.1109/access.2023.3325198
8. Xu J, Zeng Y, Zhang R. UAV-Enabled Wireless Power Transfer: Trajectory Design and Energy Optimization. IEEE Transactions on Wireless Communications. 2018, 17(8): 5092-5106. doi: 10.1109/twc.2018.2838134
9. Quy VK, Ban NT, Van Anh D, et al. An Adaptive Gateway Selection Mechanism for MANET-IoT Applications in 5G Networks. IEEE Sensors Journal. 2023, 23(19): 23704-23712. doi: 10.1109/jsen.2023.3307617
10. Ijaz H, Ahmad R, Ahmed R, et al. A UAV-Assisted Edge Framework for Real-Time Disaster Management. IEEE Transactions on Geoscience and Remote Sensing. 2023, 61: 1-13. doi: 10.1109/tgrs.2023.3306151
11. Wei J, Gao X, Cheng P, et al. Coordinated Post-Disaster Recovery and Assessment Method for Integrated Electricity-Gas-Transportation System. IEEE Access. 2023, 11: 11685-11699. doi: 10.1109/access.2023.3242130
12. Christy E, Astuti RP, Syihabuddin B, et al. Optimum UAV flying path for Device-to-Device communications in disaster area. In: Proceedings of the 2017 International Conference on Signals and Systems (ICSigSys); 16-18 May 2017; Bali, Indonesia.
13. Tran Minh Q, Nguyen K, Borcea C, Yamada S. On-the-Fly Establishment of Multihop Wireless Access Networks for Disaster Recovery. IEEE Communications Magazine. 2014, 52(10): 60-66. doi: 10.1109/MCOM.2014.6917403
14. Sun X, Chen J, Zhao H, et al. Sequential Disaster Recovery Strategy for Resilient Distribution Network Based on Cyber–Physical Collaborative Optimization. IEEE Transactions on Smart Grid. 2023, 14(2): 1173-1187. doi: 10.1109/tsg.2022.3198696
15. Ali IQ. Security Issues of Solar Energy Harvesting Road Side Unit (RSU). Iraqi Journal for Electrical and Electronic Engineering. 2015, 11(1): 18-31. doi: 10.33762/eeej.2015.102711
16. Ali IQ. Enhanced power management scheme for embedded road side units. IET Computers & Digital Techniques. Available online: www.ietdl.org (accessed on 12 November 2023).
17. Ali IQ. Solar Powered SCADA Infrastructure Serving Different Smart Grid Applications. JJEE Journal. 2016, 2(1).
18. Qaddoori S, Ali Q. An Efficient Security Model for Industrial Internet of Things (IIoT) System Based on Machine Learning Principles. Al-Rafidain Engineering Journal (AREJ). 2023, 28(1): 329-340. doi: 10.33899/rengj.2022.134932.1191
19. Alsharbaty F, Ali Q. An Enhanced Industrial Wireless Communication Network for Hard Real Time Performance Substation Automation Purposes. Al-Rafidain Engineering Journal (AREJ). 2022, 27(2): 216-226. doi: 10.33899/rengj.2022.133860.1173
20. Yasser S, M. Abdul-Jabbar DrJ, Ali Q. Design and Performance Evaluation of Lattice Daubechies Wavelet Filter Banks for Less Complex Cognitive Transceivers. Al-Rafidain Engineering Journal (AREJ). 2020, 25(1): 61-69. doi: 10.33899/rengj.2020.126799.1021

Energy Storage and Conversion 2023; 1(1): 275.
Review Article

Research progress on hydroxide fluoride-based electrode materials for supercapacitors

Zijin Xu, Zeshuo Meng*

Key Laboratory of Automobile Materials of MOE, School of Materials Science and Engineering, Jilin University, Changchun 130012, Jilin Province, China

*** Corresponding author:** Zeshuo Meng, mengzs21@jlu.edu.cn

ARTICLE INFO

Received: 23 October 2023
Accepted: 7 December 2023
Available online: 16 December 2023

doi: 10.59400/esc.v1i1.275

ABSTRACT: Supercapacitors have attracted much attention due to their high-power density and long cycle life, making them a potential substitute for traditional batteries. Research on hydroxide fluorides as electrode materials for supercapacitors has been increasing. Hydroxide fluorides exhibit higher specific capacitance due to the redox reactions between transition metal elements in different oxidation states. However, their high resistance limits their rate performance and cycling stability, which hinders their large-scale application. This article summarizes the main synthesis methods of hydroxide fluorides, and by controlling the reaction conditions, hydroxide fluorides with different morphologies and structures can be obtained to meet various application requirements. In addition, considering the limitations of hydroxide fluorides, this article systematically introduces the main approaches to improving their electrode performance and summarizes the electrochemical characteristics and latest research progress of hydroxide fluorides.

KEYWORDS: supercapacitors; hydroxide fluoride; electrode materials; elemental doping

1. Introduction

As global energy demand continues to grow, the depletion of fossil fuels and the worsening environmental pollution highlight the increasing importance of developing sustainable and renewable energy sources[1–3]. New energy sources such as solar power, wind energy, and tidal energy have been developed as alternatives to traditional fossil fuels. However, these energy sources are intermittent in their availability. To ensure a continuous energy supply, there is an urgent need to develop efficient energy storage devices[4,5]. Supercapacitors have the potential to serve as an alternative electrochemical energy storage technology, replacing widely commercialized rechargeable batteries[3,6,7].

According to energy storage principles, supercapacitors can be divided into three main categories: double-layer capacitors, pseudocapacitors, and hybrid capacitors[8–11]. Double-layer supercapacitors store energy based on the adsorption of ions in the electrolyte onto the positive and negative charges on the electrode surface[12–16]. Pseudocapacitors store energy based on the adsorption resulting from redox reactions between ions in the electrolyte and the electrode material[17–20]. Hybrid capacitors are composed of carbon materials that can form a double layer as the negative electrode and metal oxides/hydroxides, conductive polymers, or traditional battery materials as the positive electrode[21–26]. Compared to double-layer capacitors and pseudocapacitors, hybrid capacitors can meet higher power density and energy density requirements, making them more widely used[27–31]. Supercapacitors possess higher capacitance

compared to conventional electrochemical capacitors, but they have a lower energy density than batteries[32–37]. However, supercapacitors have gained significant research attention due to their favorable characteristics, including excellent cycling stability and lifespan, high power density, wide operating temperature range, relatively lower cost, enhanced safety, and environmental friendliness, when compared to batteries[38,39]. However, the construction of high-performance supercapacitors with both high energy density and high power density remains a challenging task[40]. Therefore, the continuous exploration of high-energy-density materials has been a primary objective in the development of supercapacitors[41–44].

Hydroxide fluorides have been extensively studied as electrode materials for supercapacitors due to their simple and versatile synthesis methods, high specific surface area, high theoretical capacitance, and excellent electronic transport capabilities. However, the high resistance of hydroxide fluorides has limited their widespread application. Therefore, strategies such as doping and compositing have been employed to improve the performance of hydroxide fluorides. Although there have been reports on the use of hydroxide fluorides in energy storage applications such as lithium batteries[45–48] and supercapacitors[49–52], their current performance is not sufficient to support large-scale energy storage applications. There is a wide variety of hydroxide fluorides, and common metal cations found in hydroxide fluorides include Mg, Co, Ni, Cu, Zn, and Cd, among others[53–56]. Metal hydroxide fluorides, due to their simple synthesis routes, controllable morphology, strong oxidation resistance, stability in air, and unique electronic band structures, have been widely applied in the development of new functional materials. Low-dimensional nanostructures can self-assemble to form materials with a high specific surface area and abundant pore structures. Mixed transition metal oxides and their derivatives exhibit reversible valence state transitions during charge and discharge processes, offering advantages of high specific capacitance and structural stability. In particular, mixed transition metal hydroxide fluorides, composed of two individual transition metal hydroxide fluorides, exhibit higher conductivity due to the lower activation energy for electron transfer. The strong synergistic effect also enables them to demonstrate characteristics that are difficult to achieve with single-metal hydroxide fluorides. Therefore, hydroxide fluorides hold promising potential as electrode materials for supercapacitors, capable of meeting the energy storage demands of supercapacitor electrodes[57].

According to the factors influencing the performance of electrode materials for supercapacitors, the performance of hydroxide fluoride electrode materials can be influenced by the following factors: 1) specific surface area; 2) electronic transport capability; 3) conductivity; and 4) unique nanostructures. Different nanostructures, such as nanorods, nanowires, and nanoplate arrays, can result in different performances of hydroxide fluorides. As long as the dispersion is uniform, the electronic transport performance will be better. However, if the distribution is too aggregated or too dispersed, it can lead to a decrease in electrochemical performance. The high specific surface area of hollow nanostructures allows for sufficient contact between the electrode material and the electrolyte, thereby enhancing electrochemical performance. The anisotropy of hydroxide fluorides also contributes to their large specific surface area, exposure to low-energy surfaces, significant size effects, and good electronic transport capability. Rapid electron transfer in electrode materials enhances their conductivity. Moreover, improving the specific surface area by controlling the nanostructure of the electrode can further enhance the performance of supercapacitors, facilitating fast redox reactions and ion/electron transfer at the electrode/electrolyte interface. Activated materials with nanowire structures can provide a higher spectral surface area, accelerating ion diffusion and electron transfer, resulting in higher specific capacitance.

This review provides a comprehensive overview of the synthesis methods of hydroxide fluorides and strategies to enhance their performance as electrode materials for supercapacitors, aiming to facilitate their more effective application. Firstly, the article summarizes the main synthesis methods of hydroxide fluorides, emphasizing the ability to obtain hydroxide fluorides with diverse morphologies and structures by controlling reaction conditions to meet various application requirements. Secondly, addressing the limitations of hydroxide fluorides, the article systematically introduces key methods to improve their electrode performance and summarizes the electrochemical characteristics and latest research progress of hydroxide fluorides. These insights provide a more comprehensive understanding of the potential applications of hydroxide fluorides in fields such as supercapacitors, offering practical guidance and inspiration for related research. This article's exposition enables readers to better grasp the potential applications of hydroxide fluorides in the realm of supercapacitors, providing important references and inspiration for future research (**Figure 1**).

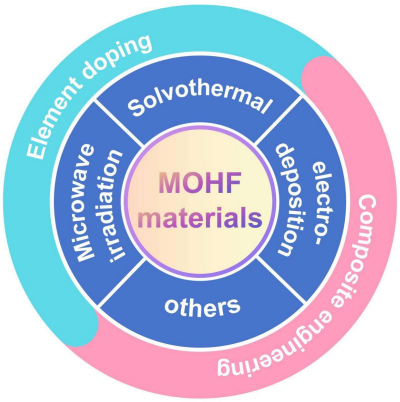

Figure 1. The challenges and strategies for promising hydroxide fluorides as the next-generation energy storage materials.

2. Synthesis strategies of hydroxide fluoride

There are several methods commonly used for the preparation of hydroxide fluorides, including hydrothermal synthesis, solvothermal synthesis, microwave-assisted synthesis, and electrodeposition. These methods are relatively simple and offer flexibility to control reaction conditions for synthesizing materials with different morphologies and properties. Hydrothermal synthesis is a commonly used method for preparing hydroxide fluorides. It involves a reaction in a high-temperature and high-pressure water environment, utilizing water's solubility and thermal stability to facilitate the reaction. In hydrothermal synthesis, fluoride and metal ions are commonly used as reactants, and by reacting at specific temperatures and pressures for a certain period of time, hydroxide fluorides can be obtained. Solvothermal synthesis is another commonly used method for preparing hydroxide fluorides. It utilizes the thermal stability and solubility of organic solvents to facilitate the reaction. In solvothermal synthesis, fluoride and metal salts are dissolved in an organic solvent, and the reaction mixture is heated to induce the reaction. By controlling the temperature and reaction time, hydroxide fluorides can be obtained. Microwave-assisted synthesis is a method developed in recent years for preparing hydroxide fluorides. It utilizes the heating effect of microwaves to rapidly and uniformly heat the reaction system, promoting the reaction. This method offers advantages such as fast reaction rates and low energy consumption, allowing for the synthesis of hydroxide fluorides in a shorter time period. Electrodeposition is a method that utilizes electrochemical principles to prepare hydroxide fluorides. By applying a current in an electrolyte solution, metal ions are reduced to metal at the electrode, simultaneously reacting with fluorides to form hydroxide fluorides. Electrodeposition enables control over the reaction rate and

morphology, allowing for the preparation of materials with different properties at different current densities. In summary, the preparation methods for hydroxide fluorides are relatively simple, and suitable methods can be chosen depending on the specific requirements. By adjusting the reaction conditions, materials with different morphologies and properties can be synthesized. These methods hold broad application prospects in the fields of materials science and chemistry.

2.1. Solvothermal method

Hydrothermal synthesis involves using a water-based solution as the medium and heating the reaction vessel, typically a high-pressure autoclave lined with polytetrafluoroethylene (PTFE), to create a high-temperature and high-pressure environment. This allows for the dissolution and recrystallization of substances that are typically insoluble or difficult to dissolve. The morphology and size of the resulting product can be controlled by adjusting factors such as solvent ratios, pH, temperature, pressure, reaction time, and solvent concentration. In contrast, solvothermal synthesis uses solvents other than water. While water is the solvent in hydrothermal synthesis, some solutes are sensitive to water, necessitating the use of non-aqueous solvents such as methanol or ethanol.

Ni et al.[48] prepared rod-shaped Co(OH)F samples by conducting a 24-hour hydrothermal reaction at 120 °C, utilizing sodium fluoride, hexamethylenetetramine, and cobalt acetate tetrahydrate as raw materials. Excess sodium fluoride in the solution acted as a capping agent, inducing the oriented growth of Co(OH)F. Subsequently, the Co(OH)F was combined with natural graphite, acetylene black, and polyvinylidene fluoride (PVDF). The resulting mixture was coated onto a copper foil to produce a disk electrode. Charge-discharge tests were performed at a current density of 0.1 mA cm^{-2}, as illustrated in **Figure 2(a)**, demonstrating the initial discharge and charge capacities of the Co(OH)F electrode at 847.9 mAh g^{-1} and 546.2 mAh g^{-1}, respectively. The cycling performance of the Co(OH)F electrode, as shown in **Figure 2(b)**, gradually reached a stable value after 50 cycles, maintaining capacities of 332.6 mAh g^{-1} and 329 mAh g^{-1}, respectively.

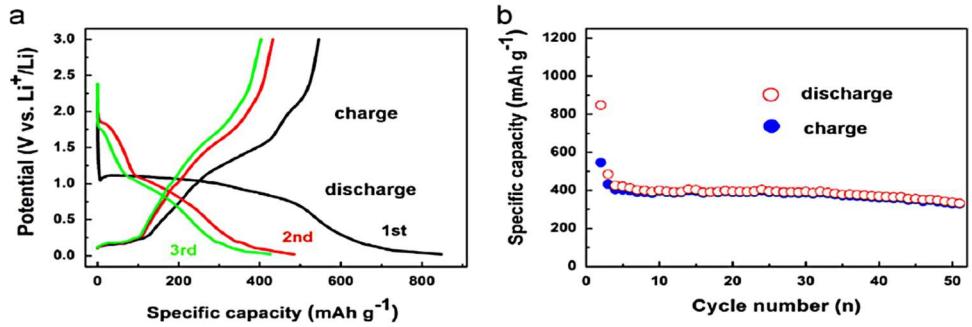

Figure 2. (a) Initial three charge-discharge curves; **(b)** cycle performance of Co(OH)F as anode for Li-ion batteries[48].

Jiang et al.[49] employed $Co(NO_3)_2{\cdot}6H_2O$ and $Zn(NO_3)_2{\cdot}6H_2O$ as starting materials and then introduced ammonium fluoride and urea to form a uniform solution. The homogeneous solution was subsequently subjected to high-pressure autoclave heating at 120 °C for a duration of 10 h, leading to the formation of three-dimensional (3D) lawn-like Co-Zn(OH)F nanoneedle arrays directly on nickel foam. The microscopic structure of the material is depicted in **Figure 3**. The highly active ordered nanoneedles, featuring a tip diameter of approximately 50 nm, contributed to the exceptional specific capacitance of 1970 F g^{-1} at a current density of 1 A g^{-1} achieved by this 3D electrode structure. Additionally, it demonstrated remarkable cycling stability, retaining 105% of its initial capacity after 5000 cycles of cyclic voltammetry testing.

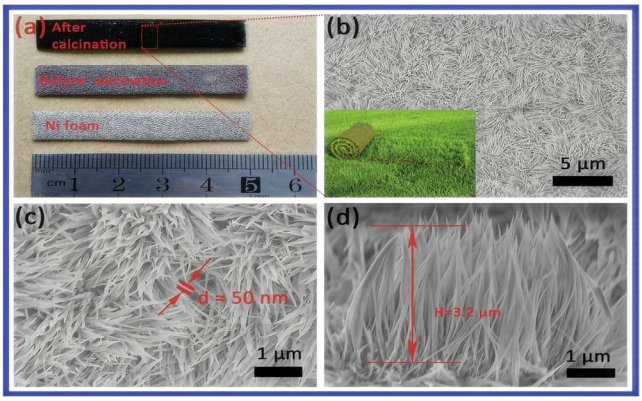

Figure 3. (a) Optical images of Ni foam substrate, Co-Zn(OH)F precursor grown directly on Ni foam and Co-Zn(OH)F nanoneedles on Ni foam. **(b, c)** The high-magnification SEM image of the region highlighted by a red rectangle in **(a)**, the photo of lawn in the inset of **(b)**. **(d)** Cross-section SEM images of Co-Zn(OH)F nanoneedles[49].

Zhang et al.[51] utilized a one-pot solvothermal synthesis approach to create a novel and distinct nickel-cobalt hydroxide fluoride (NiCo-HF) nanowire material. The research explored the impact of varying hydrothermal temperatures on the formation mechanism. Findings suggested that Ni^{2+} tended to form nanospheres, while Co^{2+} favored nanowire formation. With increasing temperature, a greater number of Co^{2+} ions engaged in the reaction, promoting increased nanowire formation. NiCo-HF synthesized at 140 °C exhibited a higher specific surface area compared to NiCo-HF prepared at other temperatures. This, combined with its mesoporous structure, not only accelerated the ion/electron transfer rate, but also provided abundant active sites during electrochemical reactions. The prepared NiCo-HF electrode displayed a high specific capacitance of 3372.6 F g^{-1} and maintained a capacitance retention of 94.3% after 10,000 cycles at a high current density of 200 A g^{-1}. The outstanding electrochemical performance of the electrode can be attributed to the synergistic effects of the nanowire morphology and the complex redox process of the active material.

The solvothermal method has the ability to dissolve a wide range of substances, allowing reactions that are not feasible or are slow under normal conditions to occur or proceed at an accelerated rate. Solvents can control the growth of crystals, and using different solvents can result in products with different shapes. Additionally, this method offers advantages such as low energy consumption, reduced aggregation, and controllable particle shapes. However, a disadvantage of this method is its relatively low yield and insufficient product purity. Moreover, the method may not always yield satisfactory uniformity in terms of the size and morphology of the products.

2.2. Electrochemical deposition method

Electrochemical deposition refers to the technique where positive and negative ions in an electrolyte continuously migrate under the influence of an external electric field and undergo oxidation-reduction reactions to form a coating on the electrode. Electrodeposition is typically conducted at low operating temperatures, often in aqueous solutions, allowing the reactants to retain their individual characteristics and resulting in products with enhanced performance.

Xu et al.[58] documented the electrochemical deposition of rhombic ZnOHF nanorod (NR) arrays in an aqueous electrolyte containing $Zn(NO_3)_2$ and sodium fluoride (NaF). The growth of the ZnOHF NR arrays was facilitated by spin-coating a zinc oxide (ZnO) nanocrystal seed layer on an ITO substrate (**Figure 4**). The study elucidated the electrochemical deposition mechanism of ZnOHF, where the preferential chemical combination of ZnF^+ complexes with the electrogenerated OH^- ions hindered the binding of free Zn^{2+} ions with OH^- ions and the formation of zinc hydroxide ($Zn(OH)_2$). The presence

of fluoride ions effectively interfered with the formation of zinc oxide. Therefore, the process was designated as fluoride ion-mediated ZnOHF electrochemical deposition. Previous reports on the synthesis of ZnOHF samples via dissolution-based synthetic routes did not yield ordered one-dimensional nanostructures. Electrochemical deposition easily achieved this objective in the present study.

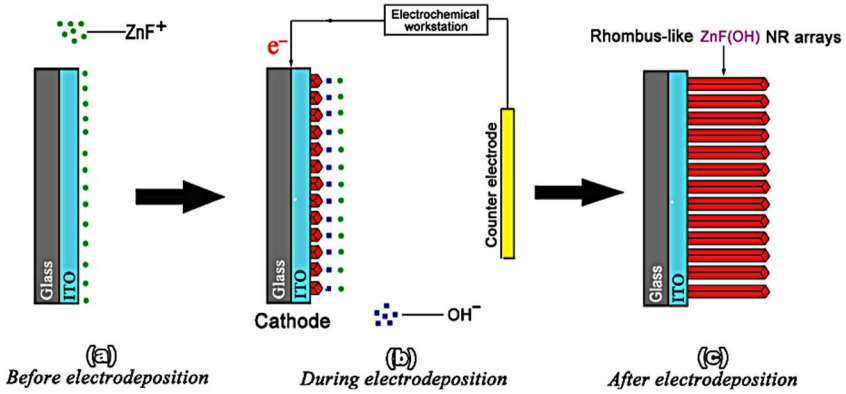

Figure 4. Schematic illustration of the electrodeposition process of the rhombus-like ZnFOH NR arrays on ITO glass substrates[58].

2.3. Microwave irradiation method

The microwave irradiation method involves placing the reactants in a reaction vessel and heating them in a microwave oven (a household microwave oven is sufficient). After complete cooling of the reaction vessel, the product is washed, centrifuged, and dried for subsequent testing.

Zhu et al.[59] initially utilized $Zn(NO_3)_2{\cdot}6H_2O$ as the raw material to synthesize $Zn_5(OH)_8(NO_3)_2{\cdot}2H_2O$, and subsequently produced Zn(OH)F nanorods for utilization in solar cells. The work demonstrated the capability of the unique microwave irradiation strategy for constructing nanostructured hydroxide fluorides. Song et al.[60] employed the ionic liquid 1-butyl-3-methylimidazolium tetrafluoroborate ([Bmim]BF_4) as both the reactant and template to synthesize novel flower-like Zn(OH)F through a simple and rapid microwave-assisted approach. In this study, Zn(OH)F also acted as a precursor for the creation of porous ZnO nanostructures. The introduction of the ionic liquid and microwave irradiation played vital roles in shaping the unique structure of Zn(OH)F. Microwave irradiation notably reduced the heating time and enhanced heating efficiency. Ionic liquids, comprising inorganic anions and organic cations, possess high polarization and conductivity. Their ionic nature makes them exceptional solvents for absorbing microwave radiation. Farshad Barzegar et al.[61] examined the influence of microwave irradiation on the performance of carbon-based electrode supercapacitors. The results showed significant changes in the specific surface area of the materials, leading to increased storage capacity of the electrode materials. By enhancing the active surface area during microwave irradiation, the specific capacitance also exhibited stability compared to before irradiation.

2.4. Other methods

Peng et al.[62]. synthesized ZnOHF using a method without any additives in their study titled "Synthesis, characterization, and photocatalytic activity of Zn(OH)F hierarchical nanofibers prepared by a simple solution-based method." Shahzad Ahmad et al.[63] used a simple and environmentally friendly method to synthesize zinc hydroxide fluoride (Zn(OH)F) by hydrolyzing $KZnF_3$, a single-source precursor, with potassium iodate at 120 ℃ in their work. The process was harmless, straightforward, and scalable. Lemoine et al.[64]. reported the synthesis and electrochemical properties of open-framework

iron hydroxyfluorides prepared by the thermal decomposition of $Fe^{2+}Fe^{3+}F_5(H_2O)_2$ and $Fe^{2+}Fe^{3+}2F_8(H_2O)_2$ under ambient air in their study titled "Synthesis by Thermal Decomposition of Two Iron Hydroxyfluorides: Structural Effects of Li Insertion." The combination of thermogravimetric analysis, X-ray thermal diffraction (XRD), and infrared spectroscopy confirmed the rapid conversion of the two unstable porous oxyfluorides into hydroxyfluorides in ambient air, resulting in $Fe^{3+}F_{2.5}(OH)_{0.5}$ and HTB-structured $Fe^{3+}F_{2.66}(OH)_{0.34}$. In the case of defluoridation, partial substitution of iron cations by other transition metals such as manganese, cobalt, or nickel could also have a positive impact on the electrochemical properties and identify a promising chemical composition with high capacity associated with long-term cycling ability as a cathode material.

In summary, the current synthesis methods often utilize solvothermal synthesis, typically using water as the solvent. This method is relatively simple, without the need for additives or templates, and allows for control over the morphology and structure of the samples by adjusting synthesis conditions such as temperature and time. However, the yield of this method is relatively low. Electrodeposition can produce pure samples with reduced impurities and operates at lower experimental temperatures. Microwave irradiation has a significant impact on the specific surface area of materials, thereby increasing the storage capacity of electrode materials. By enhancing the active surface area of the electrode material through microwave irradiation, the stability of discharge capacitance before irradiation is improved. Microwave irradiation is a promising technique as it can be conducted at room temperature in a short period of time with minimal energy consumption. Additionally, solution-based methods and hydrolysis methods for the synthesis of zinc hydroxide fluoride were introduced, which have lower environmental requirements and lower production costs compared to solvothermal synthesis. Furthermore, thermal decomposition was mentioned as a method to obtain hydroxyfluoride by decomposing mixed-valence iron fluorides at high temperatures.

3. Supercapacitor applications of hydroxide fluoride

Hydroxide fluorides exhibit characteristics such as high specific surface area, exposure to low-energy surfaces, size effects, excellent electronic transport capability, and high theoretical capacitance. As a result, they are considered electrode materials with potential for developing supercapacitors capable of meeting the energy storage demands of supercapacitor electrodes. However, compared to the currently used electrode materials for supercapacitors, hydroxide fluorides may face challenges regarding rate performance and cycling stability. To further enhance the performance of hydroxide fluoride electrode materials, researchers have explored various methods. These include doping with a certain number of other metals or compounds, as well as the fabrication of composite electrode materials through the combination of metal oxides or hydroxides. These composite electrode materials are then assembled with carbon electrodes to form supercapacitors, allowing for the evaluation of their electrochemical performance.

3.1. Elemental doping

Doping is a commonly used method to improve the performance of materials or substances. It involves intentionally introducing small amounts of other elements or compounds into the material or substrate to regulate its electronic properties, thus giving it specific value or utility. Doping can generally be categorized into two types: impurity doping and ion doping. Impurity doping refers to introducing small amounts of other elements into the material, which often have different atomic sizes, electronic structures, or chemical properties. By impurity doping, the material's conductivity, optical properties, mechanical performance, etc., can be altered. Ion doping refers to introducing small amounts

of ions (usually metal ions) into the material, which can substitute for atomic positions in the material. Through ion doping, the material's lattice structure, stability, and electronic band structure can be adjusted, thus affecting its conductivity, thermal conductivity, optical properties, etc. In summary, the purpose of doping is to give materials specific properties or functionalities to meet specific application needs. Doping is an effective method for improving the performance of materials or substances. By purposefully introducing small amounts of other elements or compounds, the material's electronic properties can be regulated, giving it specific value or utility. Doping technology has broad prospects in the fields of materials science and engineering.

Lv et al.[65] employed a one-step hydrothermal method to synthesize nitrogen-doped Co(OH)F. The raw materials used included $Co(NO_3)_2{\cdot}6H_2O$, sodium fluoride, and urea. The CFP (2 cm × 3 cm × 0.01 cm) was immersed in the reaction vessel with the mixed solution, and the resulting product was subsequently filtered, washed, and dried. The introduction of the halide anion F and heteroatom N led to the generation of a large number of oxygen vacancies, thus enhancing the OER (oxygen evolution reaction) activity. The prepared N-doped Co(OH)F-CFP (N:Co(OH)F-CFP) displayed favorable hydrophilicity, promoting interaction with the electrolyte and expediting the reversible electron transfer between the material surface and the electrolyte.

Jiang et al.[49] employed a hydrothermal approach to directly cultivate doped Co element Zn(OH)F three-dimensional nano-edge arrays on a Ni foam substrate. The resulting Zn(OH)F electrode, featuring a three-dimensional structure, attained an exceptionally high specific capacitance of 1970 F g^{-1} at a current density of 1 A g^{-1}. In **Figure 5(a)**, a cycling stability test was performed on this electrode, revealing 105% initial capacity retention after 5000 charge-discharge cycles, thus confirming its outstanding cycling stability. Additionally, **Figure 5(b)** illustrates that the impedance spectra before and after 5000 CV cycles are nearly indistinguishable. As a result of the electrode's electroactivation process, it demonstrated reduced resistance, in line with the findings of the aforementioned cycling stability test. Furthermore, an asymmetric supercapacitor (ASC) was constructed using Co-Zn(OH)F as the positive electrode and activated carbon as the negative electrode. When compared to ASCs assembled with other cobalt-based electrode materials, the Co-Zn(OH)F//AC configuration exhibited higher energy density and power density. At a power density of 285.1 W kg^{-1}, it achieved a maximum energy density of 86.2 Wh kg^{-1}, comparable to lithium-ion batteries. Even at a high power density of 5062 W kg^{-1}, the device's energy density could still be maintained at 18.8 Wh kg^{-1}.

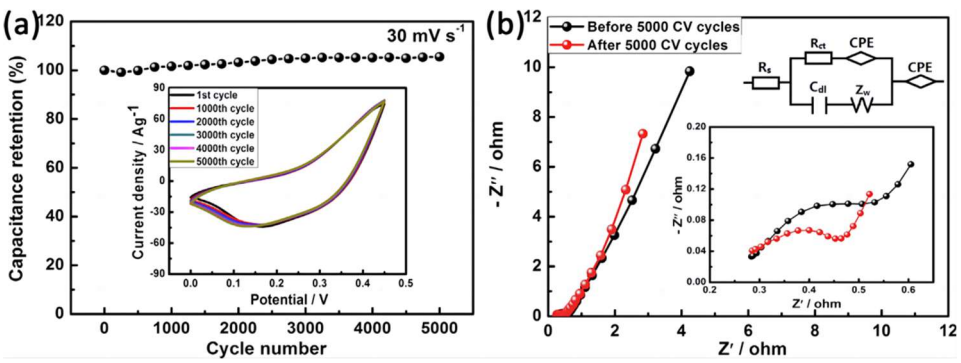

Figure 5. (a) The cycle performance of Co-Zn(OH)F electrode at a scan rate of 30 mV s^{-1}. Inset: the CV curves of the different cycles; **(b)** The electrochemical impedance spectra of Co-Zn(OH)F electrode before and after 5000 cycling tests. Inset: the electrical equivalent circuit used for fitting impedance spectra[49].

Shi et al.[57] successfully synthesized a series of Co^{2+}-doped nickel hydroxyfluorides using a one-pot solvothermal method, and the excellent conductivity resulting from Co^{2+} doping was confirmed through density of states calculations and experimental validation. Building upon a larger surface area and more defects compared to pure Ni_4OHF_7, the material achieved an ultra-high specific capacitance of 3380.2 F g^{-1} at a current density of 1 A g^{-1}, while maintaining a capacitance retention of 78.4% at a high current density of 20 A g^{-1}, demonstrating remarkable rate performance. To address the challenges of smaller interlayer spacing and lower conductivity in cobalt hydroxyfluoride, Hao et al.[66] modified it by doping with Fe. By incorporating Fe atoms with a slightly larger atomic radius, the interplanar spacing was increased, thereby enhancing ion storage capacity and significantly improving the conductivity of cobalt hydroxyfluoride. The optimized sample, CoOHF-0.06Fe, exhibited a high specific capacitance of 85.8 F g^{-1} and achieved a high energy density of 37.2 Wh kg^{-1} at a power density of 1600 W kg^{-1} in an asymmetric supercapacitor composed of activated carbon.

3.2. Material composite

Materials composite is a method of combining two or more material components with different chemical or physical properties together in a pre-designed structure, proportion, and distribution to obtain materials with excellent performance. This method has the advantage of structural designability, allowing for the preservation of the individual properties of each component material and achieving comprehensive performance that cannot be achieved by a single component material. For materials such as hydroxyfluorides with high resistance, their conductivity can be optimized by composites with other materials, such as carbon materials. Carbon materials have good electrical conductivity and can enhance the conductivity of composite materials. By mixing or compositing hydroxyfluorides with carbon materials in certain proportions, composite materials with lower resistance and good rate performance can be formed.

Composite materials can be achieved through various methods, such as physical mixing, chemical reactions, deposition, and impregnation. When preparing hydroxyfluoride composite materials, appropriate methods can be chosen to mix or composite hydroxyfluorides with carbon materials. By controlling the composition ratio, distribution, and structure of the composite materials, their conductivity can be adjusted, thereby optimizing their performance. By selecting suitable composite components and optimizing the composite structure, the electrochemical performance of hydroxyfluorides can be regulated and enhanced. In conclusion, material composites are an effective method for optimizing material performance. For materials such as hydroxyfluorides with high resistance, their conductivity can be optimized by composites with carbon materials, leading to enhanced comprehensive performance. Materials composite technology has broad prospects in the fields of materials science and engineering.

Zhu et al.[45] prepared Zn(OH)F/N-C (nitrogen-doped carbon) composite material using a hydrothermal method and utilized it as a new anode material for lithium-ion batteries (LIBs), as depicted in **Figure 6**. The Zn(OH)F/N-C electrode features a distinct porous structure, a high Li^+ diffusion coefficient, and a large specific surface area. This unique structure effectively facilitates electrolyte penetration, improves electronic conductivity, and accelerates lithium-ion diffusion. The small grain size of the Zn(OH)F/N-C material indicates its ability to form numerous grain boundaries, shortening the diffusion path of Li^+ ions, facilitating Li^+ transport, and enhancing the ion conductivity and rate performance of the battery. Additionally, the sample displays numerous surface defects, offering more

active sites for ion storage and contributing to increased specific capacity. The presence of oxygen defects significantly enhances the electrode and ion conductivity. Structures with various pore sizes provide ample space to accommodate the phase change of the active material, ensuring full contact between the electrolyte and the electrode and preventing electrode fracture, thereby enhancing the cyclic stability of the battery. As a result, the Zn(OH)F/N-C composite material demonstrates a good initial discharge capacity (946.8 mAh g^{-1}), high coulombic efficiency (87.3%), excellent cyclic stability (1050.2 mAh g^{-1} after 430 cycles), and outstanding rate capability.

Figure 6. Schematic of the synthesis routes of ZnOHF-embedded N-doped porous carbon nanocomposite[45].

Chen et al.[46] engineered a composite material consisting of $Ni_{0.33}Co_{0.66}(OH)F$ hollow hexagons interwoven with multi-walled carbon nanotubes (MWCNTs), demonstrating outstanding electrochemical performance characterized by high reversible capacity and stable cycling performance. Illustrated in **Figure 7**, the addition of carbon nanotubes resulted in the $Ni_{0.33}Co_{0.66}(OH)F$ hollow hexagons becoming smaller, well-dispersed, more uniform in size, and exhibiting a more regular shape. Simultaneously, the carbon nanotubes were seamlessly interconnected with the $Ni_{0.33}Co_{0.66}(OH)F$ hollow hexagons, forming a distinctive woven network structure that significantly enhanced the conductivity of the composite material. Leveraging this unique composite structure, the $Ni_{0.33}Co_{0.66}(OH)F$/CNTs electrode showcased a high reversible capacity of 1014 mAh g^{-1} after 100 charge-discharge cycles (at a current density of 100 mA g^{-1}), and it also achieved a high capacity of 585 mAh g^{-1} at a current density of 1000 mA g^{-1}. The exceptional electrochemical performance of the $Ni_{0.33}Co_{0.66}(OH)F$/CNTs electrode can be attributed to its three-dimensional interconnected hollow structure and the synergistic effect of each component. Firstly, the MWCNTs prevented the aggregation of $Ni_{0.33}Co_{0.66}(OH)F$, thereby increasing the surface area and greatly reducing the pressure caused by volume changes during cycling. Secondly, the MWCNTs network connected the separated $Ni_{0.33}Co_{0.66}(OH)F$ hollow hexagons into a three-dimensional structure, thereby improving the conductivity of the composite material. The interconnected hollow structure not only increased the contact area between the active material and the electrolyte but also provided a network for charge and ion conversion. Lastly, due to the high ionic nature of metal fluoride bonds, the formation of fluoride derivatives resulted in higher redox voltages.

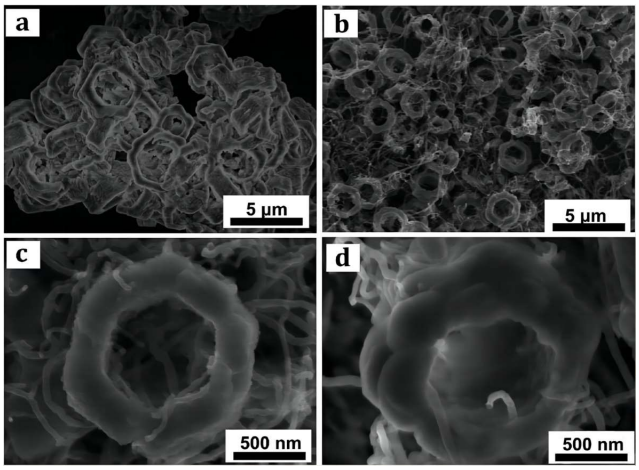

Figure 7. SEM images of (a) $Ni_{0.33}Co_{0.66}(OH)F$ and (b–d) hollow hexagon $Ni_{0.33}Co_{0.66}(OH)F$/CNTs at different magnifications[46].

Li et al.[50] produced a $Co(OH)F/Ni(OH)_2$ (Co/Ni = 3:1) hybrid material for supercapacitor electrodes using a straightforward one-pot hydrothermal method. In **Figure 8**, the specific capacitance variation of different candidate materials with varying $Co(OH)F/Ni(OH)_2$ composite ratios at different current densities is illustrated. Compared to the pre-composites and other composite ratios (Co/Ni = 1:0, 1:1, 1:3, 0:1), the $Co(OH)F/Ni(OH)_2$ (Co/Ni = 3:1) electrode demonstrated significantly enhanced specific capacitance and rate performance. Furthermore, the $Co(OH)F/Ni(OH)_2$ (Co/Ni = 3:1) electrode was subjected to a 5000-cycle stability test, retaining 116% of its capacity at a current density of 6 A g^{-1}, showcasing its exceptional cycling stability. As a result of the optimal synergistic effect between Co and Ni redox species, the material displayed high specific capacitance, rate capability, and excellent cyclic performance. Additionally, the designed AC//$Co(OH)F/Ni(OH)_2$ (Co/Ni = 3:1) asymmetric supercapacitor exhibited higher energy density, power density, and longer cycle life compared to other $Co(OH)F/Ni(OH)_2$ candidate materials (Co/Ni = 1:0, 1:1, 1:3, 0:1).

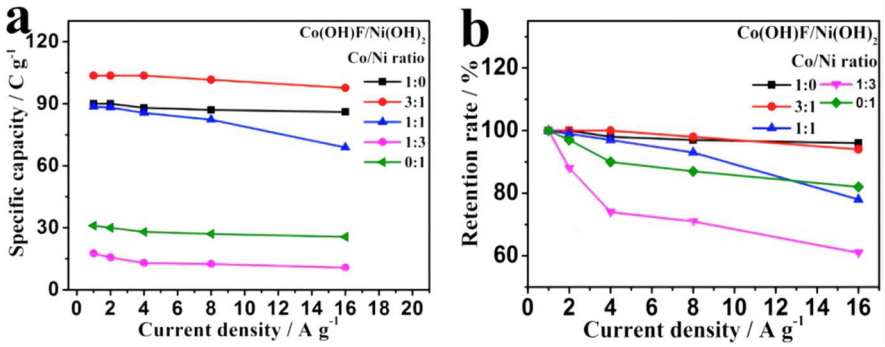

Figure 8. Specific capacity **(a)** and retention rate **(b)** as a function of current density of $Co(OH)F/Ni(OH)_2$ electrodes (Co/Ni = 1:0, 3:1, 1:1, 1:3, 0:1)[50].

Creating electrodes with unique structures can also enhance the electrochemical performance of materials. Chen et al.[67] created a core-shell structure array of Co(OH)F nanorods coated with K_xMnO_2 using electrodeposition. The electrochemical performance was assessed using Co(OH)F nanorods as the working electrode in a 0.02 M manganese acetate and 0.2 M potassium sulfate electrolyte. In **Figure 9(a)**, the transmission electron microscopy image of individual Co(OH)F nanorods obtained in ethanol through ultrasound reveals the relatively smooth surfaces of the nanorods. The transmission electron microscopy image of the Co(OH)F@K_xMnO_2 core-shell structure (**Figure 9(c)**) illustrates that the surface

of the Co(OH)F nanorods (dark region) is encompassed by K_xMnO_2 nanosheets (light region). Additionally, the high-resolution projection image (**Figure 9(d)**) corresponds well to the interplanar spacing of the (002) plane of MnO_2, further confirming the successful synthesis of the structure. Compared to Co(OH)F nanorods and K_xMnO_2 nanosheets, the core-shell structure demonstrates a larger integrated area in cyclic voltammetry, indicating higher areal capacity and suggesting the additional contribution of K_xMnO_2 as the shell to the overall value (**Figure 10(a)**). In the galvanostatic charge-discharge curves (**Figure 10(b)**), the Co(OH)F@K_xMnO_2 core-shell structure sample exhibits the longest discharge time among the three samples, indicating the highest capacitance. Calculations demonstrate a high areal capacitance of 1046 mF cm^{-2} at 1 mA cm^{-2}, and after 3000 cycles at a constant current density of 10 mA cm^{-2}, it shows a high capacitance retention of 118%. These results indicate that the core-shell array nano-composite material displays improved electrochemical performance and substantial energy storage potential.

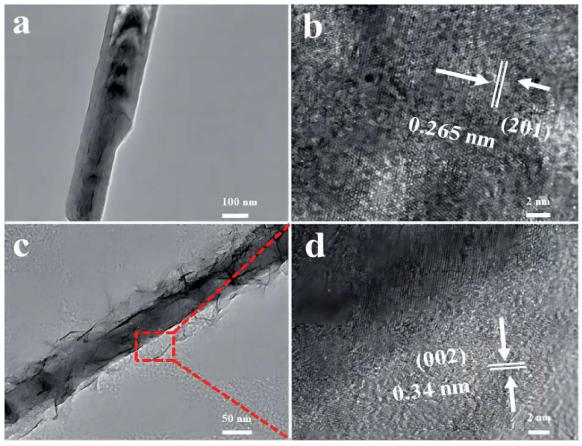

Figure 9. (a) TEM image of Co(OH)F nanorods; **(b)** HRTEM images of the Co(OH)F nanorods; **(c)** TEM image of Co(OH)F@KxMnO₂ core–shell structure; **(d)** HRTEM images of the Co(OH)F@KxMnO₂ core–shell structure[67].

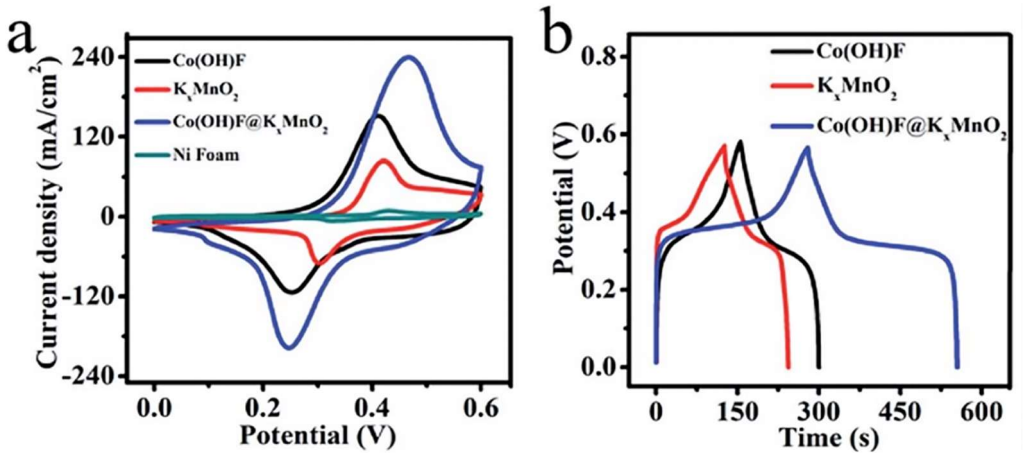

Figure 10. (a) CV curves of the Co(OH)F nanorods electrode, the KxMnO₂ nanosheets electrode, the Co(OH)F@KxMnO₂ core–shell structure electrode and the pure Ni foam at a scan rate of 100 mV s^{-1}; **(b)** galvanostatic charge–discharge curves of the Co(OH)F nanorods electrode, the KxMnO₂ nanosheets electrode and the Co(OH)F@KxMnO₂ core–shell structure electrode at a current density of 2 mA cm^{-2}[67].

In this novel non-uniform core-shell structure, both the electrochemical materials serving as the "core" and "shell" are fully utilized and exhibit excellent synergistic effects. Importantly, the direct growth on a conductive substrate avoids the resistance introduced by binders, facilitating rapid electron transfer to the conductive substrate and enhancing the electrochemical performance of the electrode.

4. Conclusions and outlook

By doping with other metal elements and utilizing synergistic effects, mixed transition metal hydroxyfluorides exhibit higher conductivity. Composites retain the advantages of each component material and achieve more comprehensive performance than single-component materials. The unique electrode structure enhances the material's electrochemical performance. Modified hydroxyfluoride electrode materials demonstrate improved conductivity, cycling stability, and the lifespan of supercapacitors. However, the large-scale application of hydroxyfluoride electrode materials still faces significant challenges, necessitating further development and exploration of higher-performance hydroxyfluorides and the adoption of more reasonable modification measures to promote their use.

Research has demonstrated that, due to their high specific surface area, theoretical capacitance, and fast electron transfer rate, hydroxyfluorides perform well in electrochemical tests. Consequently, an increasing amount of research is applying hydroxyfluorides in electrode materials for supercapacitors and lithium-ion batteries, which is crucial for enhancing energy storage capabilities. With their straightforward and cost-effective preparation methods, hydroxyfluorides have the potential for large-scale applications in the future. However, hydroxyfluoride materials themselves suffer from poor rate performance and stability, necessitating improvement through modification measures. Additionally, further refinement of hydroxyfluoride preparation methods is needed to optimize product structure and properties. Furthermore, research on hydroxyfluorides is still relatively limited, and continued exploration of the preparation of other transition metal hydroxyfluorides and their application in supercapacitor electrode materials requires significant effort.

Despite the potential of hydroxyfluorides as efficient catalysts, they still face significant challenges in both fundamental and practical aspects. This includes: 1) developing advanced scaling-up methods that are simple, convenient, and cost-effective, in addition to refining synthesis strategies; 2) precise control of the composition, size, morphology, pore structure, phase, and impurities in the nanostructures of efficient catalysts to improve the utilization of active sites; 3) comprehensive characterization techniques for structure and composition information; 4) high-throughput methods for characterizing composition, configuration, microstructure, and catalytic performance to identify unexplored core catalysis within a vast combination of elements; 5) computational models with high accuracy, generality, and simplicity to provide a time- and cost-efficient approach for optimizing the composition and surface structure of hydroxyfluoride-based materials; 6) collaborative efforts between experimental and theoretical approaches to determine active sites and structure-performance relationships.

In conclusion, while hydroxyfluorides hold significant development potential as electrode materials for energy storage devices, addressing challenges related to rate performance and stability is essential. With continued technological advancements and further research, hydroxyfluorides are expected to play a crucial role in energy storage and contribute to efficient and sustainable energy storage solutions.

Funding

This work was financially supported by the Graduate Innovation Fund of Jilin University (Grant No. 2022177).

Conflict of interest

The authors declare that they have no conflict of interest.

References

1. Shi W, Meng Z, Xu Z, et al. Controllable vacancy strategy mediated by organic ligands of nickel fluoride alkoxides for high-performance aqueous energy storage. Journal of Materials Chemistry A. 2023, 11(3): 1369-1379. doi: 10.1039/d2ta08004d
2. Meng Z, Gong X, Xu J, et al. A general strategy for preparing hollow spherical multilayer structures of Oxygen-Rich vacancy transition metal Oxides, especially high entropy perovskite oxides. Chemical Engineering Journal. 2023, 457: 141242. doi: 10.1016/j.cej.2022.141242
3. Wang F, Wu X, Yuan X, et al. Latest advances in supercapacitors: from new electrode materials to novel device designs. Chemical Society Reviews. 2017, 46(22): 6816-6854. doi: 10.1039/c7cs00205j
4. Wang Y, Du Z, Xu J, et al. Improved Catalytic Activity and Stability of Co9S8 by Se Incorporation for Efficient Oxygen Evolution Reaction. Inorganic Chemistry. 2022, 61(51): 21139-21147. doi: 10.1021/acs.inorgchem.2c03805
5. Sun X, Meng Z, Hao Z, et al. Efficient fabrication of flower-like core–shell nanochip arrays of lanthanum manganate and nickel cobaltate for high-performance supercapacitors. Journal of Colloid and Interface Science. 2023, 630: 618-628. doi: 10.1016/j.jcis.2022.10.035
6. Olabi AG, Abbas Q, Al Makky A, et al. Supercapacitors as next generation energy storage devices: Properties and applications. Energy. 2022, 248: 123617. doi: 10.1016/j.energy.2022.123617
7. Salanne M, Rotenberg B, Naoi K, et al. Efficient storage mechanisms for building better supercapacitors. Nature Energy. 2016, 1(6). doi: 10.1038/nenergy.2016.70
8. Simon P, Gogotsi Y. Materials for electrochemical capacitors. Nature Materials. 2008, 7(11): 845-854. doi: 10.1038/nmat2297
9. Aricò AS, Bruce P, Scrosati B, et al. Nanostructured materials for advanced energy conversion and storage devices. Nature Materials. 2005, 4(5): 366-377. doi: 10.1038/nmat1368
10. Wang G, Zhang L, Zhang J. A review of electrode materials for electrochemical supercapacitors. Chemical Society Reviews. 2012, 41(2): 797-828. doi: 10.1039/c1cs15060j
11. Chhowalla M, Shin HS, Eda G, et al. The chemistry of two-dimensional layered transition metal dichalcogenide nanosheets. Nature Chemistry. 2013, 5(4): 263-275. doi: 10.1038/nchem.1589
12. Zhang LL, Zhao XS. Carbon-based materials as supercapacitor electrodes. Chemical Society Reviews. 2009, 38(9): 2520. doi: 10.1039/b813846j
13. Zhu Y, Murali S, Stoller MD, et al. Carbon-Based Supercapacitors Produced by Activation of Graphene. Science. 2011, 332(6037): 1537-1541. doi: 10.1126/science.1200770
14. Kötz R, Carlen M. Principles and applications of electrochemical capacitors. Electrochimica Acta. 2000, 45(15-16): 2483-2498. doi: 10.1016/s0013-4686(00)00354-6
15. Frackowiak E, Béguin F. Carbon materials for the electrochemical storage of energy in capacitors. Carbon. 2001, 39(6): 937-950. doi: 10.1016/s0008-6223(00)00183-4
16. Chen LF, Zhang XD, Liang HW, et al. Synthesis of Nitrogen-Doped Porous Carbon Nanofibers as an Efficient Electrode Material for Supercapacitors. ACS Nano. 2012, 6(8): 7092-7102. doi: 10.1021/nn302147s
17. Augustyn V, Simon P, Dunn B. Pseudocapacitive oxide materials for high-rate electrochemical energy storage. Energy & Environmental Science. 2014, 7(5): 1597. doi: 10.1039/c3ee44164d
18. Pandolfo AG, Hollenkamp AF. Carbon properties and their role in supercapacitors. Journal of Power Sources. 2006, 157(1): 11-27. doi: 10.1016/j.jpowsour.2006.02.065
19. Snook GA, Kao P, Best AS. Conducting-polymer-based supercapacitor devices and electrodes. Journal of Power Sources. 2011, 196(1): 1-12. doi: 10.1016/j.jpowsour.2010.06.084
20. Bonaccorso F, Colombo L, Yu G, et al. Graphene, related two-dimensional crystals, and hybrid systems for energy conversion and storage. Science. 2015, 347(6217). doi: 10.1126/science.1246501
21. Liu C, Yu Z, Neff D, et al. Graphene-Based Supercapacitor with an Ultrahigh Energy Density. Nano Letters. 2010, 10(12): 4863-4868. doi: 10.1021/nl102661q
22. Zhai Y, Dou Y, Zhao D, et al. Carbon Materials for Chemical Capacitive Energy Storage. Advanced Materials. 2011, 23(42): 4828-4850. doi: 10.1002/adma.201100984
23. Chen H, Cong TN, Yang W, et al. Progress in electrical energy storage system: A critical review. Progress in Natural Science. 2009, 19(3): 291-312. doi: 10.1016/j.pnsc.2008.07.014
24. Zhong C, Deng Y, Hu W, et al. A review of electrolyte materials and compositions for electrochemical supercapacitors. Chemical Society Reviews. 2015, 44(21): 7484-7539. doi: 10.1039/c5cs00303b
25. Luo X, Wang J, Dooner M, et al. Overview of current development in electrical energy storage technologies and the application potential in power system operation. Applied Energy. 2015, 137: 511-536. doi: 10.1016/j.apenergy.2014.09.081
26. Wang Y, Shi Z, Huang Y, et al. Supercapacitor Devices Based on Graphene Materials. The Journal of Physical Chemistry C. 2009, 113(30): 13103-13107. doi: 10.1021/jp902214f

27. Wei W, Cui X, Chen W, et al. Manganese oxide-based materials as electrochemical supercapacitor electrodes. Chemical Society Reviews. 2011, 40(3): 1697-1721. doi: 10.1039/c0cs00127a
28. Wan F, Wang X, Tang C, et al. Metallic 1T-MoS_2 coupled with MXene towards ultra-high rate-capabilities for supercapacitors. Journal of Materials Chemistry A. 2022, 10(22): 12258-12268. doi: 10.1039/d2ta01908f
29. Yu J, Xie F, Wu Z, et al. Flexible metallic fabric supercapacitor based on graphene/polyaniline composites. Electrochimica Acta. 2018, 259: 968-974. doi: 10.1016/j.electacta.2017.11.008
30. Yu Z, Tetard L, Zhai L, et al. Supercapacitor electrode materials: nanostructures from 0 to 3 dimensions. Energy & Environmental Science. 2015, 8(3): 702-730. doi: 10.1039/c4ee03229b
31. Ling Z, Ren CE, Zhao MQ, et al. Flexible and conductive MXene films and nanocomposites with high capacitance. Proceedings of the National Academy of Sciences. 2014, 111(47): 16676-16681. doi: 10.1073/pnas.1414215111
32. Zhang K, Zhang LL, Zhao XS, et al. Graphene/Polyaniline Nanofiber Composites as Supercapacitor Electrodes. Chemistry of Materials. 2010, 22(4): 1392-1401. doi: 10.1021/cm902876u
33. González A, Goikolea E, Barrena JA, et al. Review on supercapacitors: Technologies and materials. Renewable and Sustainable Energy Reviews. 2016, 58: 1189-1206. doi: 10.1016/j.rser.2015.12.249
34. Yan J, Wang Q, Wei T, et al. Recent Advances in Design and Fabrication of Electrochemical Supercapacitors with High Energy Densities. Advanced Energy Materials. 2013, 4(4). doi: 10.1002/aenm.201300816
35. Wang H, Casalongue HS, Liang Y, et al. $Ni(OH)_2$ Nanoplates Grown on Graphene as Advanced Electrochemical Pseudocapacitor Materials. Journal of the American Chemical Society. 2010, 132(21): 7472-7477. doi: 10.1021/ja102267j
36. Yan J, Fan Z, Sun W, et al. Advanced Asymmetric Supercapacitors Based on $Ni(OH)_2$/Graphene and Porous Graphene Electrodes with High Energy Density. Advanced Functional Materials. 2012, 22(12): 2632-2641. doi: 10.1002/adfm.201102839
37. Fan Z, Yan J, Wei T, et al. Asymmetric Supercapacitors Based on Graphene/MnO_2 and Activated Carbon Nanofiber Electrodes with High Power and Energy Density. Advanced Functional Materials. 2011, 21(12): 2366-2375. doi: 10.1002/adfm.201100058
38. Pershaanaa M, Bashir S, Ramesh S, et al. Every bite of Supercap: A brief review on construction and enhancement of supercapacitor. Journal of Energy Storage. 2022, 50: 104599. doi: 10.1016/j.est.2022.104599
39. Zhang J, Gong X, Li X, et al. Electron-ion conjugation sites co-constructed by defects and heteroatoms assisted carbon electrodes for high-performance aqueous energy storage. Journal of Colloid and Interface Science. 2023, 640: 600-609. doi: 10.1016/j.jcis.2023.02.147
40. Zeng F, Meng Z, Xu Z, et al. Biomass-derived porous activated carbon for ultra-high performance supercapacitor applications and high flux removal of pollutants from water. Ceramics International. 2023, 49(10): 15377-15386. doi: 10.1016/j.ceramint.2023.01.122
41. Zhi M, Xiang C, Li J, et al. Nanostructured carbon–metal oxide composite electrodes for supercapacitors: A review. Nanoscale. 2013, 5(1): 72-88. doi: 10.1039/c2nr32040a
42. Futaba DN, Hata K, Yamada T, et al. Shape-engineerable and highly densely packed single-walled carbon nanotubes and their application as super-capacitor electrodes. Nature Materials. 2006, 5(12): 987-994. doi: 10.1038/nmat1782
43. Lin T, Chen IW, Liu F, et al. Nitrogen-doped mesoporous carbon of extraordinary capacitance for electrochemical energy storage. Science. 2015, 350(6267): 1508-1513. doi: 10.1126/science.aab3798
44. Frackowiak E. Carbon materials for supercapacitor application. Physical Chemistry Chemical Physics. 2007, 9(15): 1774. doi: 10.1039/b618139m
45. Zhu B, Liu Y, Zhao H, et al. ZnOHF/N-doped carbon hybrids as a novel anode material for enhanced lithium storage. Journal of Alloys and Compounds. 2021, 889: 161705. doi: 10.1016/j.jallcom.2021.161705
46. Chen H, Zhang Y, Yang J, et al. $Ni_{0.33}Co_{0.66}$(OH)F hollow hexagons woven by MWCNTs for high-performance lithium-ion batteries. Journal of Materials Chemistry A. 2015, 3(41): 20690-20697. doi: 10.1039/c5ta05143f
47. Wu F, Ma X, Feng J, et al. 3D $Co_3O_4$and CoO@C wall arrays: morphology control, formation mechanism, and lithium-storage properties. Journal of Materials Chemistry A. 2014, 2(30): 11597. doi: 10.1039/c4ta01676a
48. Ni S, Ma J, Zhang J, et al. Facile synthesis of Co(OH)F micro-rods and its application as anode for lithium ion batteries. Materials Letters. 2015, 139: 138-140. doi: 10.1016/j.matlet.2014.10.035
49. Jiang S, Pang M, Zhao J, et al. Superior performance asymmetric supercapacitors based on a directly grown three-dimensional lawn-like cobalt-zinc hydroxyfluorides nanoneedle arrays electrode. Chemical Engineering Journal. 2017, 326: 1048-1057. doi: 10.1016/j.cej.2017.06.017
50. Li X, Ding R, Shi W, et al. Hierarchical porous Co(OH)F/$Ni(OH)_2$: A new hybrid for supercapacitors. Electrochimica Acta. 2018, 265: 455-473. doi: 10.1016/j.electacta.2018.01.194

51. Zhang JF, Wang Y, Shu X, et al. One-pot synthesis of nickel-cobalt hydroxyfluorides nanowires with ultrahigh energy density for an asymmetric supercapacitor. Science Bulletin. 2018, 63(5): 322-330. doi: 10.1016/j.scib.2018.01.024
52. Chen S, Zhou X, Ma X, et al. Asymmetric supercapacitors with excellent rate performance by integrating Co(OH)F nanorods and layered $Ti_3C_2T_x$ paper. RSC Advances. 2019, 9(53): 30957-30963. doi: 10.1039/c9ra06393e
53. Dong Q, Su T, Ge W, et al. Atomic Doping and Anion Reconstructed CoF_2 Electrocatalyst for Oxygen Evolution Reaction. Advanced Materials Interfaces. 2020, 7(7). doi: 10.1002/admi.201901939
54. Zhang B, Jiang K, Wang H, et al. Fluoride-Induced Dynamic Surface Self-Reconstruction Produces Unexpectedly Efficient Oxygen-Evolution Catalyst. Nano Letters. 2018, 19(1): 530-537. doi: 10.1021/acs.nanolett.8b04466
55. Roger I, Shipman MA, Symes MD. Earth-abundant catalysts for electrochemical and photoelectrochemical water splitting. Nature Reviews Chemistry. 2017, 1(1). doi: 10.1038/s41570-016-0003
56. Zhang L, Wang W, Xu G, et al. Facile synthesis of $Co_xFe_{1-x}P$ microcubes derived from metal-organic frameworks for efficient oxygen evolution reaction. Journal of Colloid and Interface Science. 2019, 554: 202-209. doi: 10.1016/j.jcis.2019.07.008
57. Shi W, Jiang C, Meng Z, et al. Novel Co-doped nickel hydroxyfluorides with rapid electron transfer for high-performance supercapacitors. Journal of Alloys and Compounds. 2023, 959: 170558. doi: 10.1016/j.jallcom.2023.170558
58. Xu F, Sun L, Dai M, et al. Fluorine-Ion-Mediated Electrodeposition of Rhombus-Like ZnFOH Nanorod Arrays: An Intermediate Route to Novel ZnO Nanoarchitectures. The Journal of Physical Chemistry C. 2010, 114(36): 15377-15382. doi: 10.1021/jp1066082
59. Zhu L, Zheng Y, Hao T, et al. Synthesis of hierarchical ZnO nanobelts via Zn(OH)F intermediate using ionic liquid-assistant microwave irradiation method. Materials Letters. 2009, 63(28): 2405-2408. doi: 10.1016/j.matlet.2009.07.062
60. Song J kui, Zheng M bo, Yang Z jiang, et al. Synthesis of Novel Flower-Like Zn(OH)F via a Microwave-Assisted Ionic Liquid Route and Transformation into Nanoporous ZnO by Heat Treatment. Nanoscale Research Letters. 2009, 4(12). doi: 10.1007/s11671-009-9428-1
61. Barzegar F, Bello A, Momodu DY, et al. Effect of radiation on the performance of activated carbon base supercapacitor: Part I. Influence of microwave irradiation exposure on electrodes material. Energy Procedia. 2019, 158: 4554-4559. doi: 10.1016/j.egypro.2019.01.754
62. Peng Y, Zhou HY, Wang ZH. Synthesis, characterization and photocatalytic activity of Zn(OH)F hierarchical nanofibers prepared by a simple solution-based method. CrystEngComm. 2012, 14(8): 2812. doi: 10.1039/c2ce06389a
63. Ahmad S, Rawat P, Nagarajan R. Facile green synthesis of Zn(OH)F from the single source precursor $KZnF_3$. Materials Letters. 2015, 139: 86-88. doi: 10.1016/j.matlet.2014.10.037
64. Lemoine K, Zhang L, Dambournet D, et al. Synthesis by Thermal Decomposition of Two Iron Hydroxyfluorides: Structural Effects of Li Insertion. Chemistry of Materials. 2019, 31(11): 4246-4257. doi: 10.1021/acs.chemmater.9b01252
65. Lv J, Yang X, Zang HY, et al. Ultralong needle-like N-doped Co(OH)F on carbon fiber paper with abundant oxygen vacancies as an efficient oxygen evolution reaction catalyst. Materials Chemistry Frontiers. 2018, 2(11): 2045-2053. doi: 10.1039/c8qm00405f
66. Hao Z, Jiang C, Xu Z, et al. Reasonably optimized structure of iron-doped cobalt hydroxylfluoride for high-performance supercapacitors. Journal of Colloid and Interface Science. 2023, 644: 64-72. doi: 10.1016/j.jcis.2023.04.061
67. Chen S, Song Y, Zhou X, et al. Co(OH)F nanorods@$KxMnO_2$ nanosheet core–shell structured arrays for pseudocapacitor application. RSC Advances. 2019, 9(62): 36208-36212. doi: 10.1039/c9ra07024a

Energy Storage and Conversion 2023; 1(1): 304.
Review Article

On efficiencies, emissions, and the colors of hydrogen—An update

Rudolf Holze[1,2,3,4]

[1] *State Key Laboratory of Materials-oriented Chemical Engineering, School of Energy Science and Engineering, Nan-Jing Tech University, Nanjing 211816, Jiangsu Province, China; rudolf.holze@chemie.tu-chemnitz.de*

[2] *St. Petersburg State University, Institute of Chemistry, St. Petersburg 199034, Russian Federation*

[3] *Technische Universität Chemnitz, Chemnitz D-09107, Germany*

[4] *Confucius Energy Storage Lab, School of Energy and Environment, Southeast University, Nanjing 210096, Jiangsu Province, China*

ARTICLE INFO

Received: 18 November 2023
Accepted: 15 December 2023
Available online: 21 December 2023

doi: 10.59400/esc.v1i1.304

ABSTRACT: Compared with electricity, more precisely electric energy, hydrogen as a secondary form of energy, an energy carrier, an energy storage material, and a chemical reagent are of growing importance. This change is driven mostly by ecological reasons, with hydrogen replacing fossil fuels and materials and finally reducing the emission of greenhouse gases. It is also relevant because of its conceivable use as an energy carrier in transportation. This update starts with a brief collection of common definitions and terminology and moves across a critical assessment of common misunderstandings towards current and future uses of hydrogen to future perspectives with a particular focus on efficiency.

KEYWORDS: hydrogen economy; energy efficiency; energy carrier; electromobility; fuel cells; energy storage

1. Introduction

Certainly, it is well known that hydrogen is a gas under standard conditions without any color, and even in liquefied form, it hardly has any pronounced coloration. Nevertheless, it is quite common to talk about a growing bundle of hydrogen colors. Find more details and some other aspects of the discussion in reports by Ajanovic et al.[1], Kusoglu[2] and Wu and Holze[3].

Green hydrogen is produced by the electrolysis of water using electric energy from renewable sources without any emission of greenhouse gases.

Yellow hydrogen is produced by the electrolysis of water using electric energy from solar energy alone, without any emission of greenhouse gases. Another definition assumes yellow hydrogen is produced using electric energy from the grid, with its typical mix of electric energy from various sources.

Blue hydrogen is produced from fossil fuels (at the time of writing, mostly natural gas) with carbon dioxide sequestration and storage or utilization in further processes. When run correctly, this process does not create emissions of greenhouse gases. Because CO_2 and not carbon (this difference is overlooked in the report by Ajanovic[1]) are collected and stored, this type of hydrogen should be distinguished from turquoise hydrogen.

Gray hydrogen is produced once again from fossil fuels (at the time of writing, mostly natural gas) without carbon dioxide sequestration. This process, which is currently the dominant one for hydrogen production, is produced from coal in its various forms, mostly bituminous coal, without sequestration of the carbon dioxide formed as a byproduct. The process is also known as coal gasification.

Black hydrogen is produced from coal in its various forms, mostly bituminous coal, without sequestration of the carbon dioxide formed as a byproduct. The process is also known as coal gasification.

Brown hydrogen is produced from lignite, also called brown or soft coal, similar to black hydrogen.

Turquoise hydrogen is produced by the thermal splitting of methane (from, e.g., natural gas) via a pyrolytic process, leaving solid carbon as a byproduct. The process is still in its infancy, but it would avoid the complications associated with carbon dioxide sequestration.

Purple hydrogen is produced using heat and electric energy from a nuclear power plant using electrolysis at elevated temperatures or combined chemical-electrolytic processes.

Pink hydrogen is produced using electric energy from a nuclear power plant.

Red hydrogen is produced using heat from nuclear power in a catalytic water-splitting process at high temperatures.

White hydrogen is a designation suggested for naturally occurring hydrogen. As chemists presumably know for centuries that hydrogen does not occur in nature and the environment in elemental form this assignment is a very special one. Elsewhere this color has been suggested for hydrogen generated as a byproduct in various chemical processes[1].

The preceding collection aims at reasonable completeness without discussing obvious overlaps, contradictions, or almost duplications. In current research and publications, further colors in most cases highly specific in terms of hydrogen production mode are proposed[1]. Details of the various processes have been reported and reviewed elsewhere[4–8], and some of the reports should be considered with care because of substantial misunderstandings[1].

Already at this stage, it becomes obvious that the assignment of a particular "type and color of hydrogen" is based solely on the actual mode of hydrogen production. Any further aspects, like the production of greenhouse gases during the production and installation of the hydrogen-producing facility and its components, are left out. This approach closely resembles the concept of zero-emission vehicles (ZEVs) popular since the 1980s in California, where again only the vehicle and its emissions during operation are considered without taking into account the emission of greenhouse gases during, e.g., the generation of electric energy needed to charge the batteries of said vehicles or during their production. But a careful consideration of greenhouse gas emissions related to the operation of a ZEV should take into account even those gas emissions released during production and setup of the wind turbine and the photovoltaic device later used for charging the batteries in this ZEV; opposite claims denying such emissions as reported sometimes are presumably erroneous[9]. Basically, the same considerations should be applied in a comprehensive consideration of hydrogen and its use.

Hydrogen as an energy carrier (also an "energy vector") has been a discussion topic for a few decades. Whether the term "hydrogen economy" was coined by Bockris[10] in 1972 or whether Beckmann's remark[11], that hydrogen as an energy carrier has been considered since the 1950s remains a question possibly more of interest to historians. Actually, Bockris hinted in a review of the history of the hydrogen economy that F. Lawaczek had written about hydrogen as an option for energy transport in the 1930s[10,12]. Certainly, lower losses during the transmission of hydrogen instead of electric energy have been the focus of the considerations discussed by Bockris[13]. Unfortunately, even at this stage, consideration and calculation were limited just to the transport (or transmission) of electric energy, not taking into account at least the components at the start of the chain (hydrogen production and its energetic efficiency) and at the end of the chain (energetic use of hydrogen and efficiencies of typical processes like

fuel cells or internal combustion engines). The use of hydrogen as a chemical reactant in industrial processes, wherein currently coal or natural gas are used as reducing agents (e.g., in the steel industry), has not been the focus of these earlier studies and considerations. On the other hand, given the rapid development of high-power electronics enabling conversion of AC to DC and DC to AC useful for high-voltage DC transmission of electric energy, the use of hydrogen as an energy carrier for transmission is of minor importance only.

This wider perception of hydrogen as an energy carrier, a chemical reactant beyond established uses in common hydrogenation reactions, in particular as a reductant in many chemical processes, and as a storage medium has shifted the general discussion about this chemical element into an almost euphoric mode. Sound and scientific discussion of its use in rational terms, taking into account physicochemical facts and an efficiency-oriented planning of hydrogen production, transportation, and finally application, is sometimes hard to find. Common misperceptions and excessive hopes and speculations differ widely from place to place, depending on the economic and ecological situation. As an example, the current state of discussion in Germany is considered in more detail, taking representative examples. Arguments and economic as well as technological facts are valid beyond this location; nevertheless, extrapolations or predictions beyond this place are left to the interested reader.

2. Hydrogen production

Hydrogen is a chemical commodity with significant amounts generated and consumed by various processes and applications.

2.1. Current hydrogen production

At the time of writing most of the hydrogen production is based on fossil fuels, in particular on reforming natural gas[5]. Further methods like coal gasification are of relatively minor importance[14]. Electrochemical water splitting, i.e. electrolysis, has been around for decades[15–17] with localized applications deployed for specific reasons[5,7]. During electrolysis of water isotope enrichment processes can be run, production of heavy water D_2O is thus connected with electrolyzers. At places with a stable, continuous supply of electric energy mostly from hydropower in a few places, electrolyzers have been set up. All of these installations run with alkaline (30% wt. KOH) water electrolysis at ambient or slightly (because of Joule heating, 60 °C–90 °C) elevated temperatures. A practical weakness of this type of electrolyzer is the need for continuous operation because at an open circuit, i.e. in idle mode, and even at strongly variable electricity supply some of its construction and electrode materials may become unstable and even corrode[18]. The integration of renewable energies with alkaline electrolyzers has been considered in the studies of Brauns and Turek[19] and Xia et al.[20]. Overall efficiencies range from 51% to 88% with respect to electric energy fed into the process and heat retrieved by burning the generated hydrogen (higher heating value). Pressures may go up to 50 bar. Electrolyzer cell stacks in the megawatt range are commercially available.

Replacing the liquid electrolyte solution of the alkaline electrolysis with a solid ionically conducting membrane as an electrolyte yields the polymer electrolyte membrane electrolyzer PEMEL, basically the polymer electrolyte membrane fuel cell running in reverse mode[21–23]. For a comprehensive review see Carmo et al.[24]. Somewhat confusingly this concept has resulted in the acronym RHFC (regenerative hydrogen fuel cell) in Pellow et al.[25]. Such a device has been examined and discussed in detail by Ahn and Holze[22,23], finally, a combination of an electrolyzer and a PEM fuel cell was recommended for both

technical and economic reasons when hydrogen is used as a storage medium. This combination and not a fuel cell is actually studied by Pellow et al.[25].

Because of the still costly cation exchange membranes specific expenses for cells are larger than with alkaline electrolysis. Electrolyzers of this type can be scaled up and down economically more easily and in a wider range than alkaline electrolyzers. They are less sensitive to changes in electricity supply. This makes PEMEL particularly attractive as a recipient of fluctuating excess electric energy from existing renewable systems and grid operators (flexible market) as well as a reliable user (firm market) for new renewable systems. The membrane of currently available types acts like an acidic electrolyte, most electrode materials well-established and stable within alkaline electrolyzers cannot be used. Unfortunately, most of the promising electrode materials (electrocatalysts) or PEMEL seem to depend on the use of expensive noble metals. Overall efficiencies of PEMEL are about the same as those of alkaline electrolyzers. Cell stacks (assemblies of single cells mounted electrically in series) with up to 1.5 MW electric power are available. A comparison of the two technologies described above is available[26]. With an optimized separator (or membrane) alkaline electrolyzers are slightly more efficient than acidic ones.

Electrolyzers using solid oxides as electrolytes (actually the reverse version of the solid oxide fuel cell) have been studied intensely when waste heat at an elevated level from nuclear power plants appeared to be available. There are various technological options using heat as an added energy input aiming at reduced cell voltages and thus lower input of electric energy these options appear to be of decreasing relevance because the assumed sources of heat were mostly nuclear power plants which have been phased out in Germany already. Elsewhere plans may differ. A look at extremely long construction times, exploding expenses, vastly delayed time of going online, and further unwelcome events cast at least some doubts on the future of nuclear power plants as an energy source and thus conceivable uses of waste heat for electrolysis of water at elevated temperatures. Accordingly, research activities fluctuate; currently, they appear to be a rather limited research and development focus. Energy efficiencies for this process appear slightly higher than for both previously mentioned processes because the thermal energy needed for operation is not factored into efficiency calculations.

Ohmic resistances in the electrolyzer cause corresponding voltage drops, and in addition, non-ideally slow electrode kinetics show some hindrances. An increase in current density j (i.e., current per area with $j = I/A$) results in an increase in needed cell voltage. As a result, the efficiency of the cell and the process will decrease with growing j and the corresponding electric input. Reducing current densities is no solution since it may increase overall production costs because of lower utilization of the installed hardware.

Because of the fluctuating supply of electric energy, electrolyzers capable of handling variable energy inputs and even temporary shut-downs are welcome, particularly in areas where the electric energy from these sources is fed into a national or even international, continent-wide electric grid with electrolyzers operating to some extent as buffers receiving electric energy not useful elsewhere in the grid and with other users. This buffering function is welcome and actually required for grid stability and to avoid economically as well as ecologically unwelcome shut-downs of windmills and photovoltaics on all grid levels; it is also welcome in small and even micro-grids.

2.2. Future hydrogen production

Green hydrogen production based on renewable energies means electrolysis, i.e., electrochemical decomposition of water. The processes briefly reviewed in the preceding section are still subject to

optimization[27,28]. In the case of PEMEL substitution of the still rather expensive membranes, in particular the cation exchange membrane, is an intensely pursued path. Replacement of the noble metals used as catalysts on both electrodes is another subject. Even at reduced use of e.g., iridium the conceivable metal supplies are completely insufficient for a scaled-up hydrogen production. The state of the art of electrocatalysts for water electrolysis has been reviewed[29]. Although some concepts for electrolyzers may be not entirely new, their application towards more efficient water splitting as with capillary designs may provide incremental improvements or even more[30].

A promising alternative to the chemically speaking acidic cation exchange membrane (a proton conductor) is substitution with an anion-conducting membrane (i.e., an alkaline membrane)[31]. When successful, the catalysts and construction materials known from alkaline electrolysis may be employed again. The chemical stability of the available membranes is still disappointing. In addition to improvements regarding this performance detail, further alternative membrane concepts (e.g., filled polymers) are studied[15].

A lack of sources of heat at the temperature level needed for water electrolysis with solid oxide electrolytes makes this option rather unlikely. Attempts to use solid proton-conducting membrane ceramic materials instead with sufficient ionic conductivity at significantly lower temperatures (500 °C to 600 °C) appear to be a relief at first sight, but again, the question of suitable heat sources may be the major barrier.

Further electrochemical options, e.g., co-electrolysis of water and CO_2 are still in the research stage[15]. This also applies to other processes, basically always including steps for carbon capture and storage. Further processes, like solar thermochemical ones, are still in the laboratory stage, according to Steinfeld[32].

3. Uses of hydrogen with a focus on efficiency

In addition to consideration of actual uses of hydrogen as a chemical reactant at the time of writing, its use as an energy carrier and storage option is in its developmental or pilot installation stage, with considerable variations from country to country. Safety aspects, infrastructure, public opinion, and further topics related to hydrogen and its use need further discussion and study; for reviews, see, e.g., Kovač et al.[33].

Because in many current (mostly chemical) uses of hydrogen as a reactant, efficiency considerations and comparisons with further options are not relevant in the following text, particular attention will be paid to its use, in particular non-chemical use, in the upcoming future.

3.1. Current uses of hydrogen

When looking at the broader picture from the viewpoint of greenhouse gas emissions and their mitigation, even at current energy mixes (in terms of energies from various primary energy sources), electrification of transport and heating will result in a reduction of said emissions[34]. An earlier study focused just on vehicles and was less optimistic for countries with a high fraction of electric energy produced using fossil fuels[35].

3.2. Future uses of hydrogen

The current situation wherein there is a surplus of electric energy from renewable sources because of poor grid infrastructure and lacking storage facilities sometimes encountered, e.g., in Germany, will be a thing of the past once these obviously and deeply deplored shortcomings are corrected. The time of

surplus electric energy, which sometimes has been considered "for free" and has been included in wide-ranging comparisons[36] will soon be over, everywhere. Because most—if not all—hydrogen will be green hydrogen produced by electrolysis, there will be no surplus of hydrogen either. Actually, in highly industrialized and densely populated countries, e.g., in central Europe, there will be a larger demand than supply. Accordingly, hydrogen use should be planned with careful attention to efficiency, with the term used in a broader sense going beyond the narrow thermodynamic meaning. **Table 1** summarizes essentials without taking into account further details like using e-fuels instead of hydrogen (based on a suggestion, see the report by Energiewende et al.[37]).

Table 1. Efficiencies of uses of hydrogen.

	Area of application			
Efficiency	**Industry**	**Transport**	**Energy grid**	**Residential and buildings**
High	Reducing agent, chemical reagent	Long-range aviation and shipping	-	Support of district heating
Questionable	high-temperature heating	Trucks, buses, trains, short-range aviation and shipping	Storage medium for grid support	-
Bad	Low-temperature heating	Cars and light vehicles	-	Residential heating

Although the use of hydrogen and fuel cells as energy sources in vehicles appears less attractive in terms of overall energetic efficiency their use in trucks seems to be reasonable because of the limitations of using batteries as storage devices in such vehicles and because the overall energy consumption of this class of vehicles amounts to about 4.1% only of overall energy consumption for vehicles[38].

The euphorically touted use of E-fuels certainly gives advantages like the possibility of keeping the current fleet of vehicles and the established fuel distribution infrastructure[39] will most likely not be matched by the availability of enough E-fuels. The high energy demand in its production will restrict its synthesis to places where all ingredients (beyond cheap electric energy) are abundantly available. As of today, their use should be limited to those cases where direct use of electric energy via batteries and supercapacitors or at least via hydrogen and fuel cells, both showing much higher efficiencies, is impossible e.g., in long-range aviation.

When considering emissions from vehicles with internal combustion engines beyond CO_2, further greenhouse effect-relevant emissions, in particular of N_2O and methane, must be considered when overall contributions and effects should be compared[40]. The calculation of CO_2-emission based simply on the chemical reaction equation of the combustion process is not wrong, but with respect to the effects of emitted combustion products, it is incomplete. The consideration gets even more complicated when, beyond efficiency and CO_2-emission per run kilometer, further emissions and consumption of resources are considered. In so-called ecological assessments or environmental footprints, this is tried; it will not be pursued further in this report. Beyond the obvious considerations of efficiencies, the various uses of hydrogen might get out of focus—such approaches have been frequently used to provide tilted criticism. e.g., the high "water consumption" during lithium production may just be water evaporation during brine treatment within the process, and the numbers almost disappear anyway when compared with current numbers reported for agriculture and textile production[41]. Most regrettably, in the latter report on current energy use in mobility, surprisingly small energy consumption is attributed to BEVs and an equally surprisingly large one to vehicles operated with fuel cells. This trivial but somewhat disturbing observation and its confusing consequences have been addressed in a report by Buchal et al.[36]. Therein two midsize cars with a diesel internal combustion engine (ICV) and a battery-fed electric engine (BEV)

are compared with respect to CO_2 emissions during operation. For the BEV, two boundary cases are considered: Electricity from the German mix of 2018 and electricity exclusively from renewables. CO_2 emissions during battery production are at least addressed. Finally, an ICV fed with methane is compared. The latter example is connected to renewable energies by assuming that methane produced with hydrogen from electrolysis with renewable energies is used. In conclusion, Buchal et al. report that for a BEV, in the best case, CO_2 emissions per kilometer are 10% higher than those of a diesel-fueled car; in the worst case, this grows to 25%. At this point, the authors refer to CO_2 emissions from the transport sector as being stagnant in Germany for years already. The causes are well known (the rapidly growing fraction of heavy cars, in particular SUVs, with high specific emissions), but too nasty to address them[42]. Knobloch et al.[34] arrive at a slightly different conclusion: Even with the electricity mix of 2020 in 53 world regions covering 95% of worldwide energy and heating demand, the CO_2-emissions per kilometer, including the battery, and assuming a lifetime of 150,000 km, just as done by Buchal et al.[36] of a BEV are smaller than those of a vehicle with ICE. In countries with a large fraction of renewable or nuclear energy (e.g., Island, Sweden, or Switzerland), it may be lower by 70%, whereas in countries with, e.g., a large fraction of oil shale in the mix, it may be 40% higher. The contradiction to Buchal et al. is obvious, but because Knobloch et al. don't quote this report, the reader is left alone in gentle confusion. The interested reader will find out quickly that the reports are hardly comparable because Buchal et al. compared only two relatively big cars, whereas Knobloch et al. took into account the actual mix of cars in a given region. This problem has been noted before by Woo and Choi[35]. Consequently, the results reported by Knobloch et al. without their limitation to a specific class of cars are of much wider validity. This finding is further supported by the fact that these authors refrain from any speculation about technologies and their future, as done by Buchal et al. and one of the coauthors before[43]. Both studies ignore the possibilities and effects of e-fuels[9,39,44,45] whether of the 1.[46], 2.[46], 3.[47], or 4. generation[48]. Given the large number of process steps of the synthetic pathways towards e-fuels proposed so far, energetic efficiency will be small, most likely[49–51] and may be acceptable only when taking into account further arguments like the possibly long distance between production and usage or the absence of any other viable option (as in air transport). Definitely, the consumer will enjoy them; certainly, they merit consideration, at least for a transitional time[44].

This interpretation of the observed difference between the conclusions of Buchal et al.[36] and Knobloch et al.[34] is supported by a much wider consideration with more details in a book edited by Klell et al.[51]. **Figure 1** shows the energy consumption per driven kilometer of vehicles with various engines.

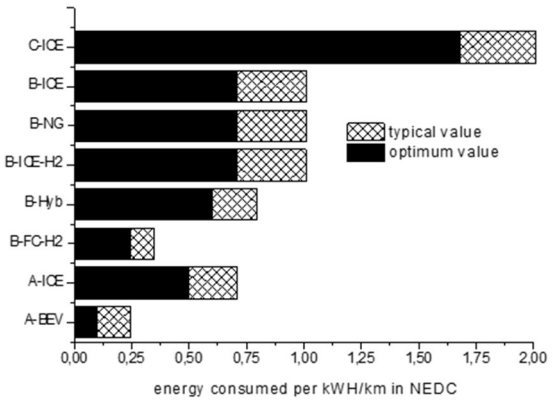

Figure 1. Energy consumed per driven kilometer for A: compact car; B: medium class car; C: luxury car. Operated with: ICE: internal combustion engine with gasoline/Diesel; NG: natural gas with internal combustion engine; ICE-H2: internal combustion engine with hydrogen; Hyb: hybrid; FC-H2: fuel cell with hydrogen; BEV: battery; NEDC: new European driving cycle[51].

Unfortunately, there are no details in the report by Knobloch et al.[34] enabling the assignment of the two selected cars to the categories used in **Figure 1** and the collection edited by Klell et al.[51], the present author refrains from any speculation. Taking in the next step a plain combustion reaction and assuming (as usual) only tailpipe emissions **Figure 2** can be obtained.

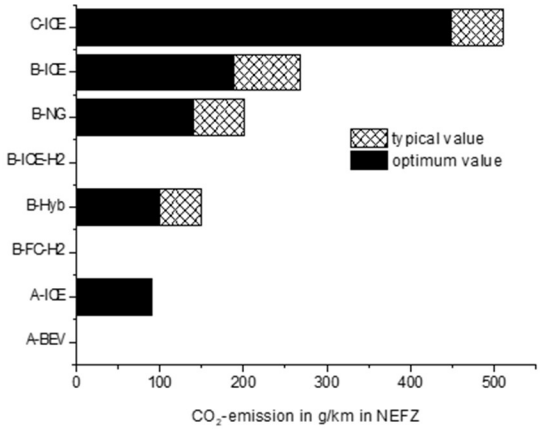

Figure 2. CO_2-emissions per driven kilometer für A: compact car; B: medium class car; C: luxury car. Operated with: ICE: internal combustion engine with gasoline/Diesel; NG: internal combustion engine with natural gas; ICE-H2: internal combustion engine with hydrogen; Hyb: hybrid; FC-H2: fuel cell with hydrogen; BEV: Battery; NEDC: new European driving cycle[51].

The authors obtain overall efficiencies containing the chain from the energy content of the primary energy carrier up to moving the vehicle yielding **Figure 3**[51].

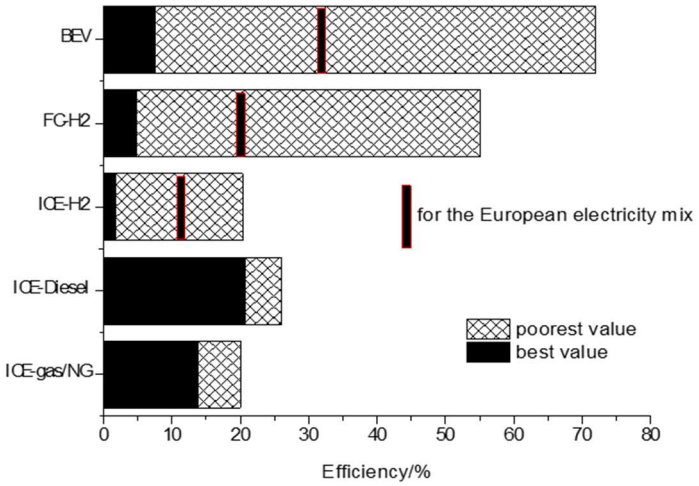

Figure 3. Efficiencies for different driving systems BEV: battery; FC-H2: fuel cell with hydrogen; ICE-H2: internal combustion engine with hydrogen; ICE-Diesel: internal combustion engine Diesel; ICE-gas/NG: internal combustion engine with gasoline or natural gas[51].

The lowest efficiency of a BEV results from using electricity from a lignite-fired power station; the best results from using hydroelectricity. Using hydrogen in the car results in the highest efficiency when using hydrogen from a methane reformer and a fuel cell; the poorest efficiency follows from using an electrolyzer fed from a lignite-fired power station and an internal combustion engine.

Inclusion of the European electricity mix provides an even more realistic picture of efficiency. Already before considering CO_2-emissions obviously electricity from renewable sources and hydrogen

produced with these sources is desirable. An answer to the initially addressed question for CO_2-emissions during operation of a vehicle is finally obtained[51], results are displayed in **Figure 4**.

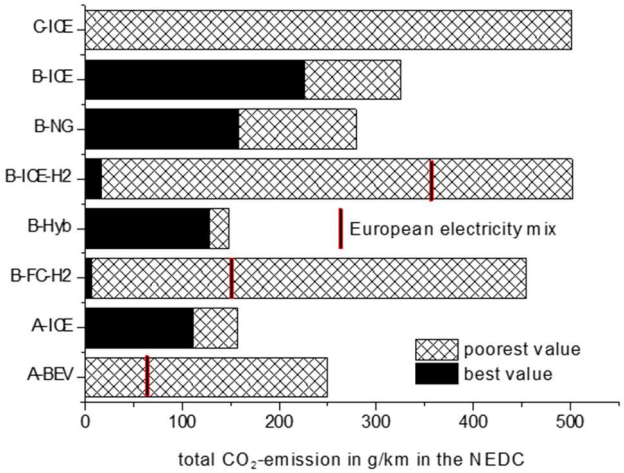

Figure 4. CO_2 emissions per driven kilometer for A: compact car; B: medium class car; C: luxury car. Operated with: ICE: internal combustion engine with gasoline/Diesel; NG: Internal combustion engine with natural gas; ICE-H2: internal combustion engine with hydrogen; Hyb: hybrid; FC-H2: Fuel cell with hydrogen; BEV: Battery; NEDC: new European driving cycle[51].

Once again electric vehicles display their advantage of low CO_2 emissions in particular when electricity from renewable sources is used directly with a BEV or indirectly with hydrogen for storage. Taking instead for a BEV the worst case CO_2 emissions are indeed larger than with the best case with an ICE. This might be taken at first glance as a confirmation of the conclusions by Buchal et al.[36], but already after a look at the more realistic European electricity mix, this apparent confirmation evaporates.

Energetic efficiencies and CO_2 emissions as addressed above are only two of several criteria applied when assessing options. They have their merits and their limitations. Further options are the consideration of energy put into setting up a system vs. the energy stored and released to the grid over the lifetime (net energy analysis) or energy return on investment as demonstrated by Pellow et al.[25].

4. Outlook and perspectives

The scientist's perspective based on thinking in yields and efficiencies will turn out to be insufficient when a topic with far-reaching social and economic implications is considered. As demonstrated above just taking the use of hydrogen in transportation inclusion of more criteria and dimensions tend to result in less clear-cut outcomes and rather relative recommendations. These in addition will be exposed to a critical discussion by non-experts in society and must turn out to be both comprehensible and convincing for the non-scientist. If insufficient care is exercised and the perspective of the non-expert is not taken into account adequately, decisions may be made which most likely will not help to avoid catastrophic developments.

Funding

Preparation of this contribution has been supported in various ways by the Alexander von Humboldt-Foundation, Deutscher Akademischer Austauschdienst, Fonds der Chemischen Indus-trie, Deutsche Forschungsgemeinschaft, National Basic Research Program of China, the Natural Science Foundation of China (Grant # 51425301) and the National Key R & D Program of China (2021YFB2400400). It includes insights obtained within research projects at St. Petersburg State

University supported by grants No. 26455158 and No. 70037840.

Conflict of interest

The author declares no conflict of interest.

References

1. Ajanovic A, Sayer M, Haas R. The economics and the environmental benignity of different colors of hydrogen. International Journal of Hydrogen Energy. 2022, 47(57): 24136-24154. doi: 10.1016/j.ijhydene.2022.02.094
2. Kusoglu A. The many colors of hydrogen. The Electrochemical Society Interface. 2021, 30(4): 44-48. doi: 10.1149/2.f12214if
3. Wu Y, Holze R. Are there green hydrogen or zero-emission vehicles? (German). Bunsen-Magazin. 2020, 22(3): 50-53.
4. Nikolaidis P, Poullikkas A. A comparative overview of hydrogen production processes. Renewable and Sustainable Energy Reviews. 2017, 67: 597-611. doi: 10.1016/j.rser.2016.09.044
5. Newborough M, Cooley G. Developments in the global hydrogen market: Electrolyser deployment rationale and renewable hydrogen strategies and policies. Fuel Cells Bulletin. 2020, 2020(10): 16-22. doi: 10.1016/s1464-2859(20)30486-7
6. Dawood F, Anda M, Shafiullah GM. Hydrogen production for energy: An overview. International Journal of Hydrogen Energy. 2020, 45(7): 3847-3869. doi: 10.1016/j.ijhydene.2019.12.059
7. Newborough M, Cooley G. Developments in the global hydrogen market: The spectrum of hydrogen colours. Fuel Cells Bulletin. 2020, 2020(11): 16-22. doi: 10.1016/s1464-2859(20)30546-0
8. El-Shafie M, Kambara S, Hayakawa Y. Hydrogen production technologies overview. Journal of Power and Energy Engineering. 2019, 7(1): 107-154. doi: 10.4236/jpee.2019.71007
9. Maus W (editor). Future Fuels: Energy Transition in Transport as a Global Climate Goal (ATZ/MTZ Specialist Book) (German). Springer Vieweg; 2019.
10. Bockris JOM. A hydrogen economy. Science. 1972, 176(40-41): 1323-1323. doi: 10.1126/science.176.4041.1323
11. Beckmann G. Hydrogen—An energy source (German)? Nachrichten aus Chemie, Technik und Laboratorium. 1991, 39(5): 503-508. doi: 10.1002/nadc.19910390505
12. Bockris JOM (editor). The hydrogen economy. In: Environmental Chemistry. Springer; 1977. pp. 549-582. doi: 10.1007/978-1-4615-6921-3_17
13. Bockris JOM. The hydrogen economy: Its history. International Journal of Hydrogen Energy. 2013, 38(6): 2579-2588. doi: 10.1016/j.ijhydene.2012.12.026
14. Midilli A, Kucuk H, Topal ME, et al. A comprehensive review on hydrogen production from coal gasification: Challenges and Opportunities. International Journal of Hydrogen Energy. 2021, 46(50): 25385-25412. doi: 10.1016/j.ijhydene.2021.05.088
15. Neugebauer R (editor). Hydrogen Technologies (German). Springer Vieweg; 2022.
16. David M, Ocampo-Martinez C. Current status of water electrolysis for energy storage. In: Comprehensive Renewable Energy. Elsevier; 2022. pp. 533-552. doi: 10.1016/b978-0-12-819727-1.00039-x
17. Dincer I, Al Zahrani AA. Electrolyzers. Comprehensive Energy Systems. 2018, 4: 985-1025. doi: 10.1016/B978-0-12-809597-3.00442-9
18. Amireh SF, Heineman NN, Vermeulen P, et al. Impact of power supply fluctuation and part load operation on the efficiency of alkaline water electrolysis. Journal of Power Sources. 2023, 560: 232629. doi: 10.1016/j.jpowsour.2023.232629
19. Brauns J, Turek T. Alkaline water electrolysis powered by renewable energy: A review. Processes. 2020, 8(2): 248. doi: 10.3390/pr8020248
20. Xia Y, Cheng H, He H, et al. Efficiency and consistency enhancement for alkaline electrolyzers driven by renewable energy sources. Communications Engineering. 2023, 2(1). doi: 10.1038/s44172-023-00070-7
21. Wu Y, Holze R. Electrochemical Energy Conversion and Storage. Wiley-VCH; 2022.
22. Ahn J, Holze R. Bifunctional electrodes for an integrated water-electrolysis and hydrogen-oxygen fuel cell with a solid polymer electrolyte. Journal of Applied Electrochemistry. 1992, 22(12): 1167-1174. doi: 10.1007/bf01297419
23. Holze R, Ahn J. Advances in the use of perfluorinated cation exchange membranes in integrated water electrolysis and hydrogen/oxygen fuel cell systems. Journal of Membrane Science. 1992, 73(1): 87-97. doi: 10.1016/0376-7388(92)80188-p
24. Carmo M, Fritz DL, Mergel J, et al. A comprehensive review on PEM water electrolysis. International

Journal of Hydrogen Energy. 2013, 38(12): 4901-4934. doi: 10.1016/j.ijhydene.2013.01.151
25. Pellow MA, Emmott CJM, Barnhart CJ, et al. Hydrogen or batteries for grid storage? A net energy analysis. Energy & Environmental Science. 2015, 8(7): 1938-1952. doi: 10.1039/c4ee04041d
26. Schalenbach M, Tjarks G, Carmo M, et al. Acidic or alkaline? Towards a new perspective on the efficiency of water electrolysis. Journal of The Electrochemical Society. 2016, 163(11): F3197-F3208. doi: 10.1149/2.0271611jes
27. Ehlers JC, Feidenhans'l AA, Therkildsen KT, et al. Affordable green hydrogen from alkaline water electrolysis: Key research needs from an industrial perspective. ACS Energy Letters. 2023, 8(3): 1502-1509. doi: 10.1021/acsenergylett.2c02897
28. Zayat B, Mitra D, Narayanan SR. Inexpensive and efficient alkaline water electrolyzer with robust steel-based electrodes. Journal of the Electrochemical Society. 2020, 167(11): 114513. doi: 10.1149/1945-7111/aba792
29. Chatenet M, Pollet BG, Dekel DR, et al. Water electrolysis: from textbook knowledge to the latest scientific strategies and industrial developments. Chemical Society Reviews. 2022, 51(11): 4583-4762. doi: 10.1039/d0cs01079k
30. Hodges A, Hoang AL, Tsekouras G, et al. A high-performance capillary-fed electrolysis cell promises more cost-competitive renewable hydrogen. Nature Communications. 2022, 13(1). doi: 10.1038/s41467-022-28953-x
31. Vincent I, Bessarabov D. Low cost hydrogen production by anion exchange membrane electrolysis: A review. Renewable and Sustainable Energy Reviews. 2018, 81: 1690-1704. doi: 10.1016/j.rser.2017.05.258
32. Steinfeld A. Solar thermochemical production of hydrogen—A review. Solar Energy. 2005, 78: 603-615. doi: 10.1016/j.solener.2003.12.012
33. Kovač A, Paranos M, Marciuš D. Hydrogen in energy transition: A review. International Journal of Hydrogen Energy. 2021, 46: 10016-10035. doi: 10.1016/j.ijhydene.2020.11.256
34. Knobloch F, Hanssen SV, Lam A, et al. Net emission reductions from electric cars and heat pumps in 59 world regions over time. Nature Sustainability. 2020, 3: 437-447. doi: 10.1038/s41893-020-0488-7
35. Woo J, Choi HA. Well-to-wheel analysis of greenhouse gas emissions for electric vehicles based on electricity generation mix: A global perspective. Transportation Research Part D: Transport and Environment. 2017, 51: 340-350. doi: 10.1016/j.trd.2017.01.005
36. Buchal C, Karl HD, Sinn HW. Coal engines, wind engines and diesel engines: What does the CO_2 balance show? (German). IFO Schnelldienst. 2019, 72(8): 40-54.
37. Energiewende A, Industry A, Torcuato F, Tella D. 12 Insights on Hydrogen—Argentina Edition. Agora, 2023.
38. Brauner G. System Efficiency for Renewable Power Generation. Springer Vieweg; 2018.
39. Ausfelder F, Wagemann K. Power-to-fuels: E-fuels as an important option for a climate-friendly mobility of the future. Chemie Ingenieur Technik. 2020, 92: 21-30. doi: 10.1002/cite.201900180.
40. JEC—Joint Research Centre-Eucar-concawe collaboration, well-to-wheels analysis of future automotive fuels and powertrains in the european context, well-to-tank (wtt) report—appendix 2, version 4a, 2014. Available online: https://ec.europa.eu/jrc/sites/jrcsh/files/wtt_appendix_2_v4a.pdf (accessed on 2 June 2023).
41. Tagesspiegel. Server-Fehler. Available online: https://www.tagesspiegel.de/berlin/archiv/2019/12/02%E2%80%9D (accessed on 20 December 2023).
42. Zellner R. Too much CO_2 from traffic: Is electromobility the solution (German)? Nachrichten aus der Chemie. 2019, 67(3): 26-31. doi: 10.1002/nadc.20194083851
43. Sinn HW. Are electric vehicles really so climate friendly? Available online: https://www.theguardian.com/environment/2019/nov/25/are-electric-vehicles-really-so-climate-friendly (accessed on 2 June 2023).
44. Sterner M, Stadler I (editors). Energy Storage—Needs, Technologies, Integration (German), 2nd ed. Springer Vieweg; 2017.
45. Leitner W, Klankermayer J, Pischinger S, et al. Advanced biofuels and beyond: Chemistry solutions for propulsion and production. Angewandte Chemie International Edition. 2017, 56(20): 5412-5452. doi: 10.1002/anie.201607257
46. Vetere A, Schrader W. Analysis of biofuels (German). GIT-Labor. 2020, 64(3): 26-29.
47. Ramirez J, Brown R, Rainey T. A review of hydrothermal liquefaction bio-crude properties and prospects for upgrading to transportation fuels. Energies. 2015, 8(7): 6765-6794. doi: 10.3390/en8076765
48. Lü J, Sheahan C, Fu P. Metabolic engineering of algae for fourth generation biofuels production. Energy & Environmental Science. 2011, 4(7): 2451. doi: 10.1039/c0ee00593b
49. Heinemann C, Kasten P, Bauknecht D, et al. The importance of electricity-based substances for climate protection in Germany (German). Available online: https://www.oeko.de/fileadmin/oekodoc/PtX-Hintergrundpapier.pdf (accessed on 20 December 2023).
50. Brauner G. System Efficiency for Renewable Power Generation (German). Springer Vieweg; 2018.

51. Agora Energiewende and Frontier Economics Ltd. The future cost of electricity-based synthetic fuels. Available online: https://www.agora-verkehrswende.de/en/publications/the-future-cost-of-electricity-based-synthetic-fuels/ (accessed on 20 December 2023).
52. Klell M, Eichlseder H, Trattner A (editors). Hydrogen in Vehicle Technology. Springer Vieweg; 2018.

Academic Publishing Pte. Ltd.

Add: 73 Upper Paya Lebar Road #07-02B-01 Centro Bianco Singapore 534818

Tel: +65 83184869

E-mail: editorial_office@acad-pub.com

Web: http://ojs.acad-pub.com/